UNIVERSITÉ LAVAL

DÉVELOPPEMENT ET ÉVALUATION DE STRATÉGIES DE CONTRÔLE AVANCÉES DES TECHNOLOGIES DE FENÊTRES INTELLIGENTES

Thèse

Jean-Michel Dussault

Doctorat en génie mécanique

Philosophiæ Doctor (Ph. D.)

Québec, Canada

DÉVELOPPEMENT ET ÉVALUATION DE STRATÉGIES DE CONTRÔLE AVANCÉES DES TECHNOLOGIES DE FENÊTRES INTELLIGENTES

Thèse

Jean-Michel Dussault

Sous la direction de :

Louis Gosselin, directeur de recherche

RÉSUMÉ

Les fenêtres intelligentes présentent un potentiel important quant à la réduction de la consommation d'énergie dans les bâtiments et permettent d'assurer le confort visuel des occupants. Depuis le début des années 90, la recherche sur les technologies de fenêtres intelligentes s'est accentuée tant au niveau des technologies elles-mêmes qu'au niveau des types de contrôle qu'on peut leur appliquer pour gérer le plus efficacement possible le rayonnement solaire qui les traverse. Plusieurs laboratoires de recherche tels que le Lawrence Berkeley National Laboratory (LBNL) se sont penché sur la question. L'évolution de la recherche dans ce domaine démontre toute la complexité associée à l'évaluation rigoureuse des performances des fenêtres intelligentes. De par sa capacité à gérer le rayonnement solaire, il va de soi que ce genre de technologies nécessite la connaissance du rayonnement solaire incident pour faciliter la prise de décision quant au contrôle à apporter. Étant donnés les coûts des technologies de capteurs de rayonnement solaire existantes et la limitation de certains quant à leur précision (lors de fluctuations du spectre électromagnétique et/ou des températures ambiantes), l'utilisation de capteurs de rayonnement solaire dédiés au contrôle de fenêtre intelligente est donc limitée. Par ailleurs, les connaissances sont encore limitées concernant les conditions permettant d'optimiser le contrôle de ce genre de technologies en termes d'énergie et de confort. L'objectif général de cette thèse est d'élargir les connaissances scientifiques sur le potentiel des technologies de fenêtres électrochromes quant à leur capacité à augmenter la performance énergétique et le confort des occupants dans les bâtiments.

Dans un premier temps, un nouveau type de capteur de rayonnement solaire à faible coût est présenté. Ce capteur utilise la différence de température entre une surface blanche et une surface noire pour estimer le flux solaire radiatif traversant les ouvertures d'un bâtiment. Les mesures de rayonnement solaire sont corrélées aux températures de surfaces à l'aide un modèle thermique du capteur en 1D. Deux différents modèles de capteur sont présentés et les résultats obtenus sont comparés aux mesures solaires de référence obtenues par un pyranomètre. Il a été démontré que les modèles de capteurs présentent des précisions suffisantes pour un contrôle efficace. Finalement, il est observé que la période de calibration des capteurs requiert minimalement une demi-journée de mesures sous des conditions de ciel clair incluant le midi solaire.

Dans un deuxième temps, l'impact des stratégies de contrôle de fenêtre intelligente sur la consommation énergétique globale est évalué. L'état des fenêtres intelligentes nécessaire à toute heure de la journée pour permettre une minimisation de la consommation d'énergie globale tout en respectant les contraintes reliées au confort thermique et visuel est déterminé à l'aide d'une stratégie d'optimisation basée sur des algorithmes génétiques. Ce contrôle quasi-optimal est alors comparé à d'autres approches qui peuvent être adaptées à des applications en temps réel, soit des contrôles fondés sur des règles et un modèle de contrôle prédictif. Les impacts de la masse thermique et de la puissance du système d'éclairage installé sont également analysés. Les résultats montrent que les quatre stratégies de contrôle à l'étude présentent une consommation énergétique similaire avec des écarts de consommation globale variant de 4% à 10%. Cette étude illustre que des stratégies de contrôle plus simple permettent d'obtenir des résultats satisfaisants.

Finalement, une analyse de sensibilité basée sur une grande variété de combinaison de paramètres de design est réalisée. Des résultats énergétiques et de confort pour un total de 7680 scénarios sont obtenus et utilisés dans cette analyse considérant l'effet principal des paramètres de design du bâtiment. L'influence relative des paramètres est présentée et les différents designs améliorant les résultats sont déterminés. Les résultats montrent que la meilleure économie d'énergie avec fenêtres intelligentes se trouve dans des climats chauds avec une exposition élevée aux rayons solaires. La présence de fenêtres intelligentes influence principalement la charge de refroidissement maximale et agit comme une solution alternative à la masse thermique en termes de réduction potentielle de cette charge maximale. Bien que le choix de la stratégie de contrôle ait un impact limité sur l'économie d'énergie réalisée et la réduction de la charge maximale, l'analyse permet de constater que ce paramètre a un impact encore plus important sur le confort visuel. L'utilisation de fenêtres intelligentes ne semble pas influencer grandement le confort thermique à l'intérieur de la zone.

ABSTRACT

Smart windows present a huge potential in terms of energy consumption reduction in buildings while also offering the possibility to assure occupants' visual comfort. Since the early nineties, research in the field of smart windows gains a lot of interest on both the technologies and the controls that could be applied on such technologies to manage more efficiently solar gains passing through these windows. Many different well-known entities such as the Lawrence Berkeley National Laboratory invested efforts in this field and demonstrated the great complexity related to the thorough evaluation of smart window performances. Given its capacity to manage solar radiation, it makes sense to benefit from solar radiation measurements to control efficiently such technology. However, the costs and other technical related limitations reduce the potential to use readily available solar sensors for smart window control. Moreover, general knowledge is still limited regarding the conditions leading to optimal control decisions of smart windows. The main objective of this thesis was to gain a better understanding of how electrochromic windows could lead to improved performances in terms of energy consumption and thermal comfort

First, a new design of low cost solar sensor is proposed. The sensor uses the difference in temperature of white and black surfaces to estimate the solar heat flux through building openings. Results of solar radiation measurements are obtained through a correlation based on a 1D thermal model of the sensor. Two designs of the sensor are presented and obtained results compared with solar measurements of a high precision pyranometer. It was shown that the new sensors present sufficient accuracy for smart window control applications. Finally, it was observed that ideal sensors calibration period should consider at least half a day of measurements, including solar peak time, and should be done during clear sky conditions.

Then, the impact of the applied control strategy on the overall energy consumption is investigated. The hour-by-hour state of the smart windows required to minimize overall energy consumption while respecting constraints related to comfort is determined through an optimization strategy based on genetic algorithms. This quasi-optimal control is compared to other approaches that could be applied in real-time applications, i.e. rule-based controls and a model predictive control. The impacts of thermal mass and installed light power density are also analyzed. Results show that the four control strategies under study presented similar energy consumption with differences in total energy consumption ranging from 4% to 10%. This study illustrates that simpler control strategies can also lead to satisfying results.

Finally, a sensitivity analysis based on a large number of different combinations of design parameters is performed. Results related to energy and for a total of 7680 scenarios were obtained and used in this analysis considering the Main effect of the building parameters. The relative influence of the parameters is presented and the different designs improving the outputs are determined. Results have shown that the greatest total energy savings considering EC windows are for warmer climates with higher solar radiation exposures. The presence of an EC window mostly influences the cooling peak load and acts as an alternative solution to thermal mass from the perspective of peak reductions. While the choice of the specific window control strategy is having a limited impact on the energy savings and peak load

reductions, the analysis revealed that this parameter has a larger impact on the visual comfort. The use of smart window does not appear to greatly influence the thermal comfort within the zone.

CONTENTS

TABLE CAPTIONS

FIGURE CAPTIONS

NOMENCLATURE

A	Surface area, m^2
ACH	Air change per hour, 1/hr
BWS	Black and white sensor
C	Thermal capacity, J/K (Chapter 4)
C	Volume heat capacity, kJ/m^3K (Chapter 5)
CDD	Annual cooling degree days considering a 18°C reference temperature, °C
CDT	Cooling design temperature, °C
CE	Cooling energy consumption reduction (or increase), kWh/m^2
CLT	Cross Laminated Timber floor
CPED	Cooling peak energy demand reduction (or increase), W/m^2
Cr	Concrete floor
Ct	Surface thermal capacity, $J/m^2 \cdot K$
D	Depth, m
DC	Discomfort Cost, Kh
Dz	Daylight zone
E	Energy consumption, kWh/m^2
E_z	Zone air distribution effectiveness
EC	Electrochromic
F	Weighting factor
f	Fraction
Fu	Utilization factor
G	Irradiance, W/m^2
GA	Genetic Algorithm
GDF	Global Depreciation Factor
H	Height, m
H_c	Control horizon
H_p	Prediction horizon
HDD	Annual heating degree days considering a 18°C reference temperature, °C
HDT	Heating design temperature, °C
HE	Heating energy consumption reduction (or increase), kWh/m^2
HEE	Heat exchanger efficiency, %
HPED	Heating peak energy demand reduction (or increase), W/m^2
I	Incident solar radiation, W/m^2
I75	Infiltration rate (rated at 75Pa gage pressure), $L/s\text{-}m^2$
IG	Internal gains, W/m^2
IGDB	International Glazing DataBase
k	thermal conductivity, $W/m \cdot K$
L	Sensor cross-section thickness, m
LDD	Luminaire Dirt Depreciation
LED	Artificial lighting system with LEDs
LLD	Lumen Lamp Depreciation
LPD	Light Power Density, W/m^2
ME	Main effect
MPC	Model Predictive Control
N	Number of parameters considered for sensitivity analysis
n	Number of capacitances (Chapter 4)
n	Number of possible designs for a parameter (Chapter 5)
Ori	Orientation
PPD	Predicted Percentage of Dissatisfied, %

Q	Heat flux, W/m^2 (Chapter 3)
Q	Load, W (Chapter 4)
r	Control setpoint
R	Thermal resistance, K/W
R_a	Outdoor air flow rate required per unit area, L/s-pers
R_p	Outdoor air flow rate required per person, L/s-pers
RBC	Rule-based Control
S	Number of possible design
SHGC	Solar heat gain coefficient
SPD	Suspended Particle device
SW	Smart Window
T	Temperature, K (Chapter 3 and 4)
T	Temperature, °C (Chapter 5)
T8	Artificial lighting system with T8 lamps
TE	Total energy consumption reduction (or increase), kWh/m^2
TM	Thermal mass
TPED	Total peak energy demand reduction (or increase), W/m^2
Tsol	Solar transmittance, %
Tvis	Visible transmittance, %
U	Inputs
UDI	Useful daylight illuminance, %
U-value	Thermal conductance, W/m^2K
W	Width, m
WP	Workplane (Chapter 4)
Wp	Workplane (Chapter 5)
WWR	Window to wall ratio
X	Set of building parameters (model inputs)
x	Building states, K (Chapter 4)
x	Building parameter (Chapter 5)
$\hat{x}$	Building states estimation, K
Y	Building output temperatures, K (Chapter 4)
Y	Model outputs (Chapter 5)
y	Output for a specific set of building parameters **X**

Subscripts

1	Interior surface of the exterior glass pane
2	Exterior surface of the interior glass pane
air	Zone air
b	Back side of sensor surface
B	Black surface
abs	Absorbed energy
airchange	Outdoor air ventilation flow rate requirement
ave	Average
c	Control
cl	Center location of the layer
cond	Conductive
conv	Convective (Chapter 3)
conv	Convective heat transfer (Chapter 4)
cool	Cooling
d	Disturbances

diff	Diffuse component of solar radiation
direct	Direct component of solar radiation
ew	Exterior wall layer of the exterior building wall (concrete)
ew1	Thermal node between the exterior and middle wall layers
f	Front side of sensor surface
fl	Floor
gains	Internal gains
gap	Insulated glazing unit argon gap
glass	Window glass panes
heat	Heating
i	Interior walls and zone air thermal node
in	Indoor
iw	Interior wall layer of the exterior building wall (gypse)
iw2	Thermal node between the middle and interior wall layers
k	k^{th} time step in MPC control (Chapter 4)
k	k^{th} building parameter (Chapter 5)
L	Light output
light	Artificial lighting system
LW	Wall section of the building façade below the glazing
max	Maximum
min	Minimum
mw	Middle wall layer of the exterior building wall (insulation)
n	Number of possible designs for parameter k
nat	Natural light illuminance
o	Over maximum temperature setpoint
out	Outdoor (Chapter4)
out	Exterior conditions (Chapter 5)
P	Light power input
p	p^{th} prediction time step
rad	Radiative (Chapter 3)
rad	Radiative heat transfer (Chapter 4)
ref	Reference measurements
req	Requirement
sum	Summer conditions
SW	Smart Window glazing
SW1	Exterior glass pane of the smart window glazing
SW2	Interior glass pane of the smart window glazing
t	t^{th} time step in ideal modulating control
u	Under minimum temperature setpoint
UW	Wall section of the building façade above the glazing
sol	Solar
st	Storage
state	State of transparency
surr	Surrounding surfaces
tot	Total
v	Vertical
W	White surface
w	Exterior wall of the building zone (Chapter 4)
w	Window (Chapter 5)
win	Winter conditions
z	Zone

zone	Zone air node
1%	Annual cumulative frequency of occurrence exceeding the given dry bulb temperature
99%	Annual cumulative frequency of occurrence exceeding the given dry bulb temperature

Greek symbols

α	Absorptivity
ε	Emissivity
ρ	Density, kg/m^3
σ	Stefan-Boltzmann constant ($\sigma = 5.670 \cdot 10^{-8}$), $W/m^2 \cdot K^4$ (Chapter 4)
σ	Standard deviation (Chapter 5)

REMERCIEMENTS

J’ai été en mesure de compléter ce projet de thèse de doctorat particulièrement dû au fait que j’ai été extrêmement bien entouré au cours des dernières années, et ce, tant du point de vue professionnel que personnel. Les lignes qui suivent présentent ces personnes et/ou organismes qui m’ont plus particulièrement soutenu dans ce projet de longue haleine et que je tiens à remercier.

Je tiens premièrement à remercier mon directeur de thèse, Louis Gosselin, qui m’a offert une place de choix dans son laboratoire, qui a cru en mes capacités de chercheur et qui m’a donné une grande latitude quant à la réalisation de ce projet. Les quatre dernières années ont été pour moi synonymes de dépassements, d’accomplissements et de réussites, et c’est en grande partie grâce à Louis que j’ai eu la chance de vivre ces expériences. Sa passion envers la recherche en transfert thermique ainsi que l’intérêt qu’il a démontré envers mon projet de recherche ont définitivement été sources de motivation.

Dans le cadre de mon projet au doctorat, j’ai eu la chance de réaliser une session d’étude au sein du Lawrence Berkeley National Laboratory (LBNL) à l’automne 2014. Cette expérience fût extrêmement enrichissante et j’ai eu la chance de côtoyer des chercheurs extrêmement compétents de qui j’ai beaucoup appris. Je tiens premièrement à remercier Dennis Anderson, LAP Manager au NFRC à l’époque, pour m’avoir permis d’entrer en contact avec le Windows and Daylight group du LBNL. Je remercie particulièrement mon superviseur immédiat Christian Kohler, ainsi que le responsable du groupe Stephen Selkowitz qui m’ont accueillis et se sont montrés extrêmement disponibles tout au long de mon séjour. Je remercie également l’ensemble des membres du groupe pour m’avoir intégré au groupe de la sorte.

Au cours des différentes étapes associées à mon parcours au doctorat, j’ai eu la chance d’être évalué par des professeurs extrêmement compétents et de surcroît bien sympathiques. Je pense entre autres à Yves St-Amant et François Mathieu Potvin qui m’ont aidé à orienter mon projet à différents niveaux. Je les remercie pour leur temps et leurs nombreux conseils.

Au jour le jour, j’ai eu la chance de côtoyer plusieurs étudiants gradués impliqués à différents niveaux au sein du Laboratoire de Transfert Thermique et d’Énergétique. Je pense particulièrement à Jonathan qui sait très bien comment se faire aimer en préparant le café tous les matins. Mis appart ses qualités en tant que "café maestro", je tiens à le remercier pour son écoute et ses différents conseils m’ayant permis d’avancer plus rapidement à certains moments critiques. Je tiens également à souligner les participations respectives de Maarten, Louis-Gabriel et Mathieu dans l’avancement de mon projet.

De plus, je remercie le CRSNG qui, de 2012 à 2015, a appuyé mon projet de recherche par l’entremise des bourses Vanier, m’offrant par la même occasion une tranquillité d’esprit financière pour la réalisation de mes travaux.

Par ailleurs, je tiens à remercier tout particulièrement ma sœur Audrey et mes parents, Sylvie et Jean, ainsi que mes amis proches Maxime, François et Jonathan qui se sont intéressés à mes projets, m’ont supporté tout au long mon cheminement et m’ont aussi fait décrocher lorsque nécessaire.

Finalement, les deux dernières personnes que je tiens à remercier, et non les moindres, ce sont les deux femmes de ma vie, c’est-à-dire ma fille de trois mois Maëva et ma fiancée Stéphanie. Je suis fortement convaincu que les réussites et accomplissements professionnels passent tout d’abord par l’épanouissement personnel. Je les remercie donc du plus profond de mon cœur de m’offrir un climat familial aussi exceptionnel.

AVANT-PROPOS

Les chapitres 1 et 2 servent à introduire les différents sujets qui seront abordés dans cette thèse. Trois articles scientifiques sont insérés aux chapitres 3, 4 et 5 et deux articles de conférences sont insérés aux Annexes A1 et A2. Biens que certaines méthodes et/ou conclusions soient propres aux articles présentés en annexe, la majorité des éléments techniques présentés dans ces conférences a été reprise dans les articles scientifiques, raison pour laquelle ces publications de conférence se retrouvent en annexe. Les différents articles scientifiques et de conférence insérés dans cette thèse, leur état de publication respectif, ainsi que mes contributions dans chaque publication sont présentés ci-dessous.

Chapitre 3 :

J.-M. Dussault, C. Kohler, H. Goudey, R. Hart, L. Gosselin, and S. E. Selkowitz, "Development and assessment of a low cost sensor for solar heat flux measurements in buildings," *Sol. Energy*, vol. 122, pp. 795–803, Dec. 2015 (publié).

Notes: Article rédigé par J-M Dussault (moi-même) et révisé par l'ensemble des coauteurs, mais plus particulièrement par L. Gosselin. J'ai développé le modèle numérique ainsi que la procédure de calibration. J'ai été assisté par C. Kohler, H. Goudey et R. Hart au niveau de la mise en place des montages expérimentaux. J'ai également dégagé les principales conclusions. L'ensemble de ce travail a été réalisé sous la supervision de S. E. Selkowitz et L. Gosselin.

Chapitre 4 :

J.-M. Dussault, M. Sourbron, and L. Gosselin, "Reduced energy consumption and enhanced comfort with smart windows: Comparison between quasi-optimal, predictive and rule-based control strategies," *Energy Build.*, vol. 127, pp. 680–691, Sep. 2016 (publié).

Notes: Article rédigé par J-M Dussault (moi-même) et révisé par M. Sourbron et L. Gosselin. J'ai développé les modèles de bâtiments dans TRNSYS et dans MATLAB et j'ai élaboré les différents modèles de contrôleurs. J'ai été assisté par M. Sourbron quant à l'implantation des modèles Matlab dans YALMIP/Gurobi. J'ai également dégagé les principales conclusions. L'ensemble de ce travail a été réalisé sous la supervision de L. Gosselin.

Chapitre 5 :

J.-M. Dussault, and L. Gosselin, "Office buildings with electrochromic windows: A sensitivity analysis of design parameters on energy performance, and thermal and visual" *Energy Build.*, Jan. 2017 (soumis).

Notes: Article rédigé par J-M Dussault (moi-même) et révisé par M. L. Gosselin. J'ai développé l'ensemble des modèles et méthodes d'analyse numériques. J'ai également dégagé les principales conclusions. L'ensemble de ce travail a été réalisé sous la supervision de L. Gosselin.

Annexe A1 :

J.-M. Dussault, M. Sourbron, and L. Gosselin, "Smart Windows Control Strategies for Building Energy Savings in Summer Conditions: A Comparison between Optimal and Model Predictive Controllers", ASHRAE Winter Conference, Orlando FL, 2016 (publié)

Notes: Article rédigé par J-M Dussault (moi-même) et révisé par M. Sourbron et L. Gosselin. J'ai développé les modèles de bâtiments dans TRNSYS et dans MATLAB et j'ai élaboré les différents modèles de contrôleurs. J'ai été assisté par M. Sourbron quant à l'implantation des modèles Matlab dans YALMIP/Gurobi pour le contrôleur MPC et pour la validation du modèle de bâtiment MATLAB. J'ai également dégagé les principales conclusions. L'ensemble de ce travail a été réalisé sous la supervision de L. Gosselin.

Annexe A2 :

J.-M. Dussault, and L. Gosselin, "Pre-design tools and procedures for efficient integration of smart windows", eSim Conference, Ottawa ON, 2014 (publié)

Notes: Article rédigé par J-M Dussault (moi-même) et révisé par L. Gosselin. J'ai développé les modèles de bâtiments dans TRNSYS et dans MATLAB et j'ai élaboré les différents modèles de contrôleurs. J'ai également dégagé les principales conclusions. L'ensemble de ce travail a été réalisé sous la supervision de L. Gosselin.

CHAPTER 1 INTRODUCTION

1.1 Mise en contexte

Dans le contexte environnemental actuel [1], la conception et les procédures d'opération des bâtiments sont de plus en plus orientées vers des concepts intégrés [2]. La conception intégrée dans le domaine des bâtiments suppose une étroite communication entre les différents intervenants de manière à, entre autres, harmoniser l'aspect esthétique, optimiser la communication entre les systèmes et favoriser le confort des occupants. Un bâtiment intelligent [3][4], dont la notion fait généralement référence à la capacité d'un bâtiment de remplir efficacement tous les objectifs de sa conception, est donc le résultat d'une conception intégrée réussi. De nos jours, le terme « intelligent » est très populaire en ce qui concerne les différents éléments des bâtiments. Parmi ces éléments, les termes qu'on retrouve fréquemment dans la littérature dans le domaine des bâtiments sont, entre autres, les réseaux intelligents [5][6][7][8], les enveloppes intelligentes [9][10], les fenêtres intelligentes [11][12][13][14][15][16] et, de façon plus générale, les matériaux intelligents [15][17]. La notion d'intelligence dans les bâtiments a donc fait l'objet de plusieurs recherches scientifiques au courant des dernières années/décennies et plusieurs nouvelles technologies ont, par le fait-même, vu le jour.

On compte plusieurs technologies récentes dont l'objectif principal est de réduire la consommation énergétique du bâtiment [18][19]. Entre autres, plusieurs nouvelles technologies sont apparues dans le domaine de l'enveloppe du bâtiment (enveloppes intelligentes). Bien que l'enveloppe des bâtiments ait longtemps été considérée comme étant un élément passif, l'avancement des connaissances dans ce domaine présente aujourd'hui un portrait différent [9][10], dû à la flexibilité et la capacité d'adaptation (aspect intelligent) que les technologies émergentes présentent [21][22][23][24][25].

Parmi ces technologies, les fenêtres intelligentes présentent un potentiel important quant à la réduction de la consommation d'énergie et des coûts qui y sont rattachés [26]. Il sera toutefois possible de tirer profit de ce potentiel uniquement lorsque des stratégies de contrôle efficaces en temps réel basées sur une compréhension approfondie des comportements en jeux seront développées et intégrées au système d'automatisation du bâtiment. En effet, la nouveauté des technologies de fenêtre intelligente présente une différence de maturité entre les technologies

elles-mêmes et l'existence de systèmes de contrôle/gestion et des connaissances quant à leurs différents comportements dans le but de minimiser la consommation énergétique globale tout en assurant un confort visuel et thermique pour les occupants.

La notion de fenêtre intelligente fait référence aux produits de vitrage appliqués à la fenestration des bâtiments dont les propriétés optiques sont modulables et auxquels un contrôle logique est appliqué. Ce contrôle permet de réduire la consommation d'énergie en chauffage/climatisation [27] ainsi que d'augmenter le confort visuel (minimiser l'éblouissement) [28]. Une fenêtre intelligente correspond typiquement à une fenêtre comportant une unité scellée dans laquelle on insère un filtre à opacité variable (propriétés optiques modulables). Typiquement, dans l'industrie de la fenestration, le filtre à opacité variable est installé sur la surface de verre #2 (voir Figure 1.1) afin de maximiser les performances énergétiques et augmenter le confort thermique.

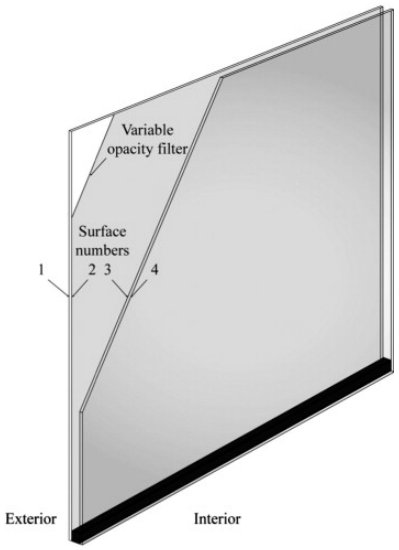

Figure 1.1 : Représentation d'une fenêtre intelligente typiquement utilisée dans les bâtiments

Certaines définitions considèrent que la notion de fenêtre intelligente fait référence aux technologies dont la modulation est due à l'application d'un courant électrique, alors que d'autres définitions sont plus générales et incluent aussi les autres stimuli tels que la luminosité, la chaleur, etc. Les types de fenêtres intelligentes incluent les vitrages de type :

1. Électrochromes [29] (Propriétés optiques modulées par une tension électrique via des réactions chimiques);

2. À cristaux liquides [30] (Propriétés optiques modulées par une tension électrique via l'orientation des cristaux liquides);
3. « SPD » [31] (Propriétés optiques modulées par une tension électrique);
4. Gasochromes [32] (Propriétés optiques modulées par le taux d'hydrogène);
5. Thermochromes [33]. (Propriétés optiques modulées par la température).

Les propriétés opto-thermiques contrôlées par les fenêtres intelligentes sont :

1. Le coefficient de gain thermique solaire (SHGC) : en modulant le flux solaire pénétrant dans le bâtiment, la fenêtre contrôle une partie des gains thermiques de celui-ci;
2. La transmission de la lumière visible : similairement, la quantité et la qualité de la lumière naturelle disponible sera affectée par le contrôle de la fenêtre.

Les avantages des fenêtres intelligentes, comparativement aux fenêtres passives, sont notamment [12]:

1. La réduction de la consommation d'énergie pour les charges de chauffage, de climatisation et d'éclairage;
2. L'amélioration du confort thermique et visuel des occupants;
3. La réduction des coûts initiaux de la mécanique du bâtiment (réduction des pics de consommation énergétique).

La technologie de fenêtre électrochrome présentant le plus grand potentiel quant à ses applications dans les bâtiments, les travaux réalisés dans le cadre de cette thèse se concentrent plus particulièrement sur cette technologie. La Figure 1.2 illustre un exemple de fenêtres électrochromes installées au Collège de Grove City en Pennsylvanie. Ces fenêtres sont contrôlées pour minimiser les gains solaires et offrir des espaces intérieurs confortables.

Figure 1.2 : Fenêtres électrochromes à l'état clair (à gauche) et dans un état coloré (à droite). Crédit: Sage Electrochromics

1.2 Revue de la littérature

Depuis la fin des années 1980, les chercheurs de la *Environmental Energy Division* du *Lawrence Berkeley National Labatory* (LBNL), aux États-Unis, ont mené des travaux importants au sujet des performances énergétiques des fenêtres intelligentes, et plus particulièrement des fenêtres électrochromes. Les premières recherches [34][35] réalisées par les chercheurs de LBNL ont porté sur l'évaluation des performances des fenêtres électrochromes et des facteurs d'importances tels les propriétés optiques, le confort thermique et visuel, les stratégies de contrôle, l'aspect esthétique et l'analyse économique associée aux surcoûts initiaux et aux économies récurrentes. Les conclusions, basées majoritairement sur des modélisations numériques de technologies idéalisées, ont démontré que les fenêtres intelligentes peuvent offrir des bénéfices en termes d'économies d'énergie et permettent d'éviter le sur dimensionnement initial des systèmes HVAC (*Heating, Ventilating and Air Conditioning*). Dans les mêmes années, ils ont aussi démontré que la stratégie de contrôle des fenêtres intelligentes basée sur la luminosité présente les meilleures performances globales [27].

Vers la fin des années 1990, l'avancement des technologies électrochromes permet aux chercheurs de LBNL de réaliser différentes analyses numériques de performances énergétiques basées sur les propriétés optiques mesurées des technologies disponibles sur le

marché [36]. Les résultats sont présentés pour différentes villes aux USA, soient Phoenix, Miami et Madisson. Les résultats pour des bâtiments commerciaux indiquent que les performances énergétiques globales sont améliorées lorsqu'un contrôle linéaire de l'état de transmission des fenêtres électrochromes est utilisé afin de fournir une luminosité minimale. Des résultats similaires sont aussi présentés pour des applications résidentielles [37] ou pour des bâtiments dominées par le chauffage [38]. Dans leurs conclusions, les auteurs mentionnent l'importance de pousser plus loin les recherches sur les stratégies de contrôle prenant en compte davantage de paramètres (radiation solaire incidente directe, radiation transmisse totale et directe, température de l'air ambient, etc). Les chercheurs de LBNL ont également mis en évidence que l'état de la fenêtre électrochrome offrant un confort visuel idéal peut potentiellement entrer en conflit avec l'état qui offre des performances énergétiques optimales [39]. Les résultats ont démontré que les fenêtres intelligentes avaient l'avantage de pouvoir offrir un confort visuel amélioré en raison de leur capacité d'adaptation de la transmission de la lumière visible et que les recherches futures devraient considérer le compromis entre confort et performances énergétiques.

Au cours des dernières années, les chercheurs de LBNL ont étudié des stratégies de contrôle plus évoluées [40] pour lesquelles l'optimisation énergétique est contrainte par l'aspect du confort visuel. Les résultats obtenus leur permettent de soumettre à la Commission de l'Énergie de la Californie une première méthode de design de bâtiments intégrant des fenêtres électrochromes [41]. Ce travail illustre bien le fait que les fenêtres électrochromes nécessitent la mise en place d'un système (capteurs, communication, etc) et que les coûts associés à ce genre de technologies sont encore très élevés. Enfin, une évaluation de l'influence du contrôle humain sur les performances énergétiques optimales (contrôle automatisé) a été menée en 2012. Les résultats démontrent qu'un contrôle automatisé adapté au confort thermique et visuel des occupants diminue grandement le risque que les occupants veuillent prendre le contrôle de l'opacité des fenêtres. Par rapport à un bâtiment de référence sans fenêtres intelligentes, ces résultats présentent des économies d'énergie potentielles de l'ordre de 50% et une diminution de la pointe de consommation de l'ordre de 35%.

De façon générale, dans l'ensemble de leurs recherches, les chercheurs de LBNL rappellent qu'encore aujourd'hui, les stratégies avancées de contrôle prédictif offriraient des avantages potentiels considérables, mais présentent des difficultés quant à leur développement en raison des effets transitoires dus aux changements non anticipés des demandes énergétiques, les variations climatiques et les taux d'occupation/inoccupation, du déphasage temporel des charges radiatives associées à la masse thermique du bâtiment ainsi que des paramètres du système HVAC tels que les performances ou les délais temporels associés au système de distribution d'air. Ces propos illustrent bien l'importance de la poursuite de la recherche de ce domaine.

Par ailleurs, plusieurs autres groupes ont mené des recherches parallèlement à LBNL. Parmi les résultats les plus pertinents, on retrouve, chronologiquement, les résultats présentés dans les paragraphes qui suivent.

En 1993, Kim et Jones [42] soulignent les avantages de l'intégration de systèmes informatiques de gestion de l'énergie des bâtiments. Parmi ces avantages, on compte, 1- La possibilité d'incorporer des fonctions avancées telles que les fonctions proportionnelles, intégrales ou dérivatives, 2- la possibilité de considérer plusieurs signaux d'entrée, 3- la possibilité d'archiver, récupérer et analyser l'information et, 4- la possibilité d'appliquer une logique booléenne aux algorithmes de contrôle. Dans leur article, Kim et Jones présentent une logique de contrôle basée sur le confort visuel, l'éclairage naturel et les besoins du système HVAC. Les notions de contrôle prédictif sont brièvement discutées en ce qui concerne l'éclairage naturel. Bien que la logique proposée soit très pertinente, cette dernière ne considère pas l'effet du déphasage temporel de la charge radiative absorbée par la masse thermique du bâtiment et les impacts qui y sont associés à l'égard de la réduction optimale de la consommation énergétique.

En 2000 [43] et 2001 [44], Karlsson et ses collègues présentent des résultats de performance énergétique similaires à ceux de LBNL [36]. Une stratégie de contrôle des fenêtres intelligentes basée sur le taux d'occupation et faisant intervenir la récupération de chaleur, un système HVAC contrôlable et des sondes de température, éclairage et d'occupation est

proposé. Cette stratégie est d'ailleurs déposée sous la forme d'un brevet au cours de 2001 [45].

En 2002, Davies [46] présente une stratégie de contrôle de fenêtres intelligentes dont l'aspect novateur provient d'une stratégie combinée faisant intervenir la variation d'opacité de la technologie de fenêtre intelligente sous la forme de sous-éléments contrôlables et l'intervention de systèmes d'ombrage passifs. Dans ses conclusions, Davies mentionne qu'il y a encore de la recherche à faire pour développer des algorithmes de contrôle plus intelligents qui devront prendre en considération, entre autres, les critères d'acceptabilité des occupants, l'environnement du bâtiment et la complexité du contrôle associée au délais de transition plutôt longs qu'offre les fenêtres électrochromes.

Au courant de la même année, Lee et DiBartolomeo [47] présentent les défis et/ou problématiques associés à l'intégration des fenêtres électrochromes aux bâtiments. Parmi ces considérations, les auteurs soulignent le fait que 1- Le contrôle de la transmission de la lumière naturelle via les fenêtres électrochromes n'assure pas le confort visuel des occupants, 2 – Il existe une adéquation entre la nécessité d'avoir une réponse rapide de la technologie pour assurer le confort et les temps de réponse qu'offrent les technologies existantes, 3- La durabilité des technologies en fonction du climat et du nombre de cycle est à évaluer de façon indépendante et, 4- Les technologies existantes ne respectent pas nécessairement la neutralité du spectre solaire, ce qui peut engendrer des inconforts visuels ou physiologiques [48].

En 2003, Gugliermetti and Bisegna [49] développent une approche de contrôle qui intègre la confort visuel et l'efficacité énergétique. Les résultats obtenus montrent que le fait de contrôler dans le but d'offrir un confort visuel ne détériore pas considérablement les performances par rapport à un contrôle uniquement axé sur les performances énergétiques. Les auteurs mentionnent aussi le fait qu'un contrôle progressif des fenêtres électrochromes et des systèmes d'éclairage présente des avantages énergétiques par rapport aux stratégies de contrôle à deux états (c'est-à-dire : « on/off »).

En 2004, Assimakopoulos et al. [50] présentent une stratégie de contrôle avancée basée sur les principes d'un « adaptive neuro-fuzzy inference system » (ANFIS). Ce type de système fait intervenir un système de contrôle utilisant une logique floue combiné à un mécanisme d'autorégulation basé sur les données/résultats antérieurs. En bref, c'est une stratégie permettant au système de logique floue d'apprendre dans le but d'optimiser le contrôle. En 2007, la suite de leurs travaux [51] leur a permis de comparer 10 différents types de stratégies de contrôle, la stratégie de contrôle la plus évoluée étant celle présentée dans leur article en 2004. Les résultats de ces avancements ont montré que la stratégie de contrôle la plus efficace était la stratégie à deux états basée sur une luminosité minimale à obtenir à l'intérieur. Leur stratégie neuro-floue (la plus évoluée), bien que très performante aussi, ne s'est pas imposée comme étant la plus performante dû au fait que l'intervalle de variation potentielle des valeurs de SHGC entre les états extrêmes des fenêtres électrochromes existantes à l'époque n'était pas suffisant pour profiter du plein potentiel de la stratégie de contrôle. Une analyse similaire sur les nouvelles technologies de fenêtres intelligentes existantes en 2013 telles que celles offertes commercialement [12] pourrait potentiellement permettre de mettre de l'avant la technologie neuro-floue présentée. Toutefois, certaines recherches expliquent que les algorithmes neuro-flouent présentent généralement des incertitudes relativement grandes et donc, la combinaison de ce genre d'algorithme à une stratégie basée sur un système expert pourrait potentiellement offrir des résultats encore plus intéressants [10].

En 2005, Gugliermetti et Bisegna [52] comparent les résultats de différentes stratégies de contrôle (à deux états et variations linéaires des états) sur des fenêtres électrochromes et des systèmes de stores automatisés basées sur la luminosité intérieure. Les résultats présentés démontrent que la meilleure combinaison technologie/stratégie de contrôle dépend grandement du climat, de la latitude et de l'orientation de la façade considérée.

En 2006, Galasiu et Veitch présentent une revue de la littérature de l'aspect du confort visuel par rapport à l'éclairage naturel. En bref, les résultats pertinents sont que les occupants préfèrent généralement travailler dans un climat offrant un apport en lumière naturelle plutôt que de la lumière artificielle. Par ailleurs, il semble que les contrôles automatiques de l'apport en lumière naturelle ne soient généralement pas bien acceptés/utilisés par les occupants. Les

auteurs mentionnent l'importance de prendre en considération l'acceptabilité des occupants envers les stratégies de contrôle qui seront développées dans le futur. Dans la même année, Clear et ses collègues [53] présentent les résultats d'une étude d'acceptabilité des fenêtres électrochromes faite sur plus d'une quarantaine de sujets dans des conditions de travail de bureau. Les résultats sont que les fenêtres éléctrochromiques améliorent le confort visuel, mais que davantage de recherches sur les algorithmes de contrôle doivent être réalisées dans le but de satisfaire les occupants des bâtiments tout en minimisant la consommation énergétique puisqu'autrement, les occupants auront tendance à prendre manuellement le contrôle des fenêtres, réduisant ainsi les économies potentielles.

En 2009, Piccolo et Simone [28] présentent une étude sur le confort visuel que peuvent procurer les fenêtres électrochromes en basant les stratégies de contrôle sur des indices d'éblouissement. Les conclusions sont qu'il est possible d'offrir un confort visuel tout en optimisant la consommation énergétique pour des fenêtres orientées vers le sud. Pour une orientation des fenêtres à l'ouest, dû à l'inclinaison du soleil en période de rayonnement direct, le confort visuel n'est atteignable qu'en ajustant les fenêtres à un très faible taux de transmission, impliquant donc la nécessité d'utiliser beaucoup d'éclairage artificiel et donc de consommer davantage d'énergie.

En 2010, Jonsson et Roos [54] utilisent des outils de simulations numériques pour évaluer le potentiel de quatre différentes stratégies de contrôle, soient 1) Une stratégie qui vise à optimiser les charges de chauffage et climatisation, 2) Une stratégie qui considère une occupation complète de jour, 3) Une stratégie qui considère le taux d'occupation et 4) Une stratégie qui limite le rayonnement horizontal afin d'éviter les situations d'éblouissement. Ces stratégies sont évaluées pour différentes façades, avec plusieurs compositions d'unités scellées et à différentes localisation géographiques. Tout comme Gugliermetti et Bisegna en 2005, la conclusion des auteurs est que les stratégies et compositions optimales diffèrent grandement selon l'orientation et la localisation géographique. En guise d'ouverture, les auteurs mentionnent que le développement de modèles simplifiés serait un outil extrêmement utile pour les architectes et designers de bâtiment afin de sélectionner les meilleurs produits et stratégies.

La littérature permet de réaliser qu'il reste encore place à des travaux de recherche qui permettraient de comprendre de quelle façon et sous quelles conditions le contrôle de ces nouvelles technologies de l'enveloppe permettrait d'offrir des performances optimales. La dynamique des transferts de chaleur et de la consommation énergétique dans les bâtiments est très complexe de par la grande quantité de facteurs qui l'influencent comme, par exemple, les conditions climatiques, les propriétés des matériaux, les systèmes mécaniques, la quantité et le type d'éclairage artificiel, les gains internes et les types et horaires d'occupation. Ces facteurs sont interdépendants, et donc, il est nécessaire de les considérer simultanément dans le développement des stratégies de contrôle optimales de fenêtres intelligentes. Par ailleurs, il est évident que ces facteurs peuvent grandement différer en fonction de la localisation géographique, de la vocation et des normes de construction en vigueur. La solution optimale de contrôle des technologies de fenêtres intelligentes n'est donc pas unique, mais doit plutôt prendre en considération le contexte dans lequel le bâtiment est construit. À cet égard, peu de résultats de recherches sur l'optimisation permettent aux concepteurs de bâtiments de s'orienter dans le développement de séquences de contrôle adaptées.

Certains travaux d'optimisation avec logiciels de simulation ont déjà été menés afin d'évaluer les performances optimales que les fenêtres intelligentes pourraient avoir dans des conditions données [26][27]. Ces simulations utilisent des données climatiques horaires connues pour toute l'année, et donc, les résultats obtenus présentent la limite théorique en termes de performances énergétiques atteignables. En situation réelle de contrôle des bâtiments, les conditions climatiques des heures à venir ne sont pas connues, ce qui entraine une incertitude dans la décision de contrôle optimale à prendre, d'où la pertinence d'approfondir les recherches dans ce secteur.

L'intégration de systèmes de fenêtres intelligentes dans les bâtiments présente encore bien des défis et offre, par le fait-même, des opportunités afin d'approfondir la recherche dans le domaine. Par exemple, plusieurs travaux ont portés sur l'amélioration des technologies de fenêtres électrochomes elles-mêmes, mais peu de travaux ont été réalisés afin de développer des outils de mesure (tels que des capteurs de rayonnement solaire) adaptés aux besoins de

ce genre de technologies et qui permettraient de réduire les coûts globaux liés à l'intégration de ce genre de systèmes. Par ailleurs, les connaissances sont encore limitées quant à la performance potentielle des différentes stratégies de contrôle plus évoluées (et à la fois plus complexes). Enfin, pour faciliter l'intégration de ce genre de technologie à plus grande échelle, il serait intéressant de généraliser les conclusions des recherches précédentes en considérant simultanément une plus grande quantité de variables de design tout en utilisant les propriétés des fenêtres intelligentes les plus à jour.

1.3 Objectifs

L'objectif général de cette thèse est d'élargir les connaissances scientifiques sur le potentiel des technologies de fenêtres électrochromes quant à leur capacité à augmenter la performance énergétique et le confort des occupants (visuel et thermique) dans les bâtiments. Pour ce faire, le projet a été élaboré autour des trois axes de recherche suivants :

1. Développement d'un capteur de rayonnement solaire intégré à faible coût intégré au système de fenestration et permettant de contrôler efficacement les diverses technologies de fenêtres intelligentes;
2. Étude comparative de la performance de différents types de contrôle (optimaux et heuristiques) des fenêtres intelligentes quant à la consommation énergétique et au confort visuel et thermique;
3. Étude de la sensibilité des paramètres de design des bâtiments avec fenêtres intelligentes.

Le développement d'un design de capteur de rayonnement solaire est associé au contenu présenté au Chapitre 3. Le contrôle des fenêtres intelligentes ayant principalement un impact sur le rayonnement solaire, la mesure du rayonnement solaire s'avère une information particulièrement utile en termes de contrôle. Les objectifs spécifiques pour cet axe sont les suivants :

1.i Développer une corrélation entre la différence de température de surfaces (blanches et noires) et le rayonnement solaire incident à l'aide d'un modèle thermique en 1D;

1.ii Concevoir différents designs de capteur de rayonnement solaire thermique intégrés au vitrage;

1.iii Élaborer une procédure d'étalonnage expérimentale des capteurs de rayonnement solaire à l'aide du modèle thermique;

1.iv Évaluer la précision des designs de capteur de rayonnement solaire ainsi que la sensibilité du processus de calibration.

Le deuxième axe de recherche concernant l'étude comparative entre les contrôles optimaux et heuristiques est couverte au Chapitre 4 de cette thèse ainsi qu'à l'Annexe A1. Les objectifs spécifiques associés à cet axe sont les suivants :

2.i Développer un modèle de bâtiment représentatif d'un espace bureau périphérique (modèle thermique dans TRNSYS et modèle visuel dans Daysim/Radiance);

2.ii Développer un type de contrôle pour fenêtres intelligentes avec modèle prédictif dans Matlab;

2.iii Définir des stratégies de références (contrôle de base dans TRNSYS et contrôle optimal par algorithmes génétiques dans MATLAB) pour des fins de comparaison avec le contrôle prédictif;

2.iv Évaluer la viabilité des stratégies de contrôle à l'étude pour des applications en temps réel;

2.v Évaluer l'amélioration potentielle des performances des stratégies de contrôle par rapport aux références de l'industrie;

Enfin, le troisième axe de recherche portant sur la sensibilité des paramètres de design des bâtiments avec fenêtres intelligentes est couvert au Chapitre 5 de cette thèse ainsi qu'à l'Annexe A2. Les objectifs spécifiques pour cet axe sont les suivants :

3.i Accroître la compréhension de l'influence simultanée de différents paramètres de design (paramètres de construction, occupation, charges internes, contrôle et/ou climat) sur les performances énergétiques et le confort des occupants;

3.ii Développer des procédures simples permettant d'évaluer le potentiel des fenêtres intelligentes;

3.iii Faire ressortir les tendances de designs favorisant l’intégration de fenêtres intelligentes dans les bâtiments;

CHAPTER 2 METHODOLOGY

This chapter introduces the different concepts and engineering tools used in the following chapters. Section 2.1 presents the building model and software used in the building simulations of Chapters 4 and 5. Section 2.2 introduces the basic concept of Model Predictive Control (MPC) and details the building model implemented in the MPC controller of Chapter 4. Finally, Section 2.3 details the different engineering tools used for optimal smart window control in Chapter 4.

2.1 Building model and software

To assess the performance of smart windows on energy and comfort, a representative office building zone was defined and used in the building simulations of Chapters 4 and 5. While some values of the design parameters under study varied between Chapters 4 and 5, the building model (presented in Figure 2.1) remained the same. The building model is defined by a box-shaped office zone with 100 m^2 of floor area. The main building design parameters were related to the location, the orientation, the Window-to-Wall ratio (WWR), the thermal mass, the internal gains and the smart window state.

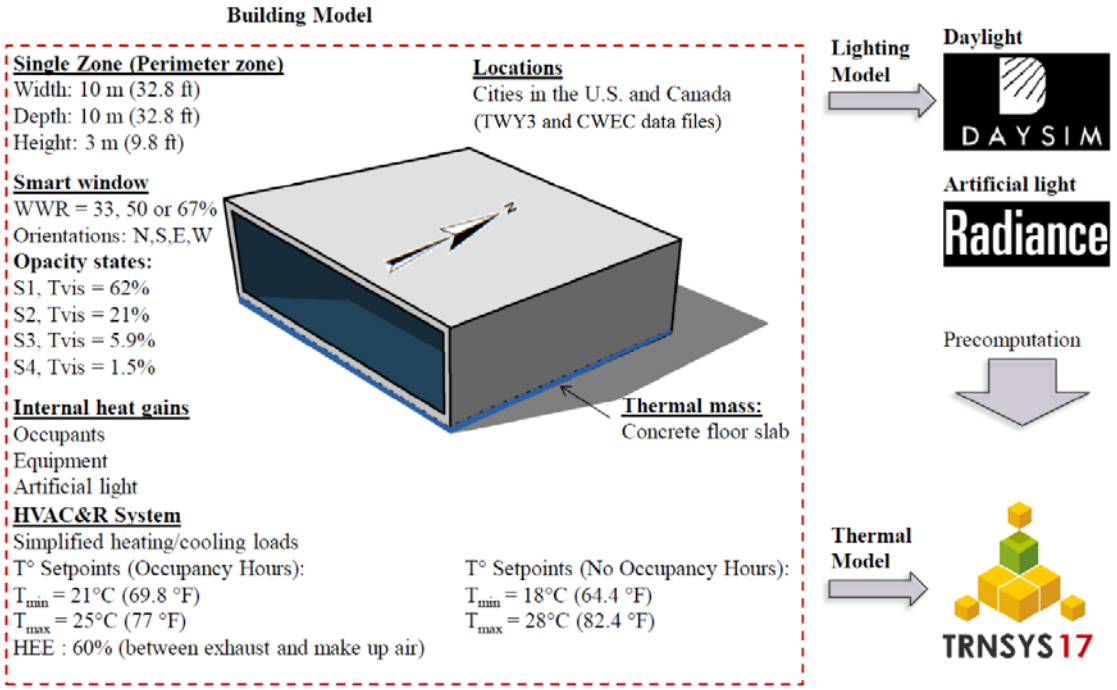

Figure 2.1: Building model description and software.

As illustrated in Figure 2.1 the thermal considerations were implemented in TRNSYS (with the Type 56). While many other powerful building simulation tools such as ESP-r, Energy Plus or DOE-2 are also based on largely validated concepts and are readily available [55], this work relies on TRNSYS since this software has a modular structure, can easily communicate with Matlab (through Type 155) and presents a great flexibility to develop complex systems such as smart window control systems. The daylight and artificial light considerations were pre-calculated in Daysim and Radiance, respectively, and then implemented in TRNSYS as user inputs.

Since this work focused on the performance of smart windows, a particular attention was devoted to the smart window modeling. Hence, the Window software (developed by the Windows and Daylighting group at Lawrence Berkeley National Laboratory) was used to model four different states of opacity of a recent electrochromic window technology from Sage Electrochromics inc. For consistency, the glazing properties were obtained with the version 6.3.74 of Window (which was the most recent version at the time this work was initiated) and were used for every simulation of this work. The optical properties of the different electrochromic states were all imported in Window using the International Glazing Database (IGDB). The IGDB IDs for the four states of interest in this work were 8902 to 8905. The glazing properties obtained in Window software for the electrochromic glazing were imported in the TRNSYS Type 56 (WinID pool). The appropriate glazing properties were then selected in TRNSYS at every time step (1 hour time step) based on the smart window control strategy.

Different heuristic (rule based control (RBC)) and optimal (based on genetic algorithm (GA) or model predictive control (MPC)) control strategies were studied for the control of the electrochromic window. While all the RBCs were directly implemented in TRNSYS, the GA and MPC controllers were complex algorithms developed in Matlab and were communicating with TRNSYS for control decisions.

2.2 Model Predictive Control (MPC)

The MPC relies on the principle of receding horizon and involves an objective function to be minimized (or maximized) [56]. In MPC, the optimal control is obtained by the minimization of some performance criterion (based on predictions) over a fixed finite horizon, i.e. a prediction horizon Hp. The predictions over that fixed finite horizon are obtained with the help of an internal model of the system to be represented. The internal model is generally a representation of the reality based on a simplified model.

In this work, a smart window controller based on MPC was developed. The system to be represented by the controller internal model is the building model. The following sections detail the internal building model (developed in Matlab) implemented within the controller as well as the verification performed to assess its accuracy (comparison of behaviors with the real building, i.e. TRNSYS model). For clarity, one should note that the building model developed in Matlab refers to the controller model (simplified model) and the TRNSYS model refers to the real system to be controlled.

2.2.1 MPC internal building model description

The internal building model implemented in the MPC consists of a simplified resistance-capacitance thermal model of the TRNSYS building zone (Figure 2.2). In order to be applied in a real-time application, the controller model needs to run fast so that optimization of the control is possible based on the predictions of this model.

Given the goal of the work presented in Chapter 4, the smart window is modelled in detail with 2 glass panes each having their own solar absorption and transmission properties based on data obtained from IGDB. Since the building zone's thermal inertia is concentrated in the concrete floor, the interior surrounding surfaces are lumped together with the air node (T_{in}/T_{walls}) in the controller model. As assumed in the TRNSYS building model (simple mode), this model supposes that, while the floor receives all the direct (geosurf = 1) and part of the diffuse solar radiation, all other interior surfaces only receiving diffuse solar radiation based on absorption-transmission weighted area ratios. Convection between the interior surfaces and the zone air was considered, while long wave radiation exchange between the different surfaces completes the energy balance in the building zone.

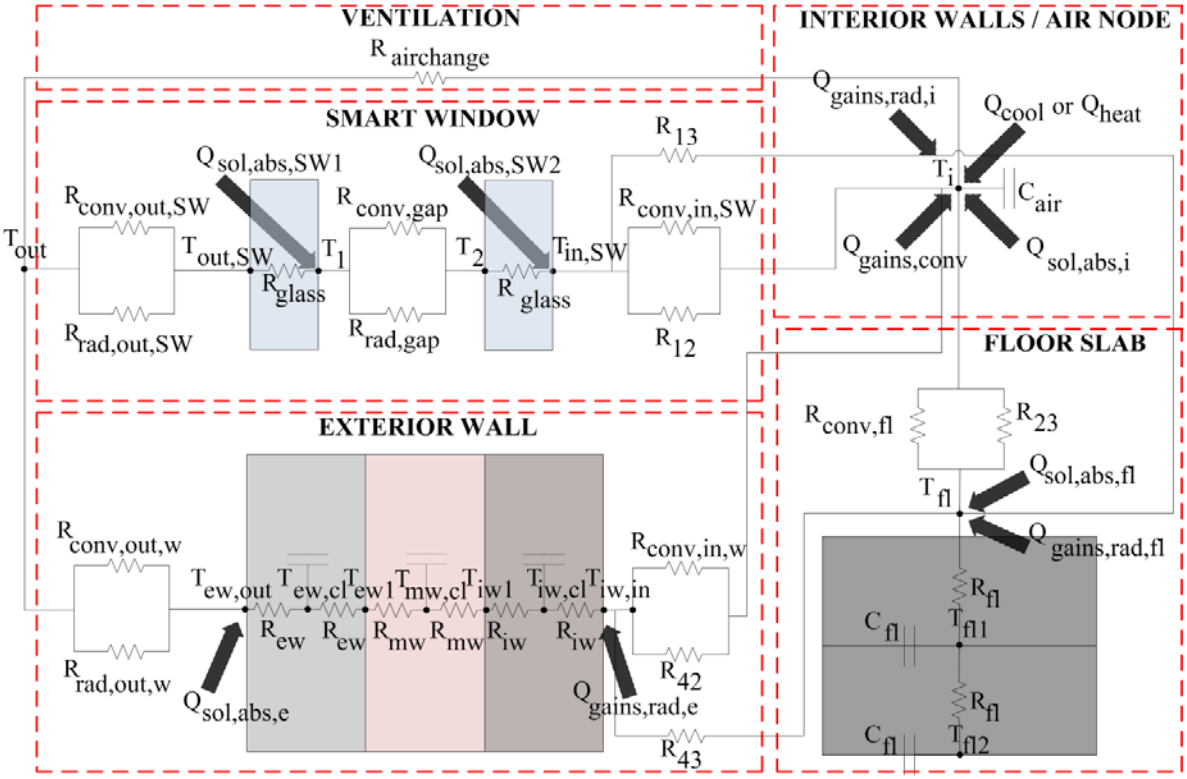

Figure 2.2: Controller building model for the MPC.

The convective portion of occupant and appliance heat gains ($Q_{gains,conv}$) is directly applied to the zone air node, while the radiative portion ($Q_{gains,radi}$, $Q_{gains,rade}$ and $Q_{gains,,radf}$) is distributed over the zone interior surfaces according to their respective weighted ratio of their area to the total interior surfaces area.

The number of capacitances n_{fl} for the thermal mass of the zone floor is determined from [57]:

$$n_{fl}^2 \geq \frac{4RC}{\pi \Delta t} \tag{2.1}$$

which results in two capacitances in the present case to accurately represent the 0.1016 m concrete slab of the building zone. Representing the floor with one capacitance was insufficient to accurately describe the transient heat storage in the floor, while more than two capacitances did not result in significant improvement to the model predictions, while increasing the time required for optimization.

The energy balance for each node of the controller model results in a discrete state-space model of the building zone with 15 nodes and 6 capacitances, and thus, a set of equations of the form:

$$C_i \frac{\left(x_i\left(t+\Delta t\right)-x_i\left(t\right)\right)}{\Delta t} = \frac{1}{R_{ij}}\left(x_i\left(t+\Delta t\right)-x_j\left(t+\Delta t\right)\right)+f(U_c\left(t+\Delta t\right)) \quad (2.2)$$

which could be rewritten as

$$AX\left(t+\Delta t\right)- B = 0 \quad (2.3)$$

with:

$$X=\left[T_{ew,out};T_{ew,c};T_{ew1};T_{mw,c};T_{iw1};T_{iw,c};T_{iw,in};T_{out,SW};T_1;T_2;T_{in,SW};T_i;T_{fl};T_{fl1};T_{fl2}\right] \quad (2.4)$$

$$U_c=\left[Q_{heat};Q_{cool};Q_{light};SW_{state}\right] \text{ the control inputs and} \quad (2.5)$$

$$A = \frac{C}{\Delta t}- \frac{1}{R} \quad (2.6)$$

$$B = \frac{C}{\Delta t}x\left(t\right)+f(U_c\left(t+\Delta t\right)) \quad (2.7)$$

with $f(U_c)$ being a function containing the control inputs as well as the different disturbance inputs (T_{out}; $Q_{sol,direct}$; $Q_{sol,diff}$).

2.2.2 MPC building controller model verification

The controller model of the zone (Section 2.1) was validated against the results of the TRNSYS simulation model using a 2-step approach: steady-state and dynamic validations. The focus of this comparison was to evaluate the ability of the simplified thermal model to correctly represent the heat flows to keep the zone temperature at a required set point.

First the steady-state output of the controller model was compared with the corresponding measurement signal from the TRNSYS building. Three cases with different boundary

conditions for T_{out} and Q_{sol} are simulated in this first validation step, as shown in Table 2.1. The chosen outdoor temperatures, exterior convection coefficients and solar fluxes are aligned with the NFRC design conditions for winter and summer. Interior convection coefficients were fixed to 5 W/m^2K. The ventilation is activated at design conditions and all internal heat gains from lighting, people and appliances are set to zero. The window is kept at its clearest state.

Table 2.1: Steady-state validation results (W/m^2 floor area)

Design condition	Q_{heat} [W/m^2]		Q_{cool} [W/m^2]	
	TRNSYS	**Controller model**	**TRNSYS**	**Controller model**
Winter	33.0	33.0	0	0
Summer	0	0	7.8	8.1
Summer with Qsol	0	0	83.0	82.4

The validation results in Table 2.1 show that the model within the controller was able to accurately reproduce the required heating and cooling loads. In summer conditions, without and with solar radiation, the controller model showed a small error for the cooling load of, respectively, +3.8% and –0.7%, which is considered acceptable. This error mainly comes from the simplifications of the controller window model and the linearization of the building model.

In the second validation phase the controller model was simulated offline using measured TRNSYS values as input values for the observer (Figure 2.3). This validation approach was used since the controller model is always applied in a closed loop situation, with measurement feedback from the building. The TRNSYS model was simulated for a whole year with the window kept at its clearest state. The heating and cooling loads were controlled to keep the zone temperature T_i between 20°C and 23°C at all time, with the heating and cooling system having perfectly modulating and unlimited thermal power, so the temperature set point is always met. This eliminates all degrees of freedom and constraints of the MPC optimizer, reducing it to a perfect set point tracker. At each time step, the building controller

model is updated with the measured TRNSYS values, the observer (Figure 2.3) is used to estimate the unmeasured temperatures ($T_{ew,cl}$, T_{ewl}, $T_{mw,cl}$, T_{iwl}, $T_{iw,cl}$, T_1, T_2, T_{fl1}, T_{fl2}) of the controller model. The MPC calculates $Q_{k+p|k}$ (forecasted heating and/or cooling energy demands (at times k + p, for p = 1 to Hp), measured at time k), where $Q_{k+1|k}$ is registered and the process moves to the next time step. The registered $Q_{k+1|k}$-vector (k = 0…8759) is compared to the system heating and cooling load measured by the TRNSYS model, using the Nash-Sutcliff model efficiency coefficient (NS) to estimate the fit:

$$NS=1-\frac{\sum_{i=1}^{n}\left(Q_{TRNSYS,n}-Q_{MPC,n}\right)^2}{\sum_{i=1}^{n}\left(Q_{TRNSYS,n}-\overline{Q_{TRNSYS,n}}\right)^2} \tag{2.8}$$

A NS-coefficient value of 1 means that the model is able to reproduce the measured output exactly. On the other hand, a value of 0 means that the controller model can only predict the heat flows as accurately as the average of the measured values.

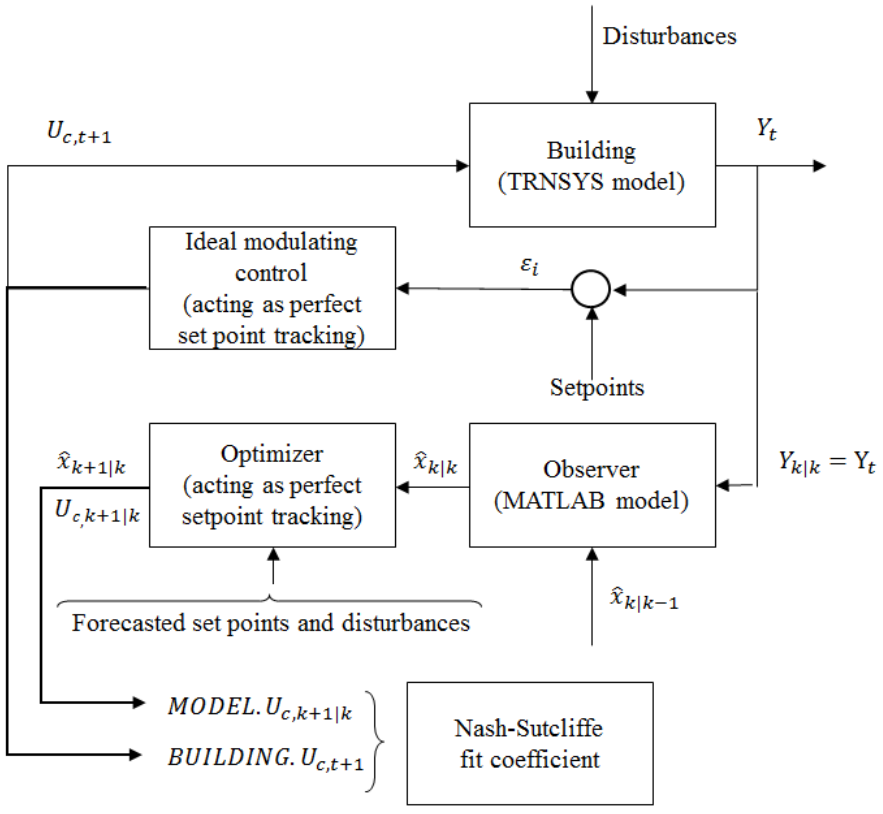

Figure 2.3: Dynamic validation scheme.

Figure 2.4 presents the monthly heating and cooling energy for both models and demonstrates that the heating load is overestimated by 2 % by the controller model (5.2 kWh/m^2 with the Matlab model compared to 5.1 kWh/m^2 with the TRNSYS model), while the annual cooling load is overestimated by 3 % by the controller model (65.1 kWh/m^2 with the Matlab model compared to 63.3 kWh/m^2 with the TRNSYS model). Moreover, the NS-coefficients are 0.980 and 0.994 for respectively Q_{heat} and Q_{cool}, which means that the controller model is able to predict the dynamic behavior of the building with a high accuracy.

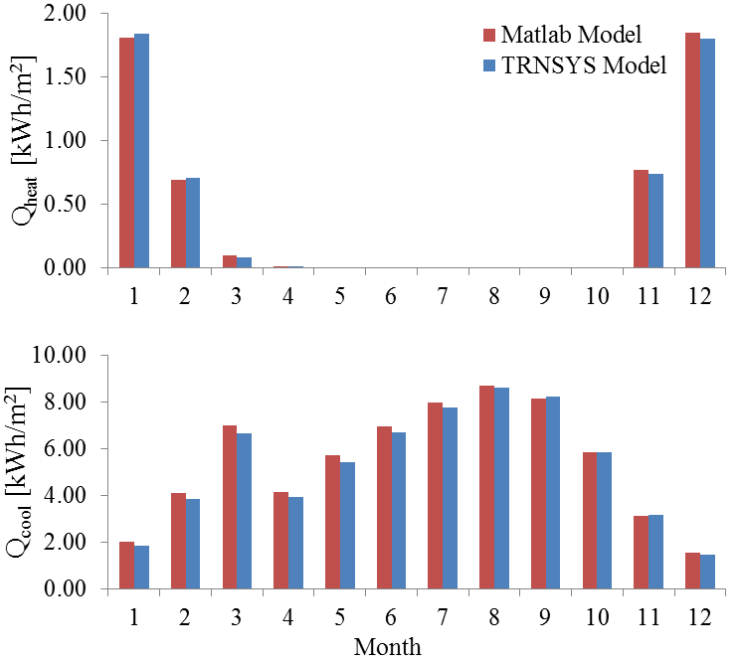

Figure 2.4: Validation result for Q_{heat} and Q_{cool}.

Both validation steps showed that the simplified building model was sufficiently accurate in order to serve as a controller model for the building zone. However, further studies should be dedicated to the assessment of the accuracy of the controller model for a longer horizon.

2.3 Optimization tools

This section introduces the two main optimization tools (i.e. Genetic algorithms and YALMIP/Gurobi) used in this work to obtain optimal control decisions for SW. Both tools aimed at minimizing the energy consumption of the building zone considering the same objective function (total energy consumption) and constraints (minimal light requirements

on the workplane during occupancy hours). The adaptation of these tools for the purpose of this work is presented in the following subsections.

2.3.1 Genetic algorithms

Genetic algorithms (GAs) are well known optimization algorithms that have gained a lot of interest in the field of heat transfer problems in the last decades [58]. As illustrated in Figure 2.5, an initial random population of individuals is first generated. A set of design variables (i.e., the SW state at each time step) represents an individual. Then, the objective function of each individual is evaluated based on the simulation results. Cross-over between individuals occurs with more probability of reproduction for best individuals. Mutations are then applied randomly to the offspring. A new generation is created from the offspring and from the few best individuals of the previous population (which is called an elitist strategy). The process is repeated until convergence of the criterion (i.e. maximal number of generations and/or maximal number of generations without improvements).

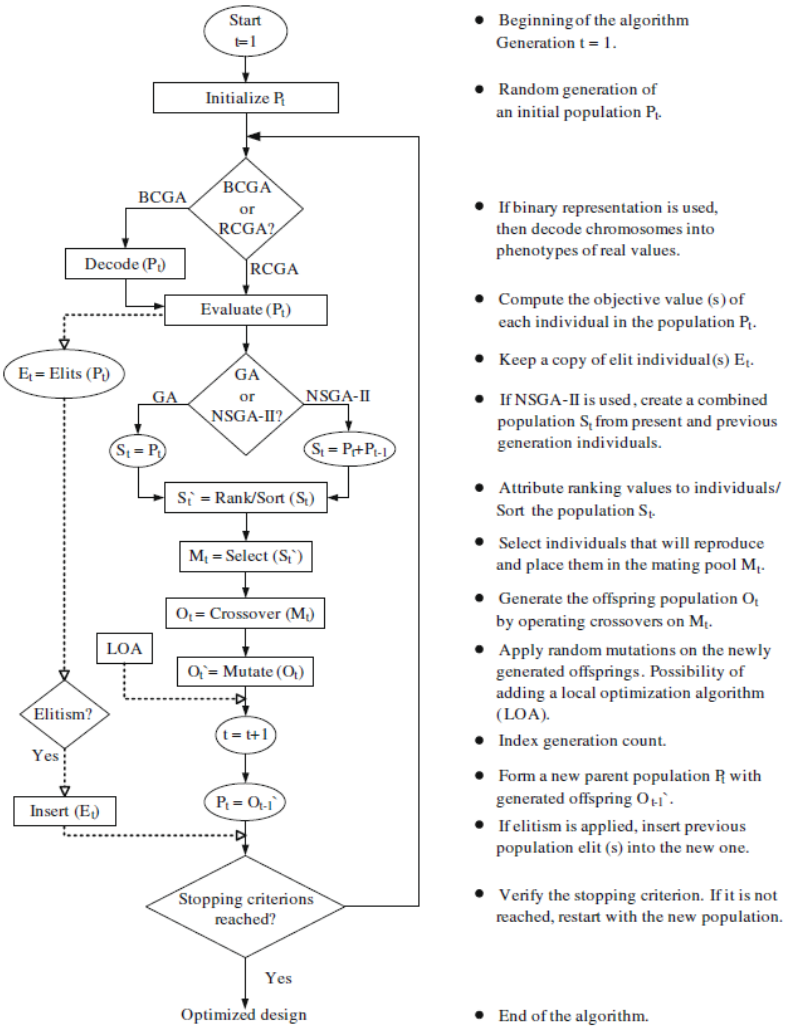

Figure 2.5: The main steps of a typical GA obtained from [58].

The use of GAs in this thesis was mainly driven by the fact that GAs are global optimization solvers (they cover the entire design space) that readily manage discrete design variables (such as SW states). However, one should note that GAs typically involve a large number of simulations that are quite computationally expensive. In the field of building simulation, too long computational times limit the use of GAs for real time applications (such as SW control). For this reason, the reader should keep in mind that the use of GAs in this work serves to establish the optimal achievable level of performance against which real-time strategies could be compared. To achieve such optimal control for SW, a controller based on GAs assuming a perfect building model representation and perfect weather forecast (i.e. one perfectly knows the future weather parameters) was considered.

2.3.2 YALMIP/Gurobi

While the previous section on GAs was used in this work to represent the best case scenario for SW control (hardly applicable for real time control), a second optimization approach was also used to assess the potential of a real-time optimal SW controller (the MPC controller detailed in Chapter 4). This second approach combines the use of the YALMIP [59] optimization toolbox and Gurobi optimizer. These tools take advantage of the linear programming to provide short computational times (required for real-time control). YALMIP is a readily available toolbox designed to develop control oriented semidefinite programming (SDP) models for convex optimization (linear optimization). The Matlab building model described in the previous section (illustrated in Figure 2.2), was linearized and defined with YALMIP for optimization of the SW control. The optimization solver called by YALMIP is Gurobi, a widely used state-of-the-art optimization tool for mathematical programming that contains a YALMIP compatible linear programming solver. Both YALMIP and Gurobi present a modeling language fully compatible with Matlab (matrix-oriented interfaces for Matlab).

CHAPTER 3 DEVELOPMENT AND ASSESSMENT OF A LOW COST SENSOR FOR SOLAR HEAT FLUX MEASUREMENTS IN BUILDINGS

Abstract

This paper presents a new type of low cost solar sensor, i.e. a black and white sensor (BWS). The BWS uses the difference in temperature of a white surface (solar energy highly reflected) and a black surface (solar energy highly absorbed) to estimate the solar heat flux through building openings. Results are obtained through a correlation based on a thermal model of the sensor. The correlation contains calibration factors determined from an initial on-site calibration. Results of estimated solar heat flux with two designs of the BWS over two different periods of time were compared with solar measurements of a high precision pyranometer. The two designs of BWS have shown mean weighted relative errors over the sampling periods under 4% for the daily integrated solar energy measured. Finally, a sensitivity analysis of the calibration period was conducted and it was observed that ideal calibration period should consider at least half a day of measurements, including solar peak time, and should be done during clear sky conditions.

Résumé

Cet article présente un nouveau type de capteur de rayonnement solaire à faible coût, c.-à-d. un capteur à surfaces noires et blanches (BWS). Le BWS utilise la différence de température entre la surface blanche (réflexion élevée de l'énergie solaire) et la surface noire (absorption élevée de l'énergie solaire) pour estimer le flux solaire radiatif traversant les ouvertures d'un bâtiment. Les résultats sont obtenus avec une corrélation basée sur un modèle thermique du capteur. La corrélation comprend des facteurs d'étalonnage obtenus via un étalonnage initial effectué sur place. Les flux solaires obtenus à l'aide de deux modèles de BWS sur des périodes de temps différentes sont comparés aux mesures solaires de référence obtenus par un pyranomètre. Les modèles de BWS ont tous deux présenté une erreur relative moyennée en dessous de 4% pour la mesure de l'énergie solaire quotidienne. Finalement, une analyse de la sensibilité de la période de calibration est réalisée et il est observé que la période idéale requiert minimalement une demi-journée de mesures sous des conditions de ciel clair (incluant la période de rayonnement solaire maximale).

3.1 Introduction

With the considerable amount of available technologies in the field of active building envelopes [60][61][62] and the continuously increasing interest of owners to enhance the energy efficiency of their buildings, a lot of opportunities emerge to develop efficient sensors and control algorithms. Among others, windows with efficiently controlled dynamic glazing offer a high potential to control solar heat gain and minimize heating, cooling and lighting loads [26][40]. To control such technologies efficiently, accurate values of solar heat gains entering the building should be measured. Since the need for these solar sensors will increase with the degree of control and intelligence in smart buildings [4], the trade-off between their cost and their accuracy will become even more relevant.

Photovoltaic detectors that have been integrated in various types of irradiance measurement systems [63][64] are typically chosen for solar heat flux measurements because of their relatively accessible prices and ease of use [65]. However, they are sensitive to the spectral distribution and ambient temperature [66][67]. In general, these sensors will experience temperature fluctuation. Also, since a wide variety of spectrally selective coatings are offered for glass [12], the spectral distribution of solar irradiance passing through different windows will be inconsistent between different glazing configurations. For these reasons, errors could be introduced when illumination and temperature conditions are different from those under which the device was calibrated. On the other hand, pyranometers [68] offer more accurate results under various skies (broadband solar heat flux) and ambient air temperatures. There exist different types of thermopile pyranometers [69] such as all black or black and white pyranometers. However these devices are also considerably more expensive.

In order to obtain more accurate results at low costs under any type of sky conditions, this paper covers the development of two different designs of a low-cost broadband BWS constructed of common and inexpensive materials. This sensor is composed of two surfaces with different absorptive properties (a highly reflective white surface and a highly absorptive black surface). Instantaneous solar heat flux measurements are obtained through an on-site calibrated correlation based on the temperature difference between those two surfaces. The two sensor designs analyzed in this paper were initially developed for smart window control

purpose. However, it is worth noticing that the sensor designs and calibration methodology presented in this paper are general enough that they could be used to calibrate sensors for other applications or spectral profiles (for ex.: IR lamps).

3.2 Sensor description and thermal model

The BWS design consists of two thin metal plates with paint coatings of different solar absorptivity values: one highly absorptive coating (i.e.: black painted surface) and one highly reflective coating (i.e.: white painted surface). The painted metal plates are positioned next to each other on the same parallel plane with the painted surfaces (front surfaces) facing the exterior of the building. Temperature sensors are installed at the center of the back side of each metal plate. The high thermal conductivity of the metal plates ensures great accuracy of the surface temperature readings by the temperature sensors by distributing the temperature uniformly over the entire plate area (enabling a 1D heat transfer analysis at the center of the surfaces, where temperature sensors are positioned). The back sides of the metal plates are covered by an insulating material to limit heat transfer through the sensor and could act as the support of the sensor. Figure 3.1 illustrates a generic design of the sensor. Depending on the purpose of the sensor, many different variations in size and spacing between the painted surfaces could be considered in order to respond to particular needs. In all cases, the design should consider some type of thermal break between the two plates to limit heat transfer between them.

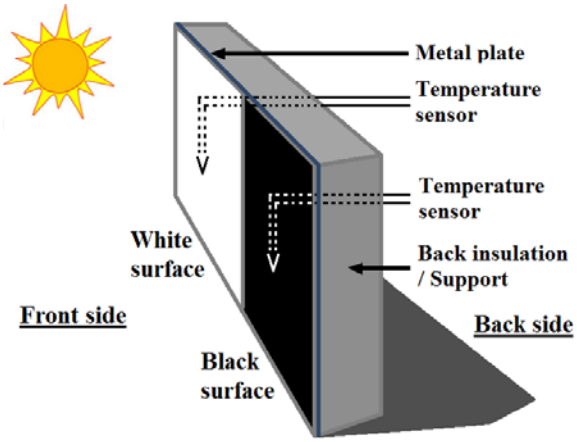

Figure 3.1: Generic representation of the sensor.

To calculate solar heat flux from surface temperature readings, the BWS needs a correlation based on a thermal model that could be calibrated on-site to properly adjust the thermal

parameters of interest. The present thermal analysis considers a 1D energy balance at the black and white surfaces of the sensor (front surfaces), as shown in Eqs. (3.1) and (3.2), respectively. The model considers the absorbed solar energy, radiative and convective heat fluxes at the front surface, conductive heat flux through the back of the sensor and the thermal capacity (heat storage) of the sensor:

$$\alpha_B G_{sol} = Q_{rad,W} + Q_{conv,f} + Q_{cond} + Q_{st,B} \tag{3.1}$$

$$\alpha_W G_{sol} = Q_{rad,W} + Q_{conv,f} + Q_{cond} + Q_{st,W} \tag{3.2}$$

Figure 3.2 illustrates a cross-section of the sensor, representative of both the black and white surfaces, to illustrate the different heat flux contributions of Eqs. (3.1) and (3.2).

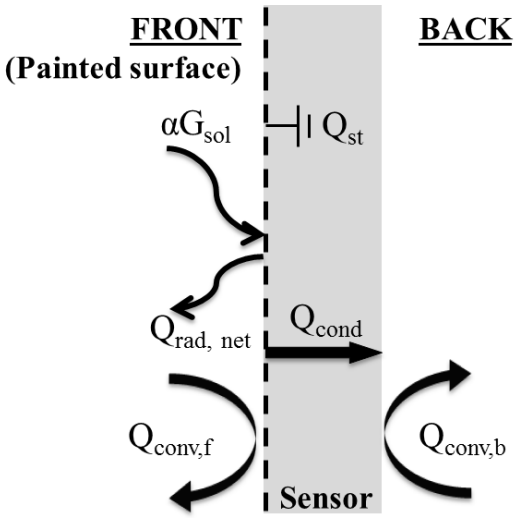

Figure 3.2: Heat balance at the sensor surfaces (cross-section view).

Considering spectrally integrated optical properties, a lumped capacitance model, see Chapter 5 of [70], for the sensor thermal capacity and identical values for the black and white surfaces regarding (i) view factors with surrounding surfaces, (ii) convection coefficient (natural convection coefficients on B&W surfaces were estimated, see Chapter 9 of [70], and presented sufficiently small differences to be neglected) and (iii) far-infrared emissivities, the energy balances become:

$$\alpha_B G_{sol} = \sigma\varepsilon(T_B^4 - T_{Surr}^4) + h_{conv}(T_B - T_{zone}) + \frac{k}{L}(T_B - T_{zone}) + C\frac{\partial T_B}{\partial t} \tag{3.3}$$

$$\alpha_W G_{sol} = \sigma\varepsilon(T_W^4 - T_{Surr}^4) + h_{conv}(T_W - T_{zone}) + \frac{k}{L}(T_W - T_{zone}) + C\frac{\partial T_W}{\partial t} \quad (3.4)$$

Subtracting Eq. (3.3) from Eq. (3.4), one achieves an expression for the total solar irradiance on the sensor as a function of the black and white surface temperature measurements:

$$G_{sol} = \frac{\sigma\varepsilon(T_B^4 - T_W^4) + h_{conv}(T_B - T_W) + \frac{k}{L}(T_B - T_W) + Ct\frac{(T_B^t - T_B^{t-1}) - (T_W^t - T_W^{t-1})}{\Delta t}}{\alpha_B - \alpha_W} \quad (3.5)$$

Note that the temporal derivatives of the temperature have been discretized to achieve this equation. Eq. (3.5) can be rewritten by grouping physical parameters into constants that it will be possible to adjust in order to fit the model with the measurements:

$$G_{sol} = A\sigma(T_B^4 - T_W^4) + B(T_B - T_W) + C\frac{(T_B^t - T_B^{t-1}) - (T_W^t - T_W^{t-1})}{\Delta t} \quad (3.6)$$

where $A = \frac{\varepsilon}{\alpha_B - \alpha_W}$ is the "radiative" term, $B = \frac{h_{conv} + \frac{k}{L}}{\alpha_B - \alpha_W}$ is the "convective" term and $C = \frac{Ct}{\alpha_B - \alpha_W}$ is the "thermal capacity" term. The calibration factors A, B and C of Eq. (3.6) can then be determined using measured values for T_B, T_W in combination with reference measurements for solar heat flux. The following section presents two different sensor designs that were calibrated for solar irradiance measurements using Eq. (3.6).

3.3 Experimental setups

The two designs of BWS presented in this paper were tested in the MoWiTT (Mobile Window Thermal Test) facility [71], located at Lawrence Berkeley National Laboratory (LBNL) in Berkeley, CA.

Sensors, both facing the exterior, were either located in the interior of the MoWiTT facility (Large Sensor) or within the interior air filled cavity of the glazing unit (Small Sensor). Both sensors were positioned parallel to the glazing in order to receive the total hemispheric solar energy that passed through the whole glazing system (and not the frame). The glazing unit was composed, from outside to inside, of 2.2 mm Cardinal loE 180 glass / exterior sealed

cavity of 11.7 mm 90% argon filled / 2 mm Cardinal clear glass / interior unsealed cavity of 28.5 mm air filled / 2.2 mm Cardinal i89 glass. The glazing unit was installed in a Pella Designer Series Fixed Casement window frame. Table 3.1 presents the window properties under standard NFRC conditions. Center-of-glass (*COG)* results of Table 3.1 refer to COG results while *Overall* results consider the overall window with frame. The installed window had dimensions of 0.914 m width by 1.219 m height (3 ft by 4 ft) and was oriented to the south. Measurements were taken during the month of August for the large sensor and during the month of September for the small sensor.

Table 3.1: Description of the window optical and thermal properties under standard NFRC conditions

Window	Gap 1 (mm)	Gap 2 (mm)	Gap Fill 1	Gap Fill 2	Emissivity Surface 1	Emissivity Surface 2	Emissivity Surface 3	Emissivity Surface 4	Emissivity Surface 5	COG U factor (Btu/h-ft^2-F)	COG U factor (W/m^2-K)	COG SHGC	COG VT	Overall U factor (Btu/h-ft^2-F)	Overall U factor (W/m^2-K)	Overall SHGC	Overall VT
Pella Designer Fixed Casement	11.7	28.5	ARGON	AIR	0.840	0.068	0.840	0.840	0.149	0.16	0.90	0.60	0.72	0.21	1.19	0.42	0.50

Table 3.2 presents the considered materials, equipment and design parameters for both sensors. The large sensor was located at approximately 0.1 m from the interior surface of the glazing (Figure 3.3). Results for the large sensor are presented in Section 3.1. The small sensor, located in the interior glazing cavity (see Figure 3.4), was positioned at approximately 2 mm from the interior surface of the center glass pane to limit the effect of natural convection of the air cavity at the sensor surfaces. The small sensor also had the advantage to be located in such a way that it could still read solar irradiance when the window shade is down. Results for this sensor are presented in Section 3.2. Both sensors were centered with the window width and located at the sill edge of glass area.

The Hobo temperature logger (large sensor temperature measurements) uses a 2.5 V excitation and the measurement is made between the thermistors and a fixed resistor (voltage divider). The Ohm to Celsius measurement conversions were managed by the HOBOware. On the other hand, the Labjack (small sensor temperature measurements) has a built-in 10 μA fixed current source. Several thermistors were chained in series with this current source including the thermistors of the small black and white sensor. The voltage drop across each thermistor was measured using the A/D (analog to digital) input channels (measured each voltage step in the resistor chain and subtracted to get each sensor). The thermistors resistance of the BWS were calculated with Ohms law from the known current and measured voltage drops. The Ohm to Celsius conversion was then achieved using parameters from the manufacturer's technical datasheet (B parameter equation). However, since the published B parameter equation parameters were found to be less accurate than desired, a second order polynomial fit was applied on top of it based on a sensor calibration (5 to 50°C in a controlled water bath Neslab RTE-221 against reference PRT probes read by an Azonix A1011).

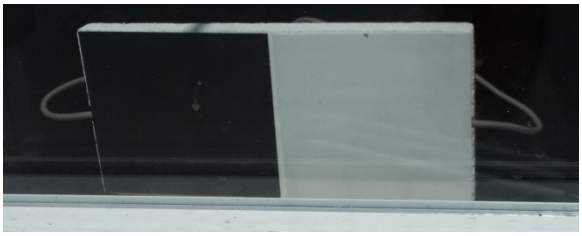

Figure 3.3: Large sensor – viewed from the exterior through the glazing.

Table 3.2: Description of the sensors

Sensor type	Metal plates	T° sensors	B&W coatings	Insulated backing	Sensor assembly dimensions	Data logger
Small sensor	Material: Copper Thickness: 0.076 mm Width: 22.8 mm Height 8.6 mm	TTF3A103F34D1BY thermistors sandwiched between two copper foils (conductivity of ~ 400 W/mK) with conductive epoxy Loctite 3873 (conductivity of 1.25 W/mK) Tolerance: ± 1% in the range (-40°C to 100°C)	Black Paint: Rustoleum flat black enamel paint (aerosol spray can) White Paint: Rustoleum flat white enamel paint (aerosol spray can)	1.5 mm thick acrylic	Overall thickness: 3.65 mm Overall width: 57.8 mm Overall height 13 mm Notes: Copper embedded T° sensors were stuck to acrylic with a 1 mm double stick foam tape. The same foam tape was stuck to the backing of the acrylic too, to increase insulation. B&W metals plates separated by a 11.4 mm gap.	Labjack T7-PRO
Large sensor	Material: Aluminum Thickness: 0.77 mm Width: 106 mm Height 99 mm	Onset TMC6-HD thermistors taped on metal plates with aluminum foil tape (conductivity of ~ 220 W/mK) Tolerance: ±0.25°C in the range (0°C to 50°C)	Black Paint: Rustoleum flat black enamel paint (aerosol spray can) White Paint: flat bright white primer	13.5 mm thick EPS foam (k≈0.34 W/mK)	Overall thickness: 14.5 mm Overall width: 217 mm Overall height 101 mm Notes: B&W metals plates separated by a 5 mm gap.	Onset Hobo U12-013

Figure 3.4: Small sensor – viewed from the exterior through the glazing.

The pyranometer (Kipp and Zonen CM11 [72]) used for calibration was positioned inside the room just above the large sensor (vertically mounted). Its accuracy corresponds to maximum errors in the hourly radiation totals of 3%.

3.3.1 Calibration method

This section presents the methodology used to calibrate the factors A, B and C in Eq. (3.6) for both types of sensors.

Readings of the temperature sensors for the black and white surfaces were taken on a one minute basis over the entire period of calibration. In the study, both sensors were calibrated considering daylight hours of a single day (a sensitivity analysis regarding the calibration period is presented in Section 3.3).

Calibration factors are optimized over the entire calibration period (m time steps) in Matlab with the interior-point algorithm of the *fmincon* solver [73]. The error function S to be minimized is defined as:

$$S=\sum_{i=1}^{m}(G_{sol,i}-G_{ref,i})^2 \tag{3.7}$$

where G_{sol} is the solar heat flux calculated from Eq. (3.6) and G_{ref} is the solar heat flux measured with the pyranometer. Bounds of the calibration factors are presented in Table 3.3.

Table 3.3: Bounds for the fitting constants A, B and C in Eq. (3.6)

Inferior limit		**Calibration factors**		**Superior limit**
0	≤	**A**	≤	5
0	≤	**B**	≤	100
0	≤	**C**	≤	2500

In developing the sensor, it was found that the sensor design and its position relative to the exterior could affect the ability of the sensor to estimate the solar flux, and that this should be taken into account in the calibration. For example, Figure 3.5 illustrates partial shading of the black surface of the large sensor due to the window frame and setback. The black surface in Figure 3.5 is mostly exposed to diffuse solar irradiance while the white surface is completely exposed to diffuse and direct solar irradiance. Since the same amount of solar irradiance is required on both surfaces for Eq. (3.6) to give accurate results, data collected when partial shading occurred was not considered in the analysis presented in the following section. Also, since solar transmittance varies significantly between different glazing types, one should keep in mind that the calibration method presented in this section should be performed again whenever the glazing is different.

Figure 3.5: Partial shading of the sensor.

3.4 Results

3.4.1 Large interior sensor

Since the large sensor was located in the interior of the room, its setback from the exterior wall of the facility created partial shading during some time intervals. In the present case, it was found that partial shading occurred from 9:45AM to 11:00AM and from 14:45 to 16:00. As mentioned earlier, data collected during these time intervals was not considered for the analysis.

The calibration period was during daylight hours of August 20th, 2014. The resulting optimized calibration factors were found to be A = 3.42 W/m^{2}K^4, B = 2.00 W/m^{2}K, C = 2500.00 J/m^{2}K. Results of solar heat flux were then estimated from the correlation up to August 27th, 2014 (range of incident angles varying between approximately 63° and 90°). Figure 3.6 presents the scatter plot of the solar heat flux obtained with Eq. (3.6) over the entire period of measurements versus measurements obtained from the pyranometer. From Figure 3.6, we can see that the correlation offers a good agreement with the reference values (1:1 slope) with 86% of calculated solar irradiance values being within ±10 W/m^2 of the reference values, 11% being between ±10 W/m^2 and ±20 W/m^2, and only 3% of occurrence being over ±20 W/m^2.

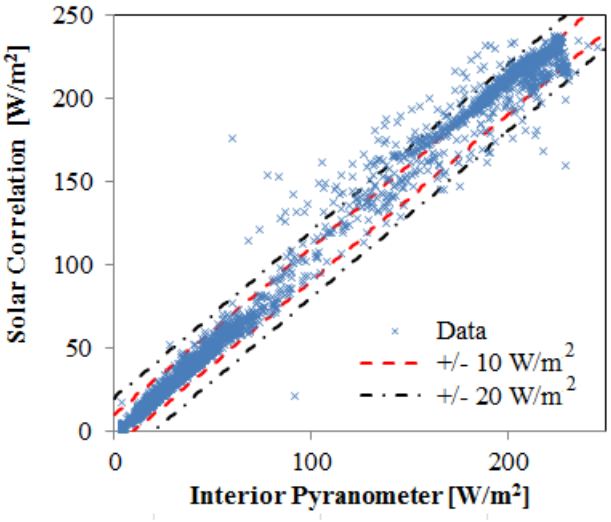

Figure 3.6: Large sensor solar irradiance obtained from the correlation, Eq. (3.6), as a function of the pyranometer measurements.

Since for several applications one will be interested in the integrated values of solar energy entering the building over a certain period of time [74] rather than in instantaneous solar intensities, it is relevant to make sure that the correlation can give accurate time integrated results. Figure 3.7 illustrates the daily integrated solar energy values calculated with the calibrated correlation and measured by the pyranometer.

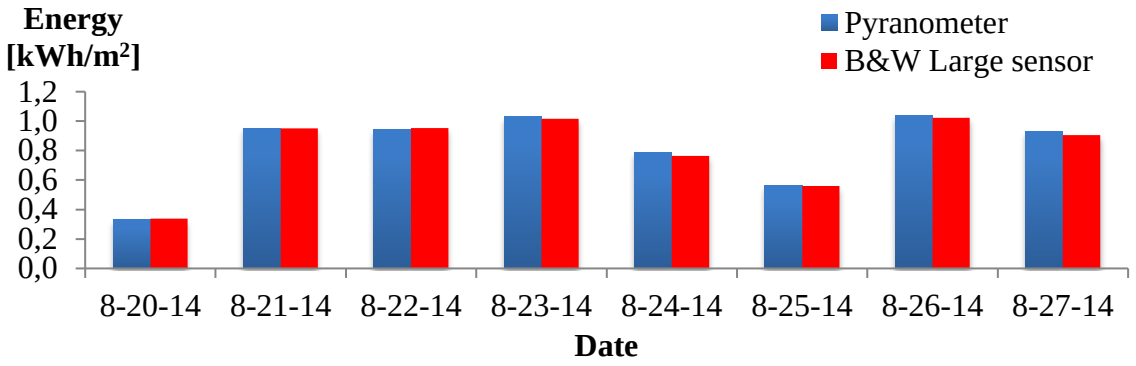

Figure 3.7: Large sensor integrated solar energy measurements on a daily basis.

From Figure 3.7 we can see that the BWS gives extremely accurate values for solar energy passing through the window with a mean weighted relative error of 1.5%. The mean weighted relative error is defined by:

$$\text{Error}=\frac{\sum_{i=1}^{n}\frac{|E_{sol,i}-E_{ref,i}|}{\overline{E}_{ref}}}{n}\cdot 100 \tag{3.8}$$

On an hourly basis, the mean weighted relative error is 3.7%. As previously said, the presented results do not consider hours of partial shading. In some applications (e.g. real time control with solar heat flux input), the large sensor design would not be appropriate because of the lack of reliable data during extended periods of time. Furthermore, since the large sensor design is quite bulky, material costs are not minimized and it cannot be easily integrated in between window glass panes for more permanent measurement applications. For these reasons, a smaller sensor was designed and tested, as presented in the next sub-section.

3.4.2 Small sensor integrated into the glazing unit

Since small sensor setback from the exterior wall plane was significantly lower than the one for the large sensor, partial shading hours were different. The setback was actually small enough to consider all data collected between 8:00 and 17:00.

The calibration period was during daylight hours of September 18th, 2014. The resulting optimized calibration factors were found to be A = 1.99 W/m^{2}K^4, B = 47.35 W/m^{2}K, C = 1963.30 J/m^{2}K. Results of solar heat flux were then estimated from the correlation up to

September 23rd, 2014 (range of incident angles varying between approximately 53° and 90°). Figure 3.8 presents the scatter plot of the solar heat flux obtained with Eq. (3.6) over the entire period of measurements versus measurements obtained from the pyranometer. From Figure 3.8, we can see that, as for the large sensor, the correlation offers a good agreement with the reference values with 74% of calculated solar irradiance values being within ±10 W/m^2 of the reference values, 18% being between ±10 W/m^2 and ±20 W/m^2, and only 8% of occurrence being over ±20 W/m^2.

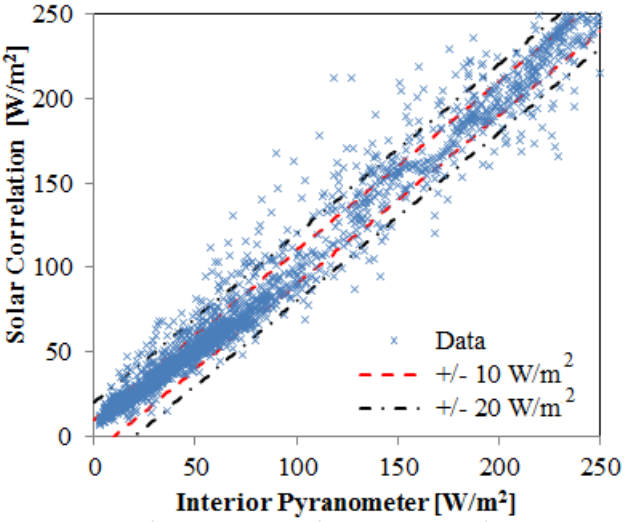

Figure 3.8: Small sensor solar irradiance obtained from the correlation, Eq. (3.6), as a function of the pyranometer measurements.

Figure 3.9 illustrates the daily integrated solar energy values calculated with the calibrated correlation and measured by the pyranometer. From Figure 3.9 we can see that the BWS gives extremely accurate values for solar energy passing through the window glazing with a mean weighted relative error (eq. 3.8) of 2.9%. The same analysis, but on an hourly basis, gave a mean weighted relative error of 3.9%.

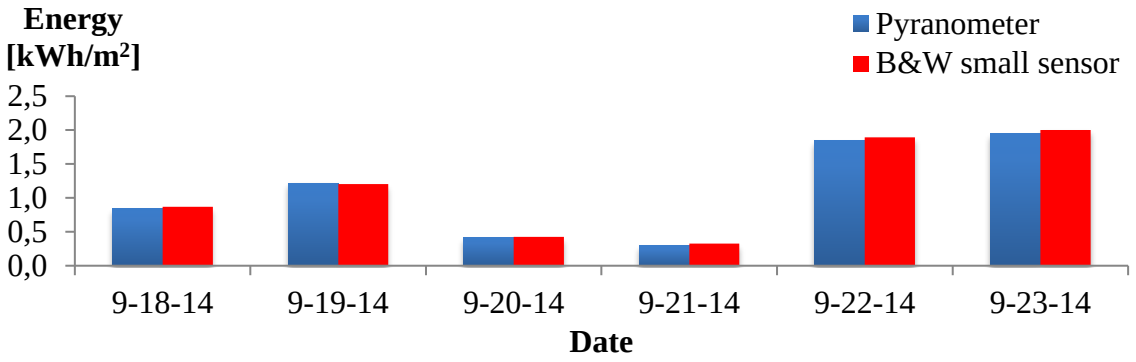

Figure 3.9: Small sensor integrated solar energy measurements on a daily basis.

Based on these results, instantaneous solar heat flux measurements obtained with the small sensor are less accurate than the ones obtained with the large sensor (solar irradiance values being 86% within ±10 W/m^2 for the large sensor compared to 74% for the small sensor). Integrated energy results present the same behavior between the two sensor designs with smaller differences in results (daily and hourly mean weighted relative errors being, respectively, 1.5% and 3.7% for the large sensor compared to 2.9% and 3.9% for the small sensor). The loss of accuracy of the small sensor could be explained by two major reasons. First, the small sensor is located in the window IGU that experiences higher variations in convection coefficient (fluctuating ambient temperature). Also, because of its size and shape, the small sensor is more sensitive to the thermal edge effects (temperature gradients parallel to the plane of the black and white surfaces) that have not been considered in the model (Eq. (3.6)). This reduction in accuracy for the small sensor is however compensated by its larger flexibility in terms of periods where collected solar heat flux data is reliable (periods without partial shading). The small sensor thus presents a very good tradeoff between accuracy and real-time control purpose since results are accurate enough for many applications and give reliable inputs for real-time control applications.

3.4.3 Effect of the calibration period

While calibrating the BWS, it is necessary to make sure that the calibration period is sufficient to ensure a good accuracy for the correlation when solar conditions change (variations in solar intensity and/or spectral distribution). For example, we can observe important changes of solar irradiance measured by the pyranometer from one day to another (see Figure 3.10). The first two days of measurements in Figure 3.10b (Sept. 18th and 19th)

present high solar irradiance values with some lower values scattered throughout the day (more importantly during the morning of Sept. 18th). These two days could be defined as partially cloudy days. The following two days (Sept. 20th and 21st) present very low solar irradiance values and are defined as overcast days. Finally, the last two days (Sept. 22nd and 23rd) present a very smooth variation of solar irradiance measurements with high solar intensity at noon and could be defined as clear sky days. Furthermore, solar irradiance changes from hour to hour in part because of sun's position. It is thus relevant to analyze the influence of the moment of the day when the calibration period is defined as well as the day itself (type of sky conditions). For this reason, this section presents different calibration periods considered to fit the constant of Eq. (3.6). In other words, for each calibration day, one set of A, B and C is thus determined. Then, the resulting models were used to verify whether they were able to predict solar irradiance for all days for which measurements with the pyranometer were available (including the calibration day, i.e. between August 20th and August 27th 2014 for the large sensor and between Sept. 18th and Sept. 23rd 2014 for the small sensor).

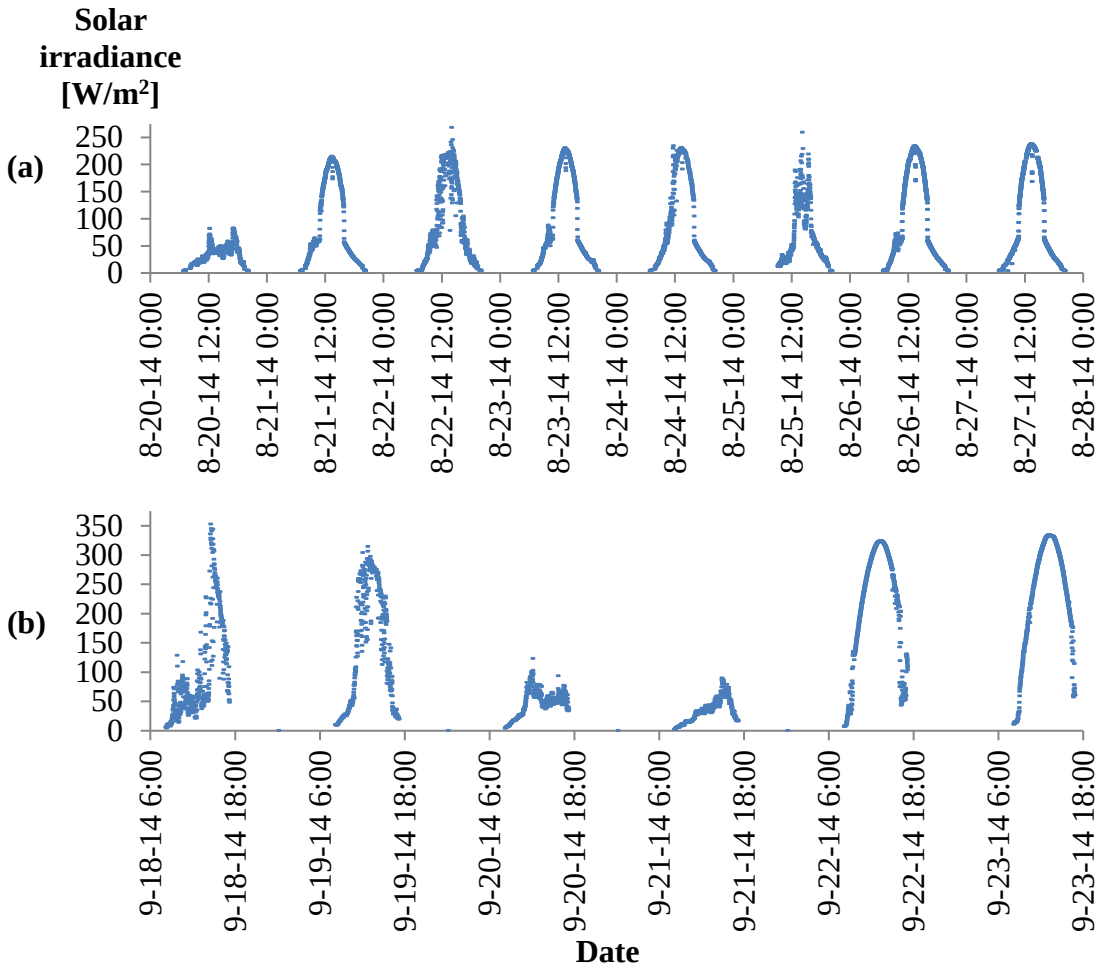

Figure 3.10: Solar heat flux measured by the pyranometer between 8:00 AM to 5:00 PM from a) August 20th, 2014 to August 27th, 2014 and b) September 18th, 2014 to September 23rd, 2014.

Figure 3.11 presents the influence of the calibration period on the BWS precision by considering different days and calibration period. The term "BWS precision" represents the percentage of calculated irradiance values obtained with the calibrated correlation that are within 10 W/m^2 compared to the measurements of the pyranometer. Each point in Figure 3.11 represents the BWS precision for a calibration period starting at 9:00AM and stopping at the calibration period stop time (x-axis). Figure 3.11a and Figure 3.11b present results for the large and small sensors, respectively. From Figure 3.11, we observe, for both sensor designs, that the precision increases as the calibration period increases and stabilizes when calibration period reaches 1:00PM (calibration period of 5 hours), i.e. after half a day of solar measurements, including the solar peak. Also, we observe that partially cloudy days (i.e.

August 22nd and 25th for the large sensor and Sept. 18th and 19th for the small sensor) and overcast days (August 20th for the large sensor and Sept. 20th and 21st for the small sensor) present a BWS precision that is more sensitive to the calibration period. On the other hand, clear sky days (August 21st, 23rd, 24th, 26th and 27th for the large sensor and Sept. 22nd and 23rd for the small sensor) present more stable results and higher precision. It is thus recommended, based on this sensitivity analysis, to choose a day with clear sky conditions for the "on-site" calibration. Also, as mentioned in the previous section, it is clear from Figure 3.11 that the sensor design influences its accuracy (large sensor precision of 93% compared to 76% for the small sensor).

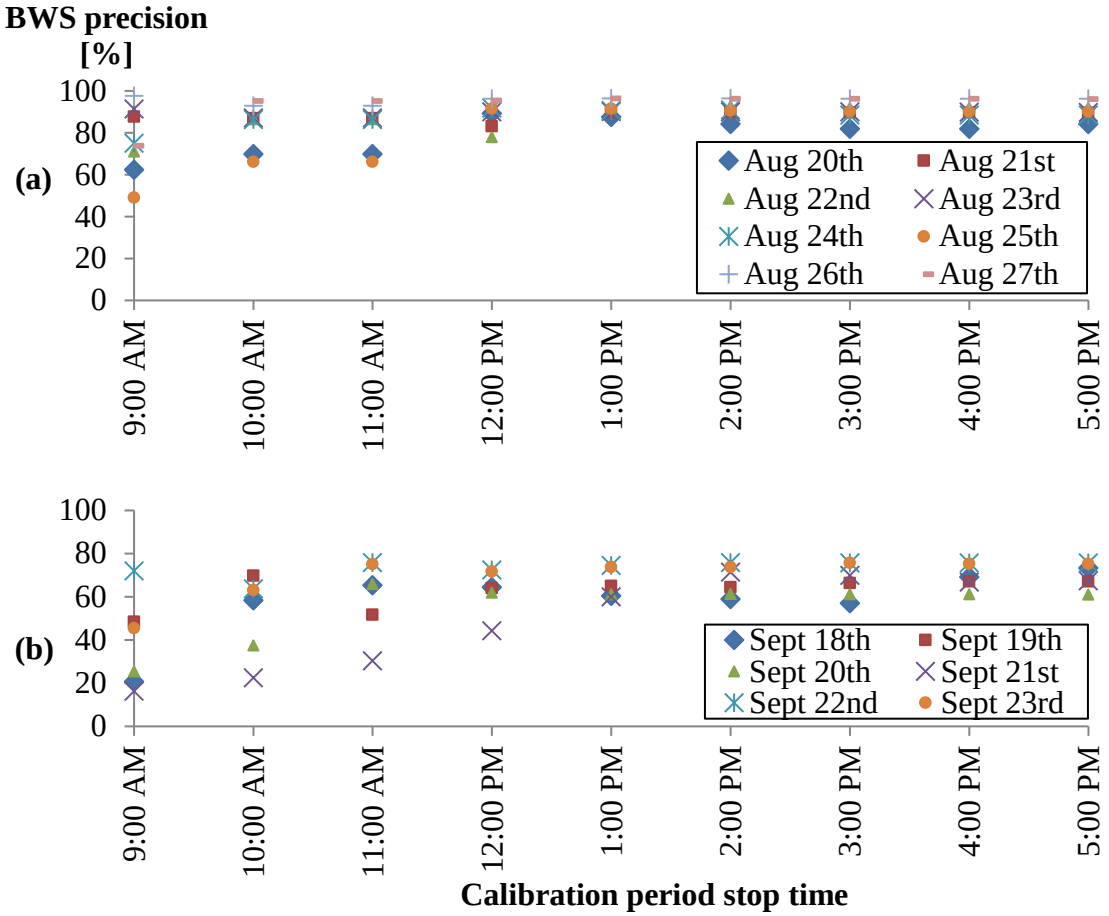

Figure 3.11: BWS precision (i.e. a) large sensor and b) small sensor) as a function of the calibration period stopping time (considering a calibration starting time of 8:00 AM) and of the calibration day.

3.5 Conclusions

This paper presents a new type of low cost solar sensor, i.e. a black and white sensor that calculates instantaneous solar heat flux based on a 1D heat transfer model. The heat transfer model contains calibration factors defining the radiative, convective/conductive and capacitive parameters of the sensor.

In the present study the sensor was calibrated on-site with a reference pyranometer prior to measurements. However, to increase the ease of use, it would be relevant in the future to develop a procedure allowing off-site or lab calibration of the sensor.

Two different designs of sensor were presented, i.e. a large sensor located in the interior of building and a small sensor located into the interior glazing cavity of a triple pane glazing. Both sensors have shown satisfactory accuracy for solar heat flux measurements. Among the two designs tested, the large sensor was more accurate, mainly due to the fact that it was exposed to more stable conditions and edge effects were limited. However, it is shown that the large sensor measurements are limited to more restricted periods of time since partial shading is occurring during extended periods of time (which is not the case for the small sensor). Moreover, if window shading is down, the large sensor could not continue to measure solar irradiance while the small sensor could. Different sizes and locations could thus be used in order to suit different applications, but further studies must be conducted in order to assess edge effects for very small sizes of the sensor black and white surfaces.

Since this study presents results gathered over a particular period of the year, further studies should determine the long term performance of the sensors calibration.

Finally, since photosensors are largely used for solar irradiance measurements, future research should compare this kind of sensor to conventional silicon sensors in order to define more precisely the pros and cons of both types (e.g., spectral sensitivity, cost, lifetime, etc.).

CHAPTER 4 REDUCED ENERGY CONSUMPTION AND ENHANCED COMFORT WITH SMART WINDOWS: COMPARISON BETWEEN QUASI-OPTIMAL, PREDICTIVE AND RULE-BASED CONTROL STRATEGIES

Abstract

Smart windows are used to reduce energy consumption and improve thermal and visual comfort mainly by controlling the solar flux entering into a building. This article presents a simulation study in which the impact of the applied control strategy on the overall energy consumption (heating, cooling and lighting) is investigated. A commercial building located in Montreal (Canada) with south-oriented integrated electrochromic windows is modeled. The hour-by-hour state of the smart windows required to minimize overall energy consumption while respecting constraints related to thermal and visual comfort is determined through an optimization strategy based on genetic algorithms (GA). Then, this quasi-optimal control is compared to other approaches that could be applied in real-time applications: (i) two types of rule-based controls (RBC), i.e. RBC1 and RBC2 and (ii) a model predictive control (MPC). The impacts of thermal mass and installed light power density are also analyzed. Results show that the four control strategies under study presented similar energy consumption with differences in total energy consumption ranging from 4% to 10%. While more complex controllers such as MPC could potentially lead to improved performances considering more design variables, complex models and extensive commissioning, this study illustrates that simpler control strategies such as RBC2 can also lead to satisfying results.

Résumé

La fenestration intelligente est utilisée pour réduire la consommation d'énergie et améliorer le confort thermique et visuel par le contrôle des flux solaires qui pénètrent un bâtiment. Cet article présente une étude numérique d'une telle technologie où l'impact des stratégies de contrôle sur la consommation énergétique globale (chauffage, refroidissement, éclairage) est évalué. Le modèle est constitué d'un bâtiment commercial situé à Montréal (Canada) comprenant une fenestration électrochrome sur une façade orientée au sud. L'état des fenêtres intelligentes nécessaire à toute heure de la journée pour permettre une minimisation de la consommation d'énergie globale tout en respectant les contraintes reliées au confort thermique et visuel est déterminé à l'aide d'une stratégie d'optimisation basée sur des algorithmes génétiques (AG). Ce contrôle quasi-optimal est alors comparé à d'autres approches qui peuvent être adaptées à des applications en temps réel : (i) deux types de contrôles fondés sur des règles (RBC), c.-à-d. RBC1 et RBC2 et (ii) un modèle de contrôle prédictif (MPC). Les impacts de la masse thermique et de la puissance du système d'éclairage installée sont également analysés. Les résultats montrent que les quatre stratégies de contrôle à l'étude présentent une consommation énergétique similaire avec des écarts de consommation globale variant de 4% à 10%. Bien que des contrôleurs plus complexes comme le MPC peuvent mener à l'amélioration des performances en considérant plus de variables de design, des modèles plus sophistiqués ainsi qu'une mise en service rigoureuse, cette étude illustre que des stratégies de contrôle plus simple comme le RBC2 permettent d'obtenir des résultats satisfaisants.

4.1 Introduction

A tradeoff between energy performance and visual comfort has to be made when selecting the window type, position and size in a building [75]. Ochoa et al. [75] state that introducing solar shading technologies considerably enlarge the search space in this field of research. Moreover, if solar shading control strategies are considered, it further increases the complexity of such an optimal design exercise.

When investigating the potential of smart window technologies [13], i.e. glazing technologies offering controllable optical properties, the determination of the control strategy is often recognized as a crucial factor in achieving the required performance [27]. Nowadays, the flexibility (large dynamic range [76]) of existing smart window technologies offers great control opportunities and challenges. Selkowitz et al. [77] present the challenges and opportunities related to dynamic control of smart windows that are judged as essential considerations in the application of smart façade technologies. The SW state influences illuminance levels, electricity consumption for artificial lighting and solar and lighting thermal loads in the building zone. These aspects should all be taken into account in order to properly assess the impact of control strategies on energy savings and on the visual and thermal comfort of occupants.

Several authors showed that the effect of smart window control strategies on energy consumption is largely influenced by the type of building zones and control strategy parameters used. Often daylight optimization strategies are applied to control smart windows. In a field study, Lee et al. [40] monitored a lighting energy reduction of 26% ± 15% and a cooling load reduction of 7 ± 4% with electrochromic windows controlled in various ways so as to optimize daylight while avoiding glare compared to a spectrally selective low-e window. Lee and Tavil [78] analyzed among other parameters the effect of control strategies based on vertical plane incident solar radiation and work plane natural illuminance control, and identified illuminance and glare based strategies as the best to decrease annual energy consumption. Shehabi et al. [79] concluded that dynamic prismatic optical element window coatings controlled to maximize performance and energy savings

available from daylighting controls could increase lighting energy savings by 85% compared to conventional daylight controls.

Assimakopoulos et al. presented a novel advanced control strategy based on an adaptive neuro-fuzzy inference system [51]. Results of that study revealed that the developed control strategy, although presenting a good performance, needed a higher range of possible SHGC values for it to fully take advantage of the complexity of the strategy. Nowadays, the advances in smart window technologies [12] could potentially justify the integration of such advanced control strategy in smart window control systems.

The various studies dedicated to improving smart window control strategies brought up to light the main challenges for a large-scale integration of smart window in current buildings. Among others, the main challenges in the development of efficient controllers are the occupancy type and the occupant's acceptance [46], the transient effects of unanticipated energy demand fluctuations, the radiative thermal load shift due to building thermal mass [35], the influence of the climate and façade orientations [54] and the HVAC parameters such as part-load performance or time delays introduced by air distribution systems [35]. Furthermore, intrinsic properties of the different smart window technologies [54] such as the required switching time between possible states or the variation of the spectral distribution of the visible transmittance [80] should be added up in the considered parameters for enhanced smart window controls.

In this paper, a building model with predefined geometry and material properties was used to explore the effect of different state-of-the-art control strategies on energy consumption for heating, cooling and lighting and on thermal discomfort, while taking into account the effect of the smart window state on the natural illuminance on the work plane. The intent of this work is to assess the performance of viable control solutions for real-time control of smart windows. The most promising rule-based controllers [81] and a model based predictive controller [82] are proposed as applicable real-time control strategies and compared to a quasi-optimal reference case based on genetic algorithms.

4.2 Building model

4.2.1 Building location, geometry and construction

A typical commercial building was considered in the present work. A 100 m^2 office zone of the building was modeled (6-sided box model of 10 m by 10 m by 3 m), with one exterior south-facing wall. The exterior building façade is composed of an electrochromic smart window (the upper 2/3 of the façade area) and an opaque exterior wall (concrete siding, lightweight frame filled with mineral wool insulation and gypsum indoor finishing) with an overall U-value of 0.45 W/m^2K. The other five faces of the box model were defined as adiabatic surfaces to represent identical building zones surrounding the considered zone. Internal walls are modelled as light weight walls. Two types of floor construction were considered, i.e.: a 10 cm concrete floor slab (C_{Cr}=191 kJ/m^2K) and a 10 cm cross-laminated timber floor (C_{CLT}=81 kJ/m^2K), representing different values of internal thermal mass (high versus medium). In this study, direct solar gains were assumed to be uniformly distributed on the floor. On the other hand, diffuse solar gains were distributed according to absorption-transmission weighted area ratios for all other surfaces. The building model was developed in TRNSYS.

Simulations were realized considering EnergyPlus weather data (epw file) for the city of Montreal, Canada. Since smart window technologies energy benefits are mostly associated to cooling load and peak demand reductions [54], the simulation period considered in this study covers the months of June and July. While the hours simulated during the month of June were used as a warm up period [83], all hours of the month of July were used for the analysis. A time step of one hour was used in all simulations.

4.2.2 Properties of smart window

The smart window considered in this study is a double glazing electrochromic window whose optical properties can be varied by an applied voltage [12]. The electrochromic layer was applied on the surface 2, i.e. the internal surface of the external glazing, in order to limit undesired solar heat gains from absorbed and reemitted heat as well as to increase thermal comfort. Four possible SW states, from clear (S1) to dark (S4), have been included in the model. Table 4.1 provides the SW center of glazing properties at normal incidence. While

properties at normal incidence of Table 4.1 are presented for readers' benefits, one should note that the model uses the complete and detailed properties, varying with incidence angle, obtained in the IGDB (International Glazing Database).

In the model, every time the state of the window is changed, the corresponding properties of that new state are also applied to the window. Since the time steps (one hour) considered in the simulation results are greater than the time required to switch from one state to the other (about 5 minutes considering an ideal window designed with a sufficient amount of bus bars) [81], it was assumed that window properties over a time step were constant.

Table 4.1: Smart window center-of-glazing properties

Smart window states	U-Value [W/m²K]	SHGC [-]	Tvis [%]	Tsol [%]
State 1 (S1) (bleached)	1.63	0.47	62.1	38.1
State 2 (S2)	1.63	0.17	21.2	8.6
State 3 (S3)	1.63	0.11	5.9	2.4
State 4 (S4) (fully tinted)	1.63	0.09	1.5	1.0

4.2.3 Gains and schedules

Internal gains are related to artificial lighting, occupancy (10 occupants doing moderate office work) and equipment. Table 4.2 presents the building zone heat gains as well as their respective radiative and convective fractions. Based on the purpose of this work, only sensible heat has been considered in the model. A remaining 120 W during off-occupancy hours was considered for appliances in standby mode.

Table 4.2: Building zone heat gains

Gain Types	Heat Gains [W]	Convective Fraction [%]	Radiative Fraction [%]
Occupants (10)	730	30	70
Equipment	800	30	70
Light	748	41	59

The building lighting model calculates the illuminance distribution on interior surfaces of the building considering combined daylight and artificial light. In order to offer proper illuminance on the work plane (0.8 m height from the floor level), a light sensor has been

positioned at the center of the room width and 7 meters depth from the glazed wall. The sensor is represented in Figure 4.1 by the circled “S” label. The illuminance requirement (WPreq) on the sensor has been set to 500 lux [84] during occupancy hours. Although more visual comfort considerations could have been included [85][86], this approach to quantify visual comfort was deemed sufficient to capture the main tradeoffs that are studied in this paper, given that the present work is more specifically oriented towards reducing energy consumption. Further studies should consider more exhaustive visual comfort models and their impacts on control strategies and building energy consumption.

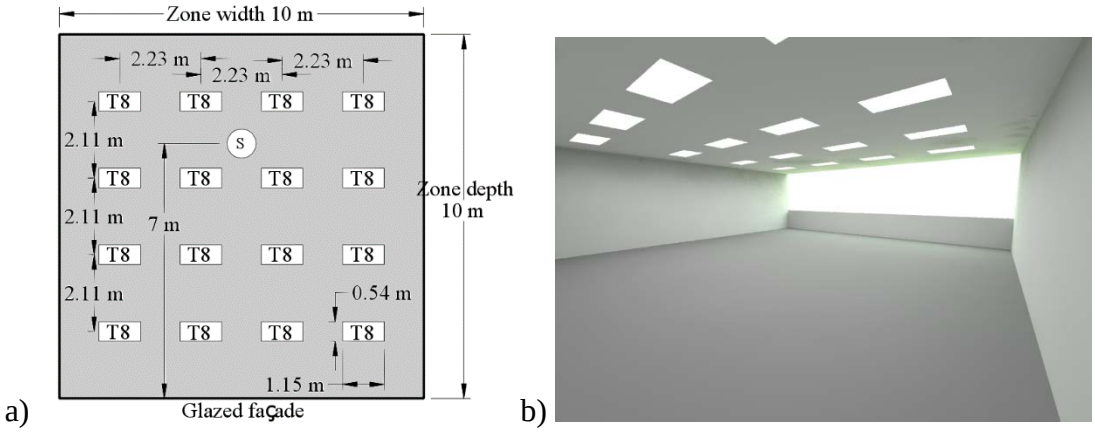

Figure 4.1: (a) Artificial lighting system disposition (Top view), (b) 3D representation of the zone natural and artificial light sources.

The daylight calculations were performed with DAYSIM [87]. A table was built with the natural illuminance on a work plane, at each hour and for all the four possible states of the window. Using this look-up table, it was possible during the thermal simulation to straightforwardly find the amount of natural light on the work plane, provided that the state of the window is known.

Radiance was used for the artificial lighting calculations [88]. Two types of artificial lighting systems were considered for the study, i.e. a conventional T8 lamps lighting system and a LED system [89]; see Table 4.3 for details.

Figure 4.1 illustrates the lamp distribution over the ceiling surface (identical for both systems). Similarly to the natural light calculation, a look up table was built for both lighting

systems directly in Radiance considering the artificial illuminance on the work plane for different lighting powers. The dimming control strategy used in this paper, summarized in Table 4.3, is similar to the EnergyPlus Continuous/OFF dimming control [90]. In Table 4.3, LLD refers to the Lumen Lamp Depreciation factor and LDD refers to the Luminaire Dirt Depreciation factor.

Table 4.3: Artificial lighting systems

Nominal LPD	10.2 W/m^2 (T8 lamps) and 4.4 W/m^2 (LED system)
Ballast factor (T8 lamps)	0.86
GDF	0.81 (GDF = LDD · LLD = 0.9 ·0.9)
Wp_{sp}	500 lux
Daylight zone dimming control	$f_P = \begin{cases} 0 & f_L = 0 \\ f_{P,min} & 0 < f_L < f_{L,min} \\ \left[f_L + (1 - f_L) f_{P,min} - f_{L,min} \right] / (1 - f_{L,min}) & f_{L,min} \le f_L \le 1 \end{cases}$

In the end, the total illuminance is simply the summation of the natural and artificial illuminances. DAYSIM and Radiance generated look up tables were used for all four control algorithms.

To represent a typical transient variation of internal gains and lighting requirements in office buildings, schedules have been created.

Figure 4.2 presents the schedule of electronic appliances, occupancy and work plane light requirement for week days. For simplicity, the only internal gains considered during week-ends were the electronic appliances at 15% of their maximal power usage.

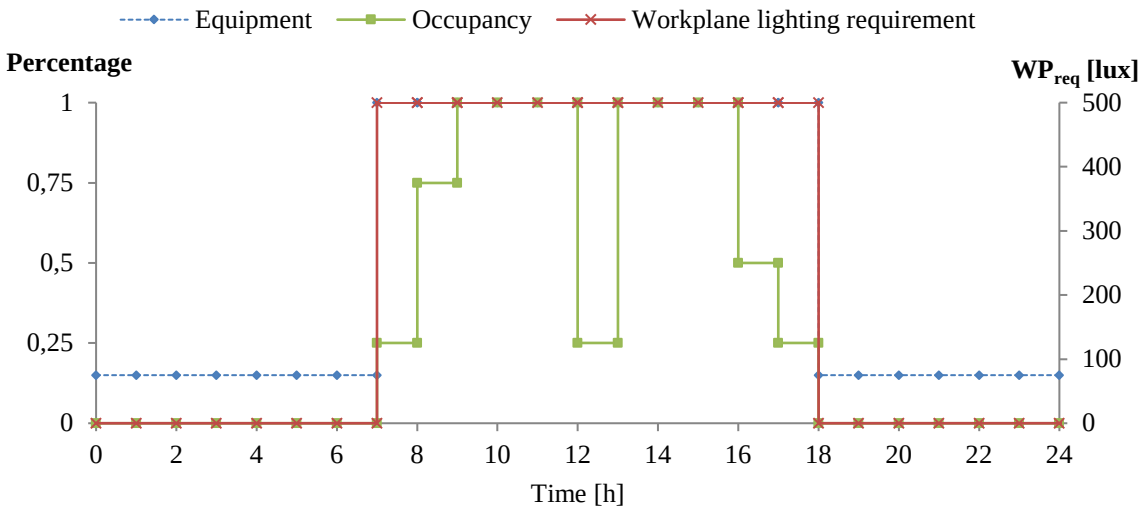

Figure 4.2: Week days schedule for equipment and occupancy (left axis) and work plane lighting requirement (right axis).

4.2.4 HVAC&R system

It was considered that the calculated heating load Q_{heat} and cooling load Q_{cool} acted directly on the air node of the building model, and were satisfied instantly by the HVAC system. Heating and cooling loads, Q_{heat} and Q_{cool} respectively, were determined by TRNSYS models except for the MPC controller. In the latter case, heating and cooling loads were determined within the controller building model (see Section 4.3.1). The cooling system considers a constant coefficient of performance (COP) of 3. A direct electric heating system is considered. The indoor temperature was allowed to vary between 21°C and 25°C during occupancy. Outside of the occupancy hours, these temperature limits are respectively lowered and raised by 3°C. Based on summer design conditions, the cooling system was sized to provide a maximum power of 8300 W considering the smart window at its clearest state. That cooling system was able to meet the cooling requirements for all hours under study. A constant air volume ventilation system was installed. The volume flow rate of outside air was roughly estimated at 340 m^3/h (200 cfm). A heat exchanger was used to transfer heat between the air exhaust and make up air with 60 % efficiency.

4.3 Implemented control strategies

Three types of control strategies are presented below. First, rule-based controllers (heuristic) are described in Section 4.3.1. Second, the optimal control is determined by a genetic

algorithm (GA) in Section 4.3.2 to establish the best scenario. Finally, a model predictive control (MPC) is detailed in Section 4.3.3. It should be noted that the rule-based control strategies of Section 4.3.1 do not involve any optimization whatsoever. On the other hand, the two other controllers minimize an objective function, as described below (Sections 4.3.2 and 4.3.3).

4.3.1 Rule-based control

Different rule-based strategies have previously been tested for the control of smart windows [54]. Rule-based control relies on predefined instructions (e.g., "if… then…") based on the difference between measured and set-point values.

Two rule-based control strategies were considered in this work. The first rule-based controller (RBC1) was designed to adjust the smart window state (control variables) in order to maximize daylight on the light sensor ('S' in Figure 4.1) without over-lighting during occupancy hours: if the light sensor reading exceeded the 500 lux threshold, the SW was switched to the next darker state that reduces the illuminance level below 500 lux. In the next time step (1 hour) this position is re-evaluated. During off-occupancy hours, this RBC1 controller was designed to set the smart window at its clearest state (S1). The second rule-based controller (RBC2) follows the same behavior as RBC1 during occupancy hours, however it was designed to switch to the darkest state (S4) during off-occupancy hours for which solar gains are still present. This second type of controller was proposed to potentially offer a more energy-efficient strategy during cooling season.

4.3.2 Procedure to determine optimal control – Genetic Algorithms (GA)

Given the state of the smart window at each hour of a certain period of time, it is possible to simulate the building thermal behavior over that time frame with the model described in Section 4.2 (TRNSYS building model). An optimization strategy was elaborated to determine the optimal state of the window at each hour. In this procedure, the states of the smart window over each time step (one hour) are the design variables. The objective is to minimize the overall energy consumption, which is:

$$Q_{Tot} = Q_{Heat} + \frac{Q_{Cool}}{COP} + Q_{Light} \tag{4.1}$$

Constraints were invoked to consider visual comfort during occupancy (W_{Preq}), as mentioned before.

The objective function was minimized with genetic algorithms (developed in Matlab) assuming a perfect building model representation, a perfect weather forecast (i.e. one perfectly knows the future weather parameters during the optimization) and perfect occupation forecast. A set of design variables (i.e., the SW state at each time step) represents an individual. An initial random population of individuals is first generated. Then, the objective function of each individual is evaluated with Eq. (4.1), based on the simulation. Cross-over between individuals occurs with more probability of reproduction for best individuals. Mutations are then applied randomly to the offspring. A new generation is created from the offspring and from the few best individuals of the previous population (which is called an elitist strategy). The process is repeated until convergence. More information on genetic algorithms can be found in [58]. Table 4.4 presents the tuning and convergence parameters of the genetic algorithms that were considered in this work.

Table 4.4: Parameters of the Genetic Algorithm

Parameters	Value	Units
Number of phenotypes per generation	40	-
Maximum number of generations	75	-
Number of generations with unchanged Q_{Tot} before convergence	30	-
Proportion of children per generation	80	%
Children mutation probability	5	%
Number of chromosomal crossovers	2	-

Formal optimization using genetic algorithms is generally quite computationally expensive [91]. For this reason, a procedure was developed to reduce computational time. In practice, the energy demand at a given time step depends only on what happened in the few previous hours or days. In other words, the SW state at a time step has influence only over a limited number of future hours. In order to take advantage of that, the optimization was first performed over the first 24h of the simulation period to determine the best SW states for each hour of that period of time. Then, the optimization was repeated for the following 24 hours considering the previous results applied to past hours, and so on, until the SW state at each

time step was optimized. Typically, it took 0.5 h to perform a 24 h period of optimization with that procedure on a 64 bits system with 2.80 GHz Intel Core i7 CPU and 8G of memory.

By definition, genetic algorithms involve probabilistic processes. As a consequence, two runs can potentially lead to two different optimization results. Although they have been able to successfully identify global optima in many situations, genetic algorithms can thus lead to local optima or nearly optimal individuals. The term quasi-optimal is used in this work to highlight this fact when required.

4.3.3 Model based predictive control (MPC)

First used in the chemical process industry, MPC is control approach currently used in a large variety of industrial applications [92]. MPC refers to a class of control algorithms that use an explicit model of a system to predict its future response over a finite-time horizon. At each control time step, the MPC algorithm optimizes the sequence of control values over the prediction horizon Hp based on the predictions of the model. In other words, the best control as predicted by the model is applied to the system. The first input of that optimal sequence (the control input at the current time) is sent to the system and the process is then repeated for the next control decision. In its standard form, the optimization is performed online (in real time) within the controller [93].

MPC has gained a lot interest in the past few years in building related applications [94] [95]. In this paper, a space-state resistance-capacitance building model developed in Matlab (called the "controller model") [26] is used within the controller as the model representation of the real building (the real building being represented by the TRNSYS model in this study). The best real time control inputs, U_c, of the HVAC system, lighting system and smart window (i.e. Q_{heat} or Q_{cool}, Fu_{light} and the window state, respectively) are obtained for each hour (time step = 1 h) based on the minimization of the total energy consumption of the building zone (electricity for heating, cooling and lighting, see Eq. (4.1)) considering a 24 h prediction horizon (H_p = 24). One should refer to Section 2.2 of Chapter 2 for technical details and model verification of the controller model.

The MPC consists of three distinct parts: the observer, the predictor and the optimizer. The work flow of the MPC is presented in Figure 4.3. It is assumed that all the control inputs (U_c) and disturbance inputs (U_d = [T_{out}, $Q_{sol,direct}$, $Q_{sol,diff}$]) are fully measurable. In Figure 4.3, the accentuation (^) on the parameters refers to the estimation (for building states x) or predictions (for building temperature outputs Y and disturbances U_d). At time step k, sensors of the building measure different temperatures ($Y_{k|k}$, i.e. measurement values of time k measured at time k), of the zone and building envelope (i.e. TRNSYS generated data used as "sensor" data for the MPC model feedback loop) that are fed to the observer. Using the MATLAB controller model, the observer estimates the unmeasured building temperature states (subset of $\hat{x}_{k|k}$) based on the measurements $Y_{k|k}$, U_c and U_d (both assumed to be perfectly measurable) as well as on the complete set of measured and estimated state temperatures of the previous step ($\hat{x}_{k|k-1}$). In parallel, the predictor predicts, for the next H_p time steps, disturbance inputs ($T_{out;}$ $Q_{sol,direct}$; $Q_{sol,diff}$). The MPC then calculates, based on the predictions and set point requirements ($r_{k+p|k}$), the model control inputs for the next control time step $U_{c,k+1|k}$ that minimize the cost function J (including electricity and discomfort costs of the building zone), according to:

$$J = \min \sum_{p=1}^{Hp} \left[\left(Q_{heat,p} + \frac{Q_{cool,p}}{COP} + Q_{light,p} \right) F_{HVAC} + \left(DC_{u,p} + DC_{o,p} \right) F_{DC} \right] \tag{4.2}$$

subject to the constraints presented in Table 4.5. FHVAC and FDC are tuning parameters used to weight the different considerations (energy and comfort) of the objective function [96]. In this study, these parameters were kept constant, i.e.: F_{HVAC} = 1e-4 and F_{DC} = 5. These parameters were sized based on the maximum estimated values, over a one hour time step, for energy and discomfort, i.e. 10000 Wh and 0.2Kh, respectively, in order to have a balanced cost between both considerations (Eq. (4.2))

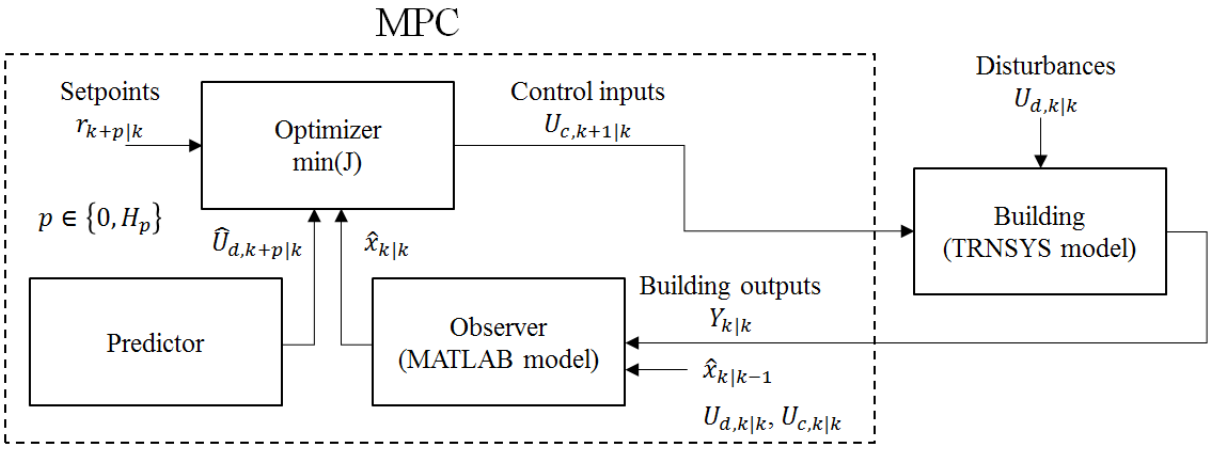

Figure 4.3: Model based predictive control architecture.

In this article, a control horizon $H_c = 1$ was chosen. A control horizon of H_c implies that the control inputs are allowed to fluctuate only over H_c of the H_p time steps during the optimization. It was chosen to implement the thermal discomfort as a soft constraint, i.e. as an element of the cost function instead of a hard constraint of the type $T_{set,min} \leq T_{in} \leq T_{set,max}$, creating a more robust MPC implementation. Using this approach, in the rare occasions when Q_{heat} or Q_{cool} are too small to keep T_{in} within the requested temperature range, the optimization routine will still find a solution, even when the cost factor F_{DC} is set to a higher value.

Table 4.5: MPC constraints

Constraints	Units
$AX(k+1) - B = 0$ (see section 4.3.1 for more details)	W
$X(0)_k = \hat{x}_{k\|k}$ (see section 4.3.1 for more details)	K
$Q_{heat} \leq Q_{heat,max} = 3295$	W
$Q_{cool} \leq Q_{cool,max} = 8304$	W
Electricity use for heating : $E_{heat,k} = Q_{heat,k}$	W
Electricity use for cooling : $E_{cool,k} = Q_{cool,k}$ / COP (COP=3)	W
Electricity use for lighting: E_{light}	W
Discomfort cost 'too cold': $DC_{u,k} = (T_{set,min} - T_{in,k}) \cdot \Delta t$	Kh
Discomfort cost 'too warm: $DC_{o,k} = (T_{in,k} - T_{set,max}) \cdot \Delta t$	Kh

The MPC controller was developed in MATLAB and the optimization procedure was handled by the YALMIP toolbox and the mixed-integer linear programming solver Gurobi.

4.4 Results

As mentioned previously, simulations were performed on an hourly basis for the months of June (warm-up period without any SW control, i.e. passive clear SW state S1) and July (period of analysis where SW states were defined by the different controllers under study).

4.4.1 Hour-by-hour SW states

Figure 4.4 presents the hourly SW states for the four controllers under study and the three different types of floor/lighting system configurations. Note that for concision, only the first week of July, which is considered "typical", is reported in that figure, and that the first day reported is a Sunday. Figure 4.4a, 4.4b and 4.4c illustrate quite different behaviors in terms of SW state evolution for the different controllers. Because of their nature, the rule-based controllers RBC1 and RBC2 present the exact same profiles of SW states for the three different floor/lighting configurations. On the other hand, SW states obtained from the GA and MPC controllers present different behaviors depending on the particular floor/lighting configuration. In Figure 4.4a, GA and MPC controllers with the LED system tend to set the SW state to S2 or a darker state over a longer period of time during occupancy hours compared to the controllers with a T8 lamps system (Figure 4.4b). This behavior is mainly due to the fact that the higher efficiency of the LED system (Figure 4.4a) calls for less daylight penetration for optimal control based on the overall energy consumption.

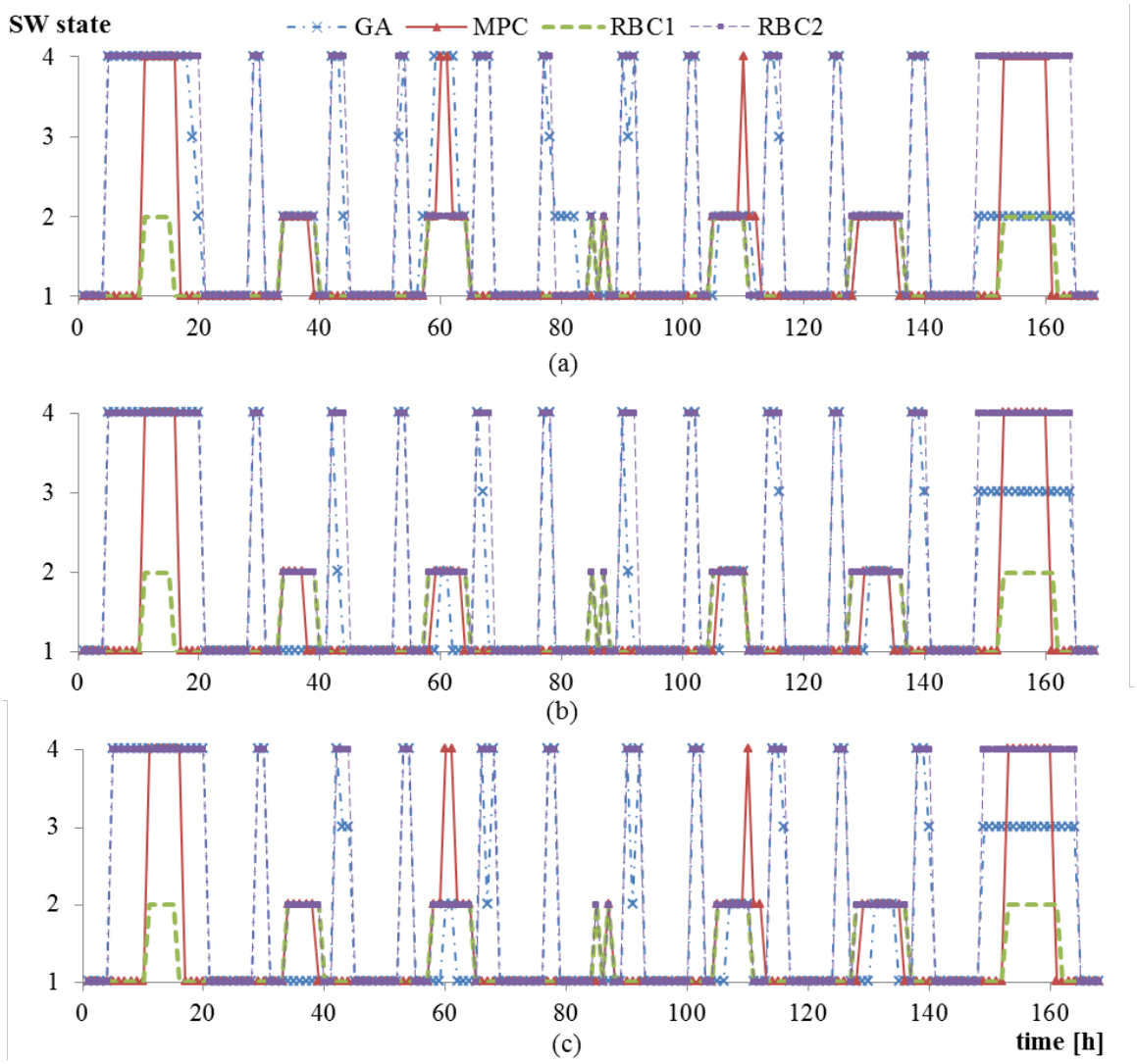

Figure 4.4: Hourly results of smart window states for the first week of July for the different control strategies considering a) a concrete floor and LED lighting system (Cr-LED), b) a concrete floor and T8 lighting system (Cr-T8) and c) a CLT floor and T8 lighting system (CLT-T8).

In all cases, one could also realize that the SW state profiles vary from one day to another. Of course, these variations come from a great combination of factors such as solar radiation and outdoor temperature. For example, the fourth day of the week (hours 72 to 95) presents lower solar radiation values (overcast day). For these hours and during occupancy, all controllers of Figure 4.4 limit the number of hours at darker SW state since solar gains are limited and daylighting tends to be maximized to limit lighting costs.

From Figure 4.4, we also realize that only two controllers (GA and RBC2) set the SW state to S4 during weekday hours with solar presence and non-occupancy, i.e. early and late daylight hours. This behavior minimizes cooling loads by keeping zone air and thermal mass temperatures to lowest values outside occupancy hours.

Figure 4.5 presents the occurrence (percentage) of each SW state for every hour of the full month of July considering the three types of floor/lighting configuration (Cr-LED in Figure 4.5a, Cr-T8 in Figure 4.5b and CLT-T8 in Figure 4.5c). Figure 4.5a and b confirm the fact that GA and MPC SW state profiles are adapted based on the artificial lighting system performance. Increasing the performance of that system will reduce the occurrence of the clearest SW state during occupancy to limit the cooling loads associated to undesired solar gains. These results highlight the fact that the full possible range of SW properties is further exploited with higher efficiency lighting systems. From Figure 4.5, it is also clear that the RBC1 controller, which is uniquely driven by daylight control, never uses the two darkest states of the SW, meaning that this type of control does not take fully advantage of the flexibility of SW technology. On the other hand, GA, MPC and RBC2 present between 10% and 31% of hours with the SW states at the darkest state S4, mostly occurring during non-occupancy hours as illustrated in Figure 4.4. GA and RBC2 are the two controllers that present the highest percentage of hours at the darkest states S3 and S4.

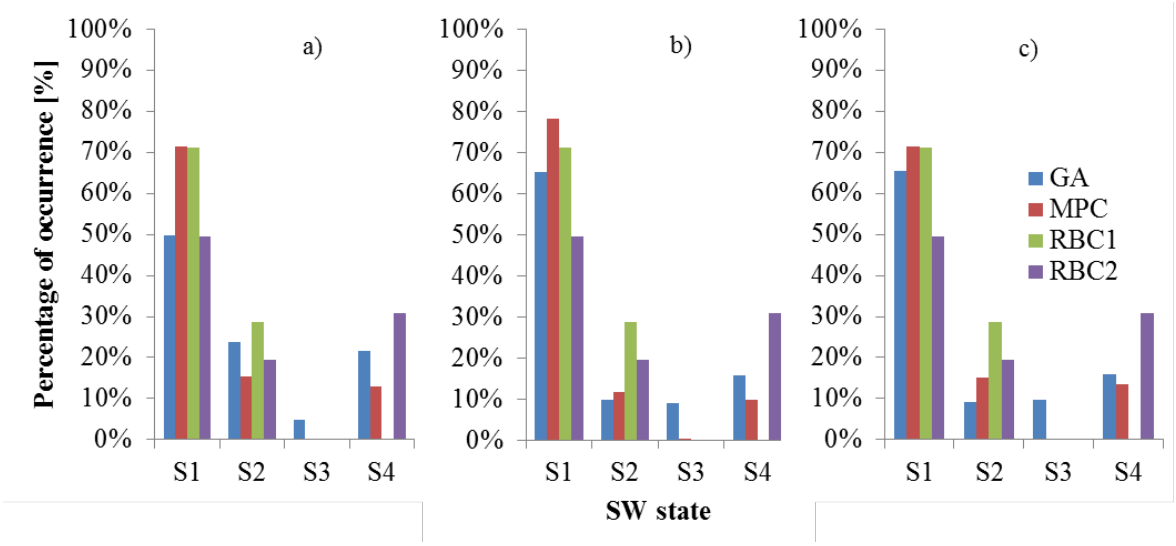

Figure 4.5: Percentage of occurrence for each SW state for every hour of the entire month of July considering a) Cr-LED, b) Cr-T8 and c) CLT-T8.

4.4.2 Respect of zone air temperature setpoints

While GA, RBC1 and RBC2 controllers considered air temperature setpoint requirements as hard constraints to be met at all time, MPC controller considered these setpoint requirements as soft constraints. This MPC particularity, designed for robustness, resulted in some hours outside setpoint requirements. Figure 4.6 presents the zone temperature overhead compared to setpoint requirements with the MPC. As illustrated in Figure 4.6, even if some hours present positive overhead temperature values, these overhead values are kept to fairly low values since too high values involve high cost penalty factors (DCo as presented in Table 4.5). While GA, RBC1 and RBC2 present 0 Kh as a thermal discomfort index (defined as the sum of the discomfort cost, see Table 4.5, of every hour), the thermal discomfort indices for MPC Cr-LED, MPC Cr-T8 and MPC CLT-T8 were 8.3 Kh, 10.5 Kh and 69.5 Kh, respectively. At the light of these results and as illustrated in Figure 4.6, the thermal discomfort index for the CLT building is higher compared to the indices for the concrete floor. One potential explanation is that the internal model of the MPC (validated for the concrete floor) presents higher estimation errors with CLT slab. These estimation errors imply that the predictions are somewhat less accurate and that the cooling system reactions are not fast enough to keep the zone temperature within the setpoints. However, one should note that air temperature increase of 0.5-0.8 K from the set-point is within the throttling range of thermostats in real building applications. Hence, even if the MPC results show slight deviations from the set point, all options would give similar indoor air temperature values in a practice.

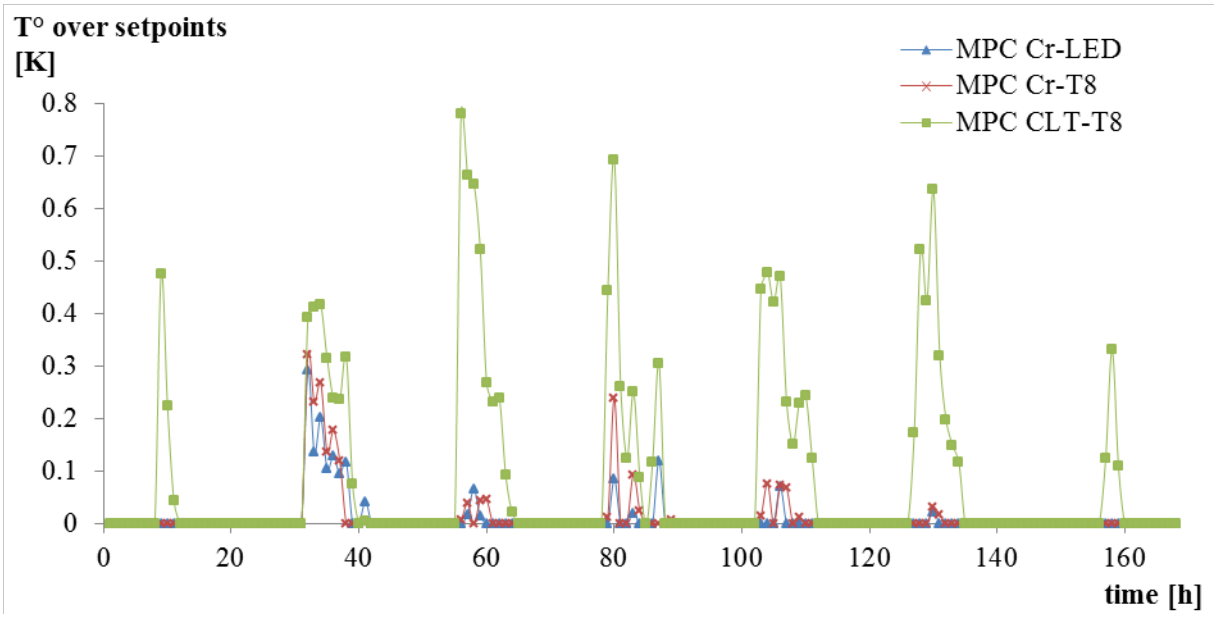

Figure 4.6: Zone temperature overhead compared to setpoint requirements with MPC.

4.4.3 Energy consumption and peak loads

Figure 4.7 presents the cooling, lighting and total energy consumption for the three different floor/lighting configurations. Figure 4.7a and b show that the trade-off between cooling and lighting energy consumption is quite different from one controller to the other. For the Cr-LED configuration, all controllers required around 0.35 kWh/m^2 of lighting energy but present different values of cooling (from 1.59 kWh/m^2 for the RBC2 up to 1.78 kWh/m^2 for the RBC1) resulting in total energy consumption of 1.95 kWh/m^2, 2.04 kWh/m^2, 2.13 kWh/m^2 and 1.94 kWh/m^2 for the GA, MPC, RBC1 and RBC2, respectively. Based on these results, the RBC2 controller presents the best overall energy consumption results of all controllers. In theory, the GA controller was considered as the optimal controller reference. However, as mentioned previously, due to the probabilistic nature of GAs, only a quasi-optimal controller reference was identified in the present case. Further simulations were performed with the GA controller with less restrictive parameters (higher values for phenotypes per generation, maximum number of generation and time steps considered, i.e. 50, 100 and 48, respectively) to determine if better results could be obtained. Indeed, total energy consumption from those new simulations with the GA controller resulted in slightly better results than those obtained and presented in this section. However, the computational time required to obtain those new results was more than tripled compared to simulations with

GA parameters presented in Table 4.4. These results highlight the fact that the GA controllers should really be considered as "quasi-optimal" rather than "optimal" if reasonable computational times are targeted, but that this nearly optimal reference is sufficient to evaluate how good the other controllers are in terms of "optimality".

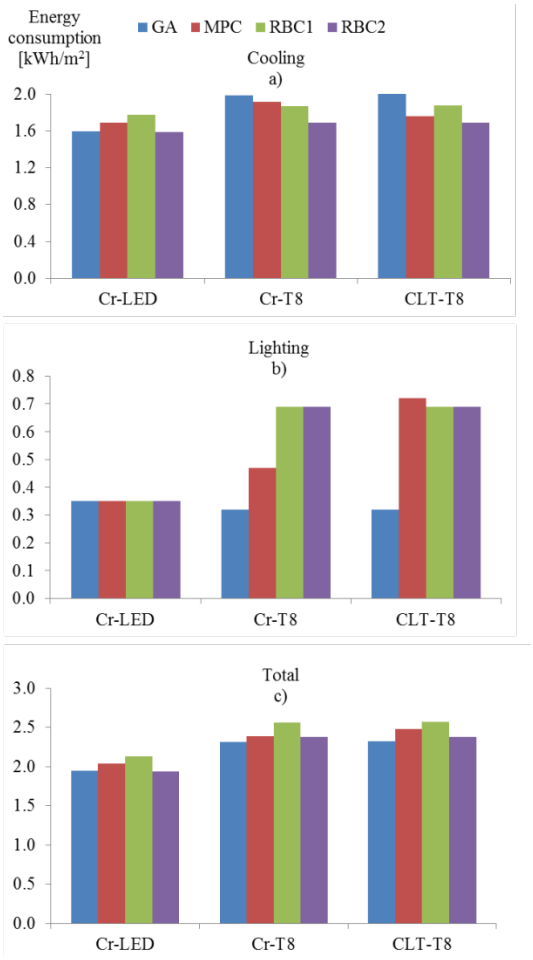

Figure 4.7: Energy consumption for a) cooling, b) lighting and c) total.

Furthermore, these results illustrate the fact that higher efficiency lighting systems reduce the need for complex controllers since the RBC2 controller achieves results that are as good as the quasi-optimal strategy. For the T8 lighting system (Cr-T8 and CLT-T8), the GA controller presents the lowest total energy consumption, followed by RBC2, MPC and RBC1, in order of performance. For all floor/lighting configurations, the difference in energy consumption performance varies from 4 % to 10% between the best and the worst case scenarios. In the light of these results, one could realize that, even if some controllers present slightly better results, all the state-of-the-art control strategies under study in this paper

present quite good performance in terms of energy efficiency. In other words, when the expertise for complex control implementation or the available budget is limited, buildings with SW technologies could be designed with a simple control strategy such as RBC1 or RBC2 and still offer very promising energy performance.

These results reveal that for the situation studied in this paper, with an office zone in summer situation, having thermal mass in the floor that is only passively interacting with the occurring heat flows, does not seem to create the required circumstances for MPC to outperform simpler controllers, although this strategy has been shown to be capable of dealing with complex thermal interactions for which it is beneficial to increase the controller intelligence.

Figure 4.8a, 4.8b and 4.8c show, respectively, the cooling, lighting and total peaks loads for the month July. Even if peak loads were not considered in the optimization objectives, it is interesting to see that the different control strategies also present different values of peak loads. For example, the GA controller with Cr-T8 configuration presents the highest cooling peak load (Figure 4.8a) of all controllers, but also presents the lowest overall energy consumption peak load (Figure 4.8c). Since some energy pricing strategies in the commercial sector include peak loads, future research should also assess the relative performance of the different controllers considering a more complex objective function that also considers peak loads.

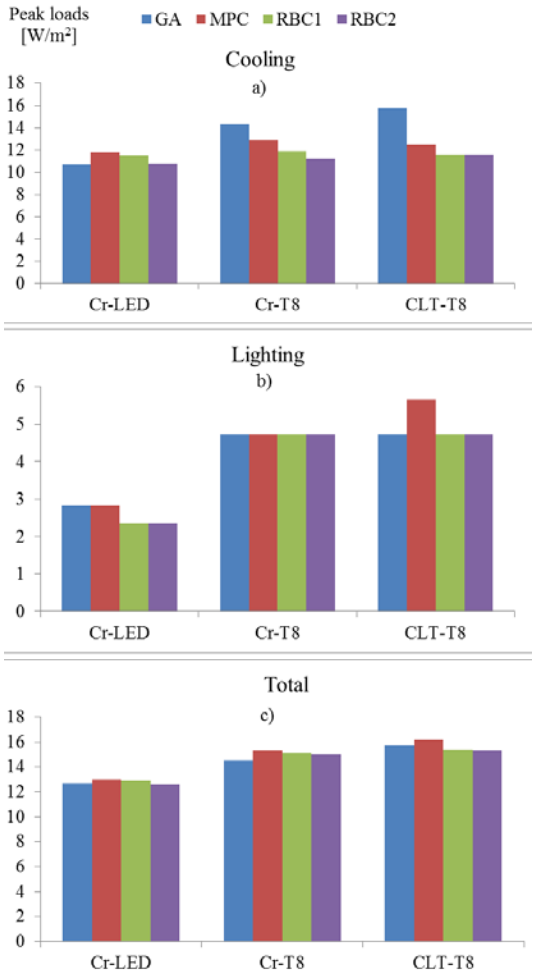

Figure 4.8: Peak loads for a) cooling, b) lighting and c) total for the month of July.

4.5 Conclusions

This paper presents and compares four state-of-the-art control strategies, i.e. controllers based on genetic algorithms, model predictive control and two similar types of rule-based controls. A building zone with smart windows was modelled in TRNSYS and a corresponding controller model was set up for the MPC.

All the results were analyzed during the month of July for a building located in Montreal, Canada. Results showed that all controllers under study were capable of handling the complex energy balance within the zone with varying temperature set points, controllable heating and cooling systems, controllable smart windows, lighting modulation and variations of heat loads (outdoor temperature, solar radiation and internal gains). The four analyzed

controllers presented different behaviors resulting in differences in terms of the total energy consumption (maximal differences between controllers of 4% to 10%). The ruled-based controller RBC2 (control based on daylight during occupancy hours and on cooling loads minimization during non-occupancy hours) presented the best real-time control strategy with results closest to quasi-optimal results obtained by the GA controllers. It was shown that the efficiency of the artificial lighting system impacts the relative performance between the different controllers. In the model under study, adopting a more efficient artificial lighting system resulted in a drop of relative performance between controllers.

In terms of comfort and energy performance, results for MPC showed that the performance of the controller relies on the accuracy of its internal building model. The investigated situation (i.e., a single office zone in summer conditions) was relatively simple, and did not offer sufficient flexibility in terms of temperature set points, thermal mass loading or unloading, multi-zone interactions, etc., so that the increased intelligence of the MPC was not that useful compared to simpler controllers. Future research should focus on the assessment of MPC model sensitivity as well as on the development of parametrization procedures for efficient MPC control for different construction types and geometries. Metamodeling [97] could also be used to predict the building dynamics.

The GA and MPC controllers based their control actions on a simple objective function aiming at minimizing the total (cooling/heating + lighting) energy consumption. While the MPC controller presented good performances, the limited number of design variables and the simplicity of the zone considered did not allow it to out stand compared to rule-based controller RBC2. Since GA and MPC algorithms are powerful tools that could easily accept more complex objective functions or scenarios, they present the potential to level up the control decisions to higher levels that include other optimization variables. For example, in this paper the peak load reduction in energy cost strategies was mentioned. Further studies should broaden the assessment of the MPC and GA controllers' performance considering more complex objective functions that include interactions with other zones and with the electromechanical systems. Since these strategies are more difficult and costly to implement

compared to rule-based strategies, it is likely that they will stand out from simpler control strategies only in situations involving complex systems, interactions, and objective functions.

It should be mentioned that several assumptions were made in this study (representative office zone, fixed occupancy and loads schedules, specific façade orientation and building location, simplified visual and thermal comfort analysis), and therefore, conclusions should be interpreted and generalized cautiously. Nevertheless, this work provided an overview of the potential of different control strategies for smart window control and a methodology to compare these strategies.

CHAPTER 5 OFFICE BUILDINGS WITH ELECTROCHROMIC WINDOWS: A SENSITIVITY ANALYSIS OF DESIGN PARAMETERS ON ENERGY PERFORMANCE, AND THERMAL AND VISUAL COMFORT

Abstract

In this paper, a representative office building zone with an electrochromic (EC) glazed façade was simulated in TRNSYS and Radiance/Daysim for a large number of different combinations of design parameters (i.e. location, façade orientation, window control, window-to-wall ratio, internal gains, thermal mass and envelope air tightness). Results of energy consumption, peak energy demand, useful daylight index (UDI) and predicted percentage of persons dissatisfied (PPD) for a total of 7680 scenarios were obtained and used in a sensitivity analysis considering the Main effect of the building parameters. The relative influence of the parameters is presented and the different designs improving the outputs are determined. Results have shown that the greatest total energy savings considering EC windows are for warmer climates with higher solar radiation exposures. The presence of an EC window mostly influences the cooling peak load and acts as an alternative solution to thermal mass from the perspective of peak reductions. While the choice of the specific window control strategy is having a limited impact on the energy savings and peak load reductions, the analysis revealed that this parameter has a larger impact on the visual comfort (UDI). The use of smart window does not appear to greatly influence the thermal comfort within the zone (small impact on the PPD).

Résumé

Dans cet article, une zone à bureaux typique incluant une fenestration électrochrome (EC) en façade est modélisé dans TRNSYS et Radiance/Daysim pour simuler une grande variété de combinaison de paramètres de design (c.-à-d. la localisation, l'orientation de la façade, le control des fenêtres, le pourcentage de fenestration, les gains internes, la masse thermique ainsi que l'étanchéité à l'air de l'enveloppe). La consommation d'énergie, la pointe de consommation, l'indice de lumière naturelle utile (UDI) et la prédiction du pourcentage d'insatisfaction (PPD) pour un total de 7680 scénarios sont obtenues et utilisé dans une analyse de sensibilité considérant l'effet principal des paramètres de design du bâtiment. L'influence relative des paramètres est présentée et les différents designs améliorant les résultats sont déterminés. Les résultats montrent que la meilleure économie d'énergie en considérant des fenêtres EC se trouve dans des climats chauds avec une exposition élevée aux rayons solaires. La présence d'une fenêtre EC influence principalement la charge de refroidissement maximale et agit comme une solution alternative à la masse thermique en termes de réduction potentielle de cette charge maximale. Bien que le choix de la stratégie de contrôle ait un impact limité sur l'économie d'énergie réalisée et la réduction de la charge maximale, l'analyse permet de constater que ce paramètre a un impact encore plus important sur le confort visuel (UDI). L'utilisation de fenêtres intelligentes ne semble pas influencer grandement le confort thermique à l'intérieur de la zone (faible impact sur le PPD).

5.1 Introduction

Smart windows (SW) are window technologies offering a control flexibility in terms of solar heat gains, daylight and glare in building perimeter zones. This flexibility is achieved through their capacity to adapt their optical properties (ranging from a clear state to a fully colored state) through different type of stimuli such as gas concentration, temperature, solar radiation or an applied voltage. Among the most promising SW technologies, electrochromic (EC) windows (whose tinted states are controlled by an applied voltage) provide views to the outside regardless of their colored states, limit glare [53] and are seen as the most reliable and promising technologies in the field of energy-efficient window technologies [12].

Although current EC window technologies are offering a great range of properties [12] [14] [98] [99], the use such technologies also requires a good understanding of the appropriate control to be implemented as well as an established communication network with other relevant systems (such as with the artificial lighting or HVAC systems) [14]. With the increasing interest toward EC technologies in the last decades, outcomes from numerical and field studies on the topic were published and has led to the diffusion of early-market design guidance information [41].

Early numerical simulations of office buildings compared a spectrally selective low-E window technology with EC technologies (reflective and idealized) in a cooling dominated location [27]. Three control strategies were considered, i.e. control based on daylight, on solar radiation or on space load. Results revealed that the total energy savings could be achieved by using EC windows compared to the conventional low-E windows and that the daylight control was offering the best overall energy performance. Similar simulation results were also obtained in other studies considering other locations [36], residential applications [37] or heating dominated climates [38].

A field study [100] analyzed the performance of electrochromic windows controlled in various ways so as to optimize daylight while avoiding glare compared to a spectrally selective low-e window. This study monitored lighting energy reduction of 26% ± 15% and a cooling load reduction of 7 ± 4%.

A recent study on advanced control strategies [101] for smart windows also has shown that heuristic controls give quite good energy and comfort performance compared to quasi optimal controllers based on genetic algorithms and model predictive control. Heuristic controls thus seem to be so far the best trade-off control strategies in terms of ease of implementation versus potential benefits (energy and comfort wise).

Nowadays, the advances in the field of EC windows have led to new field studies combining EC technologies with other complementary technologies such as photovoltaic cells [102] or ventilated façades [103].

Despite evidence that smart windows can enhance building performance in specific scenarios, there is still a lack of general and systematic design guidelines to introduce smart windows in building designs. In particular, based on literature, it is difficult to establish which building designs are the most improved by using smart windows, and to what extent. Sensitivity analysis techniques have recently been gaining a lot of attention in order to identify the most influential design variables in terms of building performance [104]. For example, a recent study has presented an uncertainty and sensitivity analysis of energy and visual performances for an office building with external venetian blind shading in a hot-dry climate [105]. It was found that glazing design parameters such as the window-to-wall ratio (WWR), the glazing type, the blind orientation and the slat angle were the most influential. Another study combined sensitivity analysis and simulation-based optimization in order to optimize the thermal and energy performance of residential buildings in the Argentine littoral region [106]. The case under study has proven that this approach could drastically improve the thermal and energy performance. These examples highlight the fact that sensitivity analysis techniques emerge as a useful tool for building design process, but no precedent was found in which they were used for building designs with smart windows.

The main objective of this study is to provide decision-making information on building design with efficiently controlled electrochromic windows. In this paper, a sensitivity analysis is presented to assess the relative effect of the main building design parameters on

energy and comfort improvements related with the use of a smart window. Section 5.2 introduces the building energy and daylight models and the sensitivity analysis technique that was developed for the present work. A series of simulations in which several building design variables were varied simultaneously was performed. Based on the concept of "Main effect", the most significant variables influencing energy consumption, peak demand and comfort in the presence of SW are reported in Section 5.3.

5.2 Methodology

5.2.1 Simulation software

In this study, energy and comfort performance data were obtained for office buildings using TRNSYS, a state-of-the-art and flexible transient system simulation tool [107]. The TRNSYS built-in multi-zone building model (Type 56) offers the possibility to adapt the window properties at every simulation time step through a variable window ID feature. This feature facilitates the assessment and comparison of different smart window control strategies. While the building thermal model (section 5.2.3), the thermal comfort model (section 5.2.4) and the control strategies (section 5.2.6) were directly implemented within TRNSYS, the daylight and artificial light simulations (section 5.2.5) were performed with Daysim [87] and Radiance [88], respectively, and inputted into TRNSYS in the form of lookup tables. Batch files for parametric study and the post-processing of results were implemented within MATLAB. A simulation time step of one hour was used in this work.

5.2.2 Climates

Simulation results were obtained for ten US and Canadian locations (see Table 5.1) selected to cover a wide range of climates. EnergyPlus weather data files (.epw files) were used for simulations. Table 5.1 presents annual heating and/or cooling features for each location, i.e. heating degree days (HDD) and averaged end-use energy consumption (total (E_{tot}), heating (E_{heat}) and cooling (E_{cool})) as well as their respective standard deviations (σ). Only the energy required for heating, cooling and lighting was included in the total energy consumption. Energy and standard deviation results in Table 5.1 are presented per unit of floor area. HDD values were calculated from the same weather data files that were used for simulations. Averaged values for E_{tot}, E_{heat} and E_{cool} and their standard deviations were obtained over a series of building designs for a given location (city) as explained later. Note that the values

of E_{tot} in Table 1 might appear to be small compared to typical total energy intensity of the current Canadian and American building stocks, but it should be mentioned that it only includes the sensible energy required for the heating, cooling and lighting of a high-performance modern building. In this study, latent loads were not considered since SWs only affect sensible loads.

Table 5.1: Climate information

Locations	HDD [°C]	E_{tot} [kWh/m^2]	$\sigma_{E,tot}$	E_{heat} [kWh/m^2]	$\sigma_{E,heat}$	E_{cool} [kWh/m^2]	$\sigma_{E,cool}$
US locations (ASHRAE 90.1 zones)							
Atlanta, GA (3A)	1673	34.3	10.5	1.5	1.9	23	8.8
Chicago, IL (5A)	3429	35.2	6.7	9.0	7.4	16	6.7
Miami, FL (1A)	68	43.5	12.8	0.0	0.0	34	10.0
New-Orleans, LA (2A)	707	37.7	11.8	0.3	0.4	28	9.3
San Francisco, CA (3C)	1557	28.5	12.0	0.1	0.3	19	9.5
Washington, D.C. (4A)	2293	32.6	8.6	3.0	3.5	20	7.9
Canadian locations (ASHRAE 90.1 zones)							
Calgary, AB (7)	5147	37.0	7.3	13.2	9.7	13.6	7.4
Montreal, QC (6A)	4493	37.5	7.6	12.5	9.6	14.9	6.9
Toronto, ON (6A)	4089	35.6	7.1	11.8	9.4	13.5	6.1
Vancouver, BC (5A)	3020	28.0	7.3	3.6	4.0	13.9	7.0

5.2.3 Building model

Building geometry and construction

A representative six-sided box-shaped office zone of the building was modeled with 100 m^2 of floor area, i.e. 10 m width (W) by 10 m depth (D), and a ceiling height of 3 m (H). The plenum zone was not modeled. Four different orientations (north, east, south and west) were simulated for the exterior façade wall. The façade is composed of an electrochromic smart window (see Section 5.2.6 for further details on the smart window system and properties) and an opaque exterior wall (concrete siding, lightweight frame filled with mineral wool

insulation and gypsum indoor finishing) with a U-value of 0.45 W/m^{2}K. All other surface boundary conditions of the model (internal walls, floor and ceiling) were modeled considering identical zone conditions for adjacent zones. In this study, direct solar gains were assumed to be uniformly distributed on the floor (geosurf = 1). On the other hand, diffuse solar gains were distributed according to absorption-transmission weighted area ratios for all surfaces (TRNSYS simple model).
Three different window-to-wall ratios (WWR = 0.33, 0.50 and 0.67) were considered in the study. For every façade configuration, the window width corresponded to the zone width (10 m) and the window sill was located at 1 m above the floor.

Two building façade air tightness ratings (rated at 75 Pa [108]) were considered in this study, i.e. a modern air tight construction (0.5 ACH) and a leakier envelope construction (2 ACH). Hourly infiltration rates were calculated in the model based on the façade rating adjusted with weather data such as outside air temperature (T_{out}) and wind speed [109].

The concrete floor slab thicknesses was varied between two values, i.e.: 0.038 m (1.5 inch) and 0.254 m (10 inches) (i.e. C=71.53 kJ/m^{2}K and 476.86 kJ/m^{2}K, respectively). These two floor constructions were selected to represent different values of the effective thermal mass of the zone (low versus high).

Gains and schedules

Internal gains account for artificial lighting, occupancy and equipment. Based on the purpose of this work, only sensible heat has been included in the model. Two scenarios were studied for internal gains, i.e. low internal gains and high internal gains [110]. Table 5.2 presents the building zone heat gains as well as their respective radiative and convective fractions for the low and high internal gain scenarios, respectively.

Table 5.2: Low and High internal gains (net sensible)

	Radiative [W]		**Convective [W]**		**Total [W]**		**Total/floor area [W/m2]**	
	Low	**High**	**Low**	**High**	**Low**	**High**	**Low**	**High**

Equipment	350	1050	150	450	500	1500	5	15
Lighting	188	375	130	261	318	636	3	6
Occupants (5)	263	525	113	225	375	750	4	8
Total	800	1950	393	936	1193	2886	12	29

To represent a typical transient variation of internal gains and lighting requirements in office buildings, week schedules have been created based on the ASHRAE 90.1 (Table G-I) schedules for office occupancy. The only internal gains considered during week-ends were the electronic appliances at 15% of their maximal power usage.

Lighting system

Two types of artificial lighting systems were considered for the study. The first type of lighting system relies on sixteen T8 lamps (64 W of nominal power per lamp) (lamp dimensions of 0.54 m width × 1.15 m long) uniformly distributed over the ceiling. Based on the technological advances in the field of artificial lighting [89], a second high-efficiency lighting system has also been simulated. For simplicity, this system presents the same lamp dimensions and position as for the first lighting system; however the T8 lamps are replaced by a more efficient LED system consuming half the power of the T8 lamps for the same illuminance output (32 W of nominal power per LED lamp). While the T8 lamps lighting system is part of the high internal gains scenario presented in the previous subsection (High gains in Table 5.2), the LED lighting system is considered in the low internal gains scenario (Low gains in Table 5.2). Artificial lighting system properties are summarized in Table 5.3. The daylight zone dimming control presented in Table 5. is based on the workplane illuminance setpoint (Wp_{sp}). The required artificial light output fraction (f_L) is calculated to respect Wp_{sp}. The light power input fraction is then obtained based on the value of f_L. Figure 5.1 illustrates the artificial lighting system layout. Note that specifications of Table 5.3 were used to define lightning gains of Table 5.2. To obtain lightings gains of Table 5.2, one should also consider the heat to return factor.

Table 5.3: Artificial lighting systems

Nominal LPD	10.2 W/m^2 (T8 lamps) and 4.4 W/m^2 (LED system)

Ballast factor (T8 lamps)	0.86
GDF	0.81 (GDF = LDD · LLD = 0.9 ·0.9)
Wp_{nat}	500 lux (on the sensor "S" in Figure 5.1)
Daylight zone dimming control	$f_P = \begin{cases} 0 & f_L = 0 \\ f_{P,min} & 0 < f_L < f_{L,min} \\ \left[f_L + (1 - f_L) f_{P,min} - f_{L,min} \right] / (1 - f_{L,min}) & f_{L,min} \le f_L \le 1 \end{cases}$

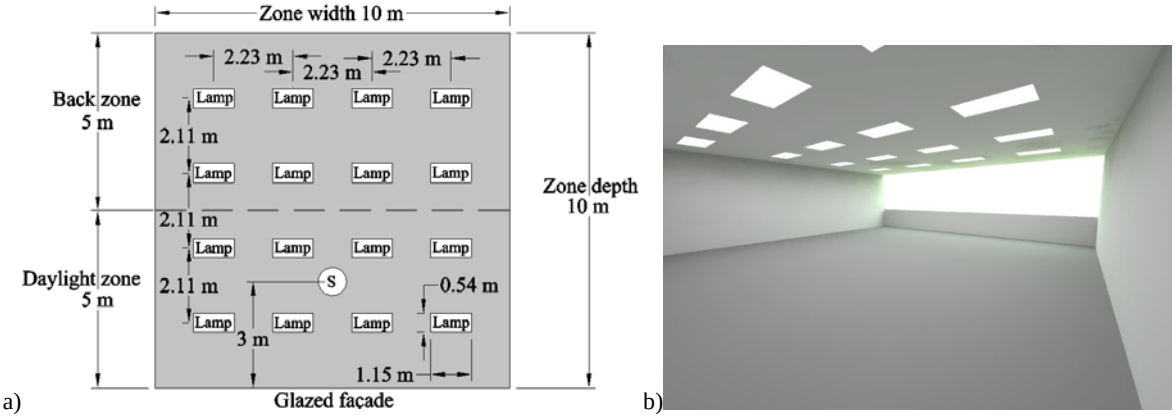

Figure 5.1: (a) Artificial lighting system disposition (Top view), (b) 3D representation of the zone natural and artificial light sources simulated with Daysim and Radiance, respectively.

HVAC system

It was assumed that the calculated heating load Q_{heat} and cooling load Q_{cool} acted directly on the air node of the building model, and were satisfied instantly by the HVAC&R system. The cooling system considers a constant coefficient of performance (COP) of 3. The indoor temperature was allowed to vary between 21°C and 25°C during occupancy, based on the acceptable ranges of temperatures provided in ASHRAE 55-2013. Outside of the occupancy hours, these temperature limits are respectively lowered and raised by 3°C. The heating and cooling systems were sized to meet the heating/cooling requirements at all time. The required flow rate of outside air was calculated based on the ASHRAE 62.1-2016 standard with the breathing zone outdoor airflow calculations considering an outdoor airflow rate per person of 2.5 L/s-pers, an outdoor airflow rate per unit area of 0.3 L/s-m^2 and a zone air distribution

effectiveness (E_z) of 0.8. A heat exchanger was used to recover heat between the air exhaust and make up air with 60 % efficiency. Note that all the heating and cooling energy needs reported in this paper are the energy consumed to satisfy the thermal loads and not the thermal loads themselves.

5.2.4 Thermal comfort model

The thermal comfort was assessed through the calculation of the Predicted Percentage of Dissatisfied (PPD) as defined in the 7730 ISO Standard [111]. Occupants' conditions (clothing, metabolic rate and relative air velocity) for typical winter and summer seasons were defined based on ASHRAE 55 requirements and are summarized in Table 5.4. The only difference between winter and summer conditions is the clothing number since people's clothing is influenced by the surrounding conditions [112]. In this work, values of PPD were calculated at each time step for both the winter (PPD_{win}) and summer clothing conditions (PPD_{sum}). The actual PPD indicator at each time step was then chosen between PPD_{win} and PPD_{sum} based on the corresponding daily averaged PPD offering the smallest percentage of dissatisfaction. This approach captures the occupants' decisions to adapt their clothing based on the surrounding conditions.

Table 5.4: Winter and summer conditions fort thermal comfort

	Winter conditions	**Summer conditions**
Clothing factor [clo]	1.0	0.5
Metabolic rate [met]	1.1	1.1
Relative air velocity [m/s]	0.1	0.1

The calculation of the PPD also involves the zone air temperature and the mean radiant temperature (T_{MR}), which are both calculated through the TRNSYS model internal calculations. This model assumes that T_{MR} is the area weighted mean surface temperature of all surfaces of the zone. Although this model would only give a rough approximation of the actual T_{MR} within a specific zone, this approach is widely used in practical engineering applications [113] and gives results accurate enough to evaluate the level of thermal comfort within the zone.

5.2.5 Lighting monitoring and visual comfort model

To offer proper lighting on the workplane (at a 0.8 m height from the floor level) in terms of minimal illuminance requirements, a light sensor has been positioned at the center of the room width and at a 3 m depth from the glazed wall (represented by the "S" symbol in Figure 5.1). Illuminance measurements on this sensor are defined as the representative values for the workplane of the daylight zone (Dz). The luminosity requirement (WP_{req}) on the sensor has been set to 500 lux [84] during occupancy hours. For both lighting system types (T8 and LED), the lamps were controlled in two separate groups (i.e. the lamps of the daylight zone and the lamps of the back zone). While the back zone lamps were fully switched on at all time during occupancy hours, the lamps of the daylight zone were dimmed in a fashion similar to the EnergyPlus Continuous/OFF dimming control [90] to assure minimal visual comfort requirements while taking advantage of daylight whenever possible (see Table 5.3 for further details regarding the daylight zone dimming control). The index used to assess the visual comfort (through useful daylight levels) in the building zone is the Useful Daylight Illuminance (UDI). In this work, the UDI is defined as the percentage of hours of the working year where daylight illuminance values on the workplane fall between 100 lx and 2000 lx, inclusively. The higher the UDI, the more likely it is that occupants feel comfortable from the visual standpoint.

While daylight is desired in building zones to improve occupant's visual comfort, natural light could also cause visual discomfort such as glare in situations of overabundance. Many indicators have been developed in the past to assess the glare potential in perimeter buildings zones [114]. In this paper, the glare potential was assessed with a maximal illuminance setpoint of 2000 lx [115]. Situations where illuminance values were over 2000 lx on more than 20% of the workplane in the daylight zone area were considered as periods of visual discomfort caused by glare.

5.2.6 Window system and control strategies

The smart window modeled in this study has a 1.63 W/m^2K U-value. The double glazing includes an electrochromic layer whose optical properties can be varied by an applied voltage

[12]. The electrochromic layer was applied on the surface 2, i.e. the internal surface of the external glazing, in order to limit undesired solar heat gains from absorbed and reemitted heat as well as to increase thermal and visual comforts. Four possible states of opacity, from clear to dark, have been included in the model. Table 5.5 provides the SW center of glazing Solar Heat Gain Coefficient (SHGC), visible transmittance (Tvis) and solar transmittance (Tsol) properties at normal incidence. While properties at normal incidence of Table 5.5 are presented for readers' benefits, one should note that the model uses the complete and detailed angle dependent properties available in the IGDB (International Glazing Database available online) and obtained through the use of Berkeley Lab WINDOW software.

Table 5.5: Smart window center-of-glazing properties

Smart window states	**SHGC [-]**	**Tvis [%]**	**Tsol [%]**
State 1 (S1) (bleached)	0.47	62.1	38.1
State 2 (S2)	0.17	21.2	8.6
State 3 (S3)	0.11	5.9	2.4
State 4 (S4) (fully tinted)	0.09	1.5	1.0

In the model, every time the state of the window is changed, the corresponding properties of that new state are also applied to the window. Since the time step (one hour) considered in the simulation results is greater than the time required to switch from one state to the other (about 5 minutes considering an ideal window designed with a sufficient amount of bus bars) [81], it was assumed that window properties over a time step were constant.

In this paper, three main types of rule based control (RBC) strategies were considered (i.e. RBC based on daylight [51][100], incident vertical solar radiation (incident on the zone façade) [51][116] and net window heat flux [117]) and are explained in the following subsections. Table 5.6 presents the main parameters considered in each RBC strategy. As illustrated in Table 5.6, every RBC considers glare control as defined in Section 5.2.5. Each type of RBC also considers either two or four possible states for control, i.e.: a 2 state (clear/dark) control and 4 state (clear/dark + 2 intermediary states) control.

Table 5.6: Smart window rule-based control (RBC) strategies

RBC ID	RBC type	RBC setpoints	Glare control	Possible SW states
RBC1	Daylight	$Wp_{nat,max}$ = 500 lx	$ill_{max,Dz}$ = 2000 lx	2 states
RBC2				4 states
RBC3	I_v	$I_{v,max}$ = 95 W/m^2	$ill_{max,Dz}$ = 2000 lx	2 states
RBC4		$I_{v,max}$ = 315 W/m^2		4 states
RBC5		$I_{v,min}$ = 63 W/m^2 $I_{v,max}$ = 95 W/m^2		2 states
RBC6		$I_{v,min}$ = 63 W/m^2 $I_{v,max}$ = 315 W/m^2		4 states
RBC7	q_{net}	T_{ave} = 23°C	$ill_{max,Dz}$ = 2000 lx	2 states
RBC8				4 states

In this paper, the use of a controlled smart window refers to a smart window considering a control logic based on one of the RBCs presented in Table 5.6.

Daylight (RBC1 and RBC2)

In these cases, the SW state decisions were based on a three level control scheme as illustrated in Figure 5.2. First of all, the controller evaluates if the building zone is in cooling mode or not. For occupancy hours where the building is in cooling mode, a control trade-off appears between the undesired solar heat gains and the desired natural light. In such situations, the control is based on the selected RBC strategy. The RBC strategies aim at selecting a SW state allowing some natural light to enter into the zone (to increase daylight and reduce lighting energy) while trying to limit overheating (to reduce cooling loads) and glare. Outside occupancy hours, the trade-off disappears and the controller selects the colored SW state, S4, to limit cooling loads as much as possible. On the other hand, when the building is not in cooling mode, the SW controller is set to maximize daylight/solar heat gains. In such situations, while the bleached SW state, S1, is selected during non-occupancy hours, the clearest state that respects glare requirements (see Section 5.2.5) is selected during occupancy hours.

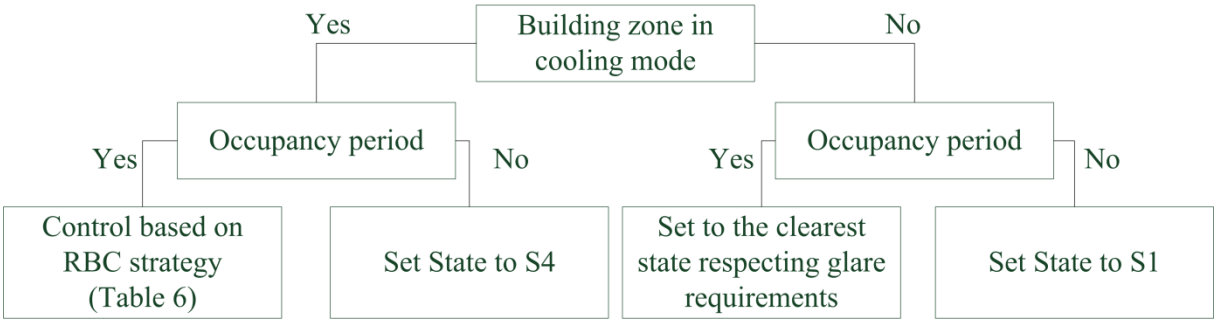

Figure 5.2: Daylight and I_v RBC schemes.

The daylight control strategies (i.e. RBC1 and RBC2 in Table 5.6) monitor the daylight illuminance on the workplane (sensor "S" Figure 5.1) and select the SW state that maximizes it without over lighting ($Wp_{nat,max}$ = 500 lx) to limit heat gains within the zone. One should note that glare control has priority over daylight control (i.e., if glare occurs in a situation where daylight on the workplane is not maximized, the SW state will still change to a darker state that meets glare control requirements). The daylight controls strategies work identically for both the 2 state and 4 state controls.

Iv – incident vertical solar radiation (RBC3 to RBC6)

The SW state decisions were based on the three level control scheme illustrated in Figure 5.2. However, in this case, the RBC (i.e. RBC3 to RBC6 in Table 5.6) is based on the vertical solar radiation (I_v) incident on the zone façade. The SW state is selected based on setpoints for I_v. For the 2 state control, only one setpoint ($I_{v,max}$) is defined. If I_v is greater than $I_{v,max}$, the SW state is switched to the colored state S4. Otherwise ($I_v \leq I_{v,max}$), the SW state is set to the bleached state S1. For the 4 state control, two setpoints ($I_{v,min}$ = 63 W/m^2 and $I_{v,max}$) were defined. While bleached state is selected when $I_v \leq I_{v,min}$, the colored state is selected when $I_v > I_{v,max}$. The two intermediate state are chosen (linear interpolation) when I_v falls between the two threshold setpoints. In this work, two values for $I_{v,max}$ were studied (i.e., $I_{v,max}$ = 95 W/m^2 and $I_{v,max}$ = 315 W/m^2) [27]. As for the daylight control, glare control has priority over the control on I_v for this type of RBC.

RBC based on incident solar radiation are seen are very promising heuristic control strategies due to their relatively simple control scheme and potentially inexpensive solar radiation sensors [118].

Net window heat flow control (RBC7 and RBC8)

This type of RBC bases its decisions according to the net heat flow, q_{net}, passing through the window:

$$q_{net} = U_w \cdot (T_{out} - T_z) + SHGC \cdot I \quad (5.1)$$

where U_w is the overall window heat transfer coefficient, T_{out} and T_z are the exterior and interior air temperatures, SHGC is the overall window solar heat gain coefficient and I is the total incident solar radiation.

In the net heat flow control [117], the state of the SW is selected based on $q_{net,}$ the zone temperature (T_z) and the average temperature value between the minimum and maximum zone temperature setpoints ($T_{ave} = (T_{z,min} + T_{z,max})/2$). If $T_z \leq T_{ave}$, the space is considered to be in heating mode (closer to heating) and the state offering the higher q_{net} will be selected. On the other hand, for $T_z > T_{ave}$, the space is considered to be in cooling mode and the SW state offering the lowest q_{net} will be selected.

While the heat transfer coefficient (U_w) of some dynamic window technologies such as blinds within the glazing could be influenced by the state of the window [117], the heat transfer coefficient of the EC window considered in this work remains the same regardless of the window color state. This being said, one could state that the net heat flow as defined in Eq. (5.1) will thus always be larger for state S1 compared to state S2, and for state S2 compared to state S3 and so on. The net heat flow control algorithm as described above thus simplifies as follows. For the 2 state control, the bleached state S1 is selected for $T_z \leq T_{ave}$ and the colored state S4 is selected for $T_z > T_{ave}$. For the 4 state control, the bleached state S1 is selected for $T_z \leq T_{z,min}$, S2 is selected for $T_{z,min} < T_z \leq T_{ave}$, S3 is selected for $T_{ave} < T_z \leq T_{z,max}$, and the colored state S4 is selected for $T_z > T_{z,max}$. Similarly to the daylight and solar radiation RBC control types, the glare control for this type of RBC has priority over the net heat flow control decisions.

5.3 Sensitivity analysis – Main effect

In this paper, a sensitivity analysis was performed to assess the effect of the principal design parameters (**X**) on different outputs (**Y)** for buildings with smart windows. Table 5.7 presents the eight building parameters (N = 8) under study. These parameters were selected based on the fact that they are common design parameters and/or relevant parameters related to smart windows. While other design parameters (such as the building envelope or other solar shading devices) could have been included in this study, the authors limited to eight the number of parameters given the scope of this study and the extensive amount of simulations involved. While the 4^{th} parameter (ID = 4) in Table 5.7 is considered in the analysis to assess the influence of replacing a reference window (represented by the passive clear state S1) by a controlled SW (with RBC), the 5^{th} parameter can be used to compare the RBCs against each other. Each parameter (e.g., location, orientation, etc.) has been attributed an ID (k) and has a finite number (n_k) of possible values (e.g., the orientation is the second parameter (k = 2) with $n_k = n_2 = 4$ possible values, i.e. north, east, south and west). All possible combinations of the different parameters were simulated. Given the number of possible values for each parameter, a total of 7680 simulations were thus performed. Depending on the parameter under study, those 7680 simulation results are then organized into different subsets for the analysis.

Table 5.7: Building design parameters studied in the sensitivity analysis

ID (k)	Parameter (X)	Possible values	Number of	S_k

			designs (n_k)	
1	Location (City)	Atlanta | Chicago | Miami | New-Orleans | San Francisco | Washington | Calgary | Montreal | Toronto | Vancouver	10	768
2	Orientation (Ori)	North | East | South | West	4	1920
3	Window to wall ratio (WWR)	0.33 | 0.50 | 0.67	3	2560
4	Presence of a smart window (SW)	Yes | No	2	3840
5	SW rule-based controls (RBC)	RBC1 to RBC8	8	960
6	Internal gains (IG)	Low | High	2	3840
7	Thermal mass	Low | High	2	3840
8	Air tightness ratings at 75Pa (I75)	0.5 ACH | 2 ACH	2	3840

The analysis was based on the Main effect [119], i.e. a global sensitivity index that focuses on how the building parameters (**X**) influence the simulation outputs (**Y**). The *main effect* of the k^{th} parameter (x_k) on **Y** is denoted ME_k(**Y**). To obtain ME_k(**Y**), the 7680 simulations are separated according to the x_k values into n_k groups. In other words, all simulations with the same x_k values are gathered together. The average of the outputs **Y** in each group is then calculated:

$$\overline{Y}_{x_{kj}} = \frac{1}{S_k}\sum_{i=1}^{s_k} Y_{i,x_{kj}} \tag{5.2}$$

where $\sum_{i=1}^{S_k} Y_{i,x_{kj}}$ includes all the simulation results (i = 1, 2…, S_k) with the j^{th} possible value for x_k. Note that S_k is the number of sample in the group over which the outputs are averaged, i.e. $S_k = 7680/n_k$. The Main effect for this parameter x_k is then obtained by taking half the difference between the maximum and the minimum values of the n_k calculated $\overline{Y}_{x_{kj}}$:

$$\mathrm{ME}_k\left(\mathrm{Y}\right)=\frac{1}{2}\left(\overline{\mathrm{Y}}_{x_k\,\max}-\overline{\mathrm{Y}}_{x_k\,\min}\right) \tag{5.3}$$

where

$$\begin{aligned}\overline{\mathrm{Y}}_{x_k\,\min}&=\min\left(\overline{\mathrm{Y}}_{x_{kj}}\right)\\ \overline{\mathrm{Y}}_{x_k\,\max}&=\max\left(\overline{\mathrm{Y}}_{x_{kj}}\right)\end{aligned} \tag{5.4}$$

Measured outputs (Y)

The outputs of interest for the sensitivity analysis, listed in Table 5.8, include energy consumption (total, heating, cooling and lighting), peak energy demand (total, heating and cooling) as well as visual and thermal comfort indices, i.e., UDI and PPD, respectively.

Table 5.8: Measured output for sensitivity analysis

Outputs (Y)	**Units**
Energy improvements	
Total energy consumption (TE)	[kWh/m^2]
Heating energy consumption (HE)	[kWh/m^2]
Cooling energy consumption (CE)	[kWh/m^2]
Lighting energy consumption (LE)	[kWh/m^2]
Peak load improvements	
Total peak energy demand (TPED)	[W/m^2]
Heating peak energy demand (HPED)	[W/m^2]
Cooling peak energy demand (CPED)	[W/m^2]
Visual comfort improvements	
Useful Daylight index (UDI)	[%]
Thermal comfort improvements	
Predicted percentage of dissatisfied (PPD)	[%]

The goal of this paper being to assess the performance of SW regarding comfort and energy, every model output (obtained with smart window control) has been compared to a base case scenario considering exactly the same set of design parameters except for the controlled SW that is replaced by a conventional passive window (state S1 at all time). The output measurements used for the sensitivity analysis are thus improvements (or reductions,

depending on the resulting signs). For example, if the total energy consumption improvement for a specific set of building parameters is reported as −10 kWh/m^2, one should understand that this specific configuration with a SW actually gives a 10 kWh/m^2 savings compared to the reference case with a passive window. Negative output values are beneficial in terms of energy, peak and PPD results (savings and thermal comfort improvements, respectively) but are detrimental for UDI (decrease of daylight availability). In this sense, the parameter ID 4 represents the improvements of the best SW control compared to the base case. One should also keep in mind that the results of the outputs presented in this section are representative for perimeter zones of office buildings only.

The sensitivity analysis is divided into three subsections (Sections 5.4 to 5.6). Results are presented in a similar fashion for every subsection, i.e. ME results are presented first. Based on the ME results, further explanations are then given for the most influential parameters (relatively high values of ME). While the sign of the output measurements could be interpreted as improvements or deteriorations, as explained in the previous paragraph, one should keep in mind that the sign of ME results is always positive by definition (i.e. ME represents the spread between maximum and minimum averaged outputs). The ME could thus illustrate if a parameter has a lot of influence or not for a specific output; however it cannot explain alone how the variation of a parameter influences the outputs. Such explanations are obtained by the subsequent analysis guided by the ME results.

Section 5.4 presents the results related to the energy use (total, heating, cooling and lighting). The total energy use is the summation of the heating, cooling and lighting energy. Section 5.5 presents the results related to the peak energy demand (total, heating and cooling). The total peak energy demand is defined as the peak load including heating, cooling and lighting. Finally, Section 5.6 presents the results related to visual and thermal comfort (i.e. UDI and PPD, respectively).

5.4 Main effects of building parameters on energy use reduction

Figure 5.3 illustrates the ME of the eight parameters on the different energy use outputs. As one would expect, the location (city), the façade orientation (ori) and the window to wall ratio (WWR) are among the most influential parameters (high ME values) regarding the total,

heating and cooling energy use outputs (illustrated in Figure 5.3a, b and c). That being said, Figure 5.3 also shows that the presence of a well controlled smart window (SW) has as much influence as these other parameters on the total and cooling energy outputs, which highlights the relevance of considering with care the integration of smart windows during the design of a building. While the presence of a smart window (SW) has a great effect on the total energy output, the choice of the specific rule-based control strategy (RBC) also has an effect on the reduction of the total energy consumption, but it is relatively limited. This effect on total energy is mainly driven by the lighting energy (high value of ME_{RBC}(LE) as illustrated in Figure 5.3d). Figure 5.3d also illustrates that the artificial lighting energy is mostly affected by the parameters related to smart windows (SW and RBC) and the light system itself (LED versus T8 lamps considered in the internal gains (IG) parameters). On the other hand, the thermal mass and the building tightness present quite small effects (small ME results) on all types of energy use outputs, i.e. the energy benefit of using a SW is not influenced by thermal mass or air tightness. In Figure 5.3, one could observe that any parameter of influence for the total energy use (Figure 5.3a) is explained by one or more of its components (i.e. heating, cooling and lighting energy, Figure 5.3 b, c and d, respectively). One should also note that the scale is greater for the cooling outputs (ME_k(CE)) compared to the heating and lighting outputs (ME_k(HE) and ME_k(LE), respectively). In other word, using a SW impacts mostly on the energy consumption for cooling.

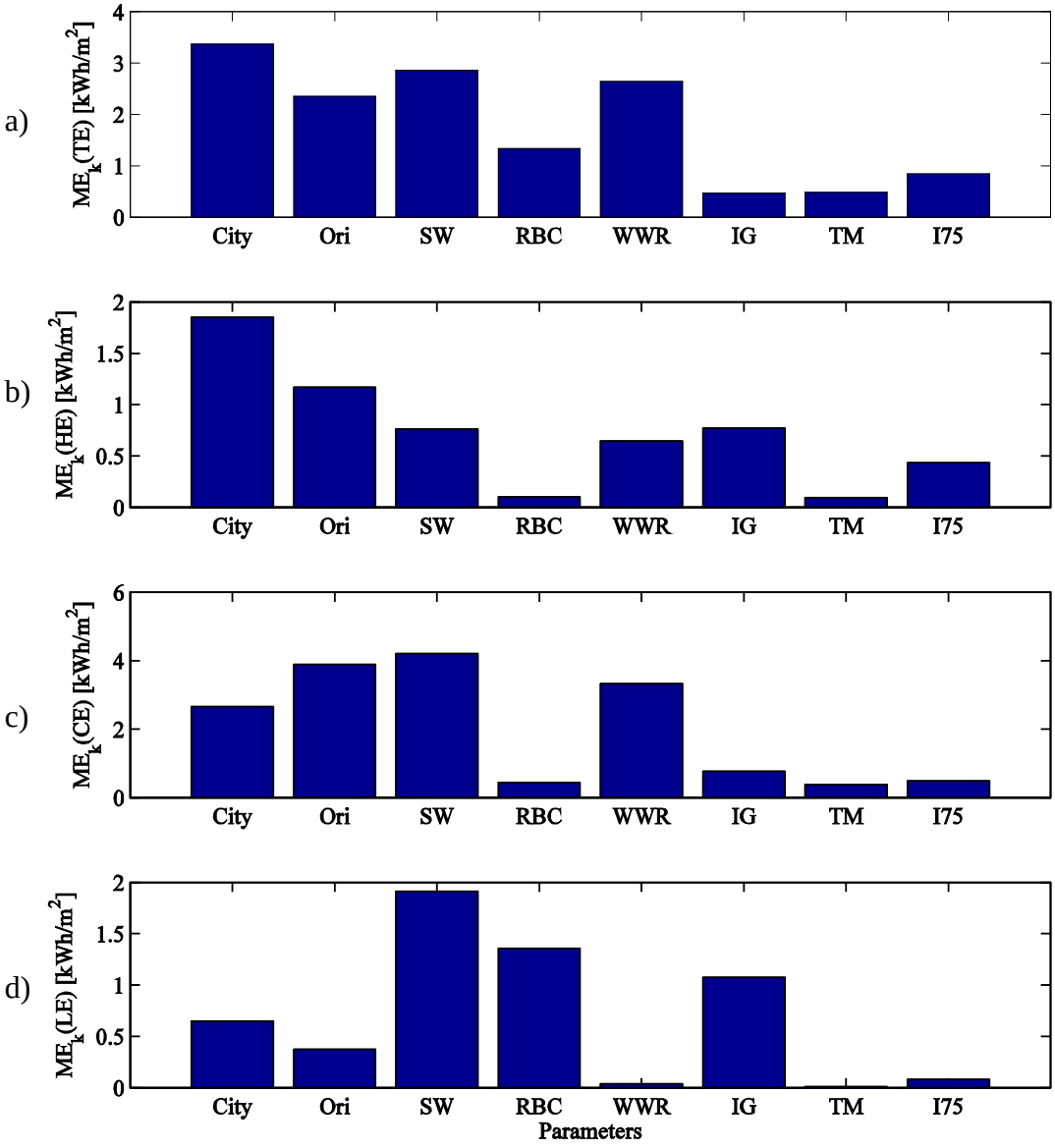

Figure 5.3: Main effect of parameters (model inputs) on change in energy consumption due to using a SW for a) total energy, b) heating, c) cooling and d) lighting.

Keeping in mind that the simulation results refer to the energy difference for buildings with SW compared to the same buildings with passive windows, a deeper analysis of the energy use outputs revealed that all the heating and lighting simulation results were positive values (i.e. increase of energy consumed due to using a SW) and that cooling results were all negative values (i.e. decrease in energy consumed due to using a SW). Since the base case scenarios consider the clear state of the SW at all time and because the use of SWs could

only lead to equal or darker states compared to the base cases, it thus makes sense that equal or lower values for heat gains and daylight are to be expected. These results reveal that the use of smart windows reduce cooling energy use, but also tend to increase the heating and lighting energy use (by limiting heat gains and daylight). These opposite trends resulted in 84.5% of the 7680 scenarios under study giving negative values of total energy use outputs (i.e. a reduction of the total energy consumption). While some situations where SWs were introduced (15.5 %) would lead to more energy being consumed, one should note that the integration of smart windows into building design generally leads to improvements in terms of total energy use. In this work, the building simulations resulting in the highest increase of total energy consumed were mostly occurring for building zones located in northern climates (such as Calgary, Montreal, Toronto and Chicago) with low internal gains and/or high infiltration rates. A particular attention should thus be paid during the design process to make sure that the design with SWs actually improves the overall energy performance. The following paragraphs provide additional indicators to support design decisions through the analysis of averaged total energy results.

Figure 5.4 presents the total energy savings for building zones with the smart windows averaged per city as a function of their respective HDD. The purpose of relating energy savings to HDD instead of the cities in Figure 5.4 is to extend the conclusions to a climate related parameter rather than specific cities. As illustrated in Figure 5.4, the reduction of the total energy use is larger for lower HDD values. Said differently, the warmer the climate is, the higher the benefits are to use smart windows in terms of overall energy use. The relatively linear relation between the total energy savings and HDD is represented by the red line in Figure 5.4. The ME of the city of Figure 5.3a is explained through the difference between the extreme results illustrated in Figure 5.4 (i.e. difference between TE_{ave} for Miami (HDD = 68°C-days) and TE_{ave} Montreal (HDD = 4493°C-days)). Note that the same approach was also applied to the cooling degree days (CDD), but was not shown in this work for the sake of brevity. While the linear relationship with CDD was very similar to the one presented in this work with HDD, the fitting presented a higher residual.

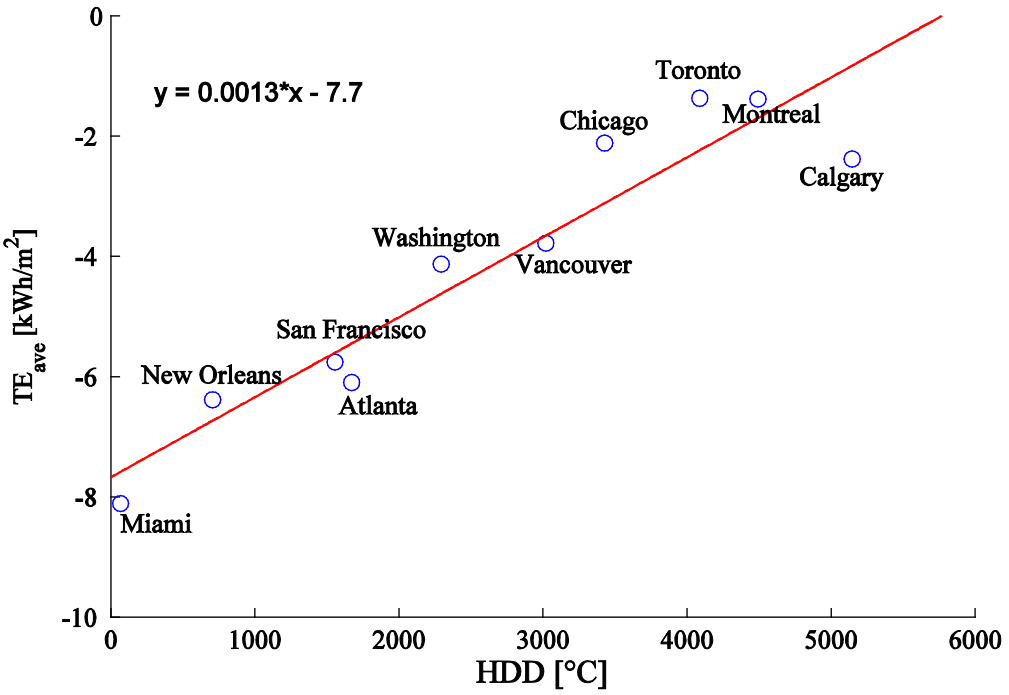

Figure 5.4: Total energy consumption reduction due to using a SW (averaged per city) as a function of the HDD

Figure 5.5 presents the averaged total energy savings for the four different façade orientations. As previously observed [26], Figure 5.5 shows that SW are offering larger benefits for east, south and west façades (savings of about 5 kWh/m^2) compared to the north façade (0.7 kWh/m^2 savings). The ME of the orientation in Figure 5.3a is explained in Figure 5.5 by the difference between the TE_{ave} for the north and the south façades.

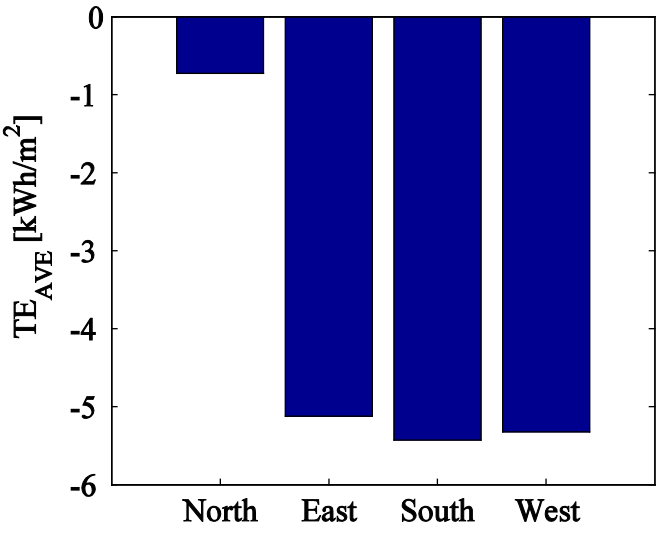

Figure 5.5: Total averaged energy use reduction due to using a SW for each orientation

Figure 5.6 presents the averaged total energy savings for the eight different smart window RBCs. Regardless of the control input (daylight, solar radiation or heat flow), the 2 state control strategies (RBC1, RBC3, RBC4 and RBC7) present lower total energy savings than their 4 state counterparts (i.e. RBC2, RBC5, RBC6 and RBC8). Overall, RBC2 and RBC6 (daylight with 4 states and Iv with 4 states with 63-315 W/m^2) give the greatest total energy savings with averaged savings on total energy use of 5.72 kWh/m^2 and 5.42 kWh/m^2, respectively. The integration of SW into office building design should thus consider at least 4 state controllers to benefit from the flexibility of the SW technology and should also integrate a control algorithm based on daylight or incident solar radiation. The ME of the RBC in Figure 5.3a is explained in Figure 5.6 by the difference between the TE_{ave} for RBC2 and RBC7.

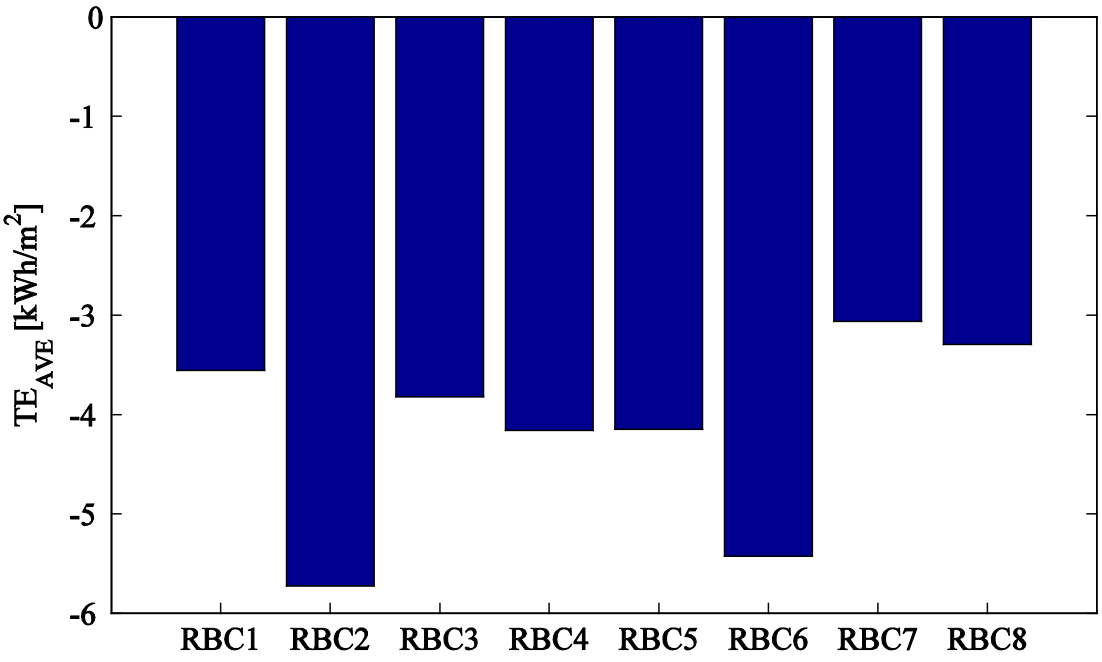

Figure 5.6: Total averaged energy use reduction due to using a SW for each RBC

Figure 5.7 presents the averaged total energy savings for the three different WWRs. As illustrated, the higher the WWR, the greater is the potential of total energy savings if controlled SWs are installed. However, even if the previous statement is true in general (or on average), one could anticipate based on the previous conclusions that some specific scenarios with high WWR would not lead to any savings (e.g. north building façades for colder climates). The ME of the WWR in Figure 5.3a is explained in Figure 5.7 through the difference between the TE_{ave} for WWR = 0.67 and WWR = 0.33.

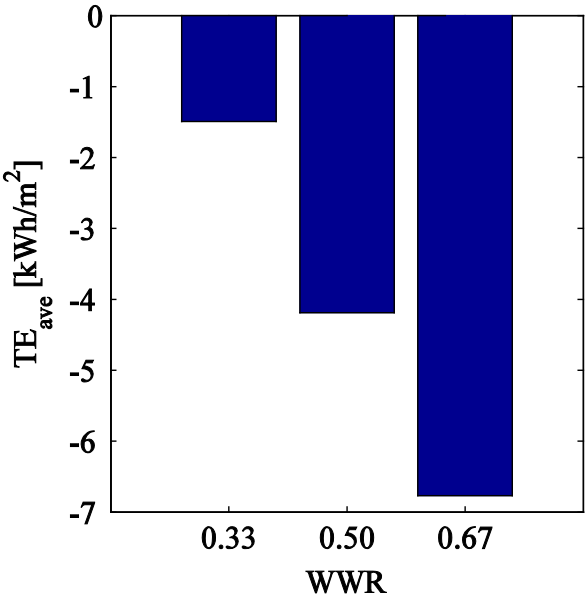

Figure 5.7: Total averaged energy reduction due to using a SW for each WWR

5.5 Main effects of building parameters on energy peak reduction

Figure 5.8 illustrates the ME of the eight parameters on the peak energy demand. While the location (City) has the most influence on the total peak demand (Figure 5.8a), other parameters such as the façade orientation (Ori), the presence of a smart window (SW), the window to wall ratio (WWR) and the thermal mass (TM) also present a significant influence on the heating and cooling peak loads. As for the energy use outputs of the previous section (Section 5.4), the presence of a SW (control on the solar heat gains) has an influence on the heating and cooling peak loads (mostly cooling). On the other hand, the type of SW control (RBC) has a negligible impact on the heating and cooling peak loads.

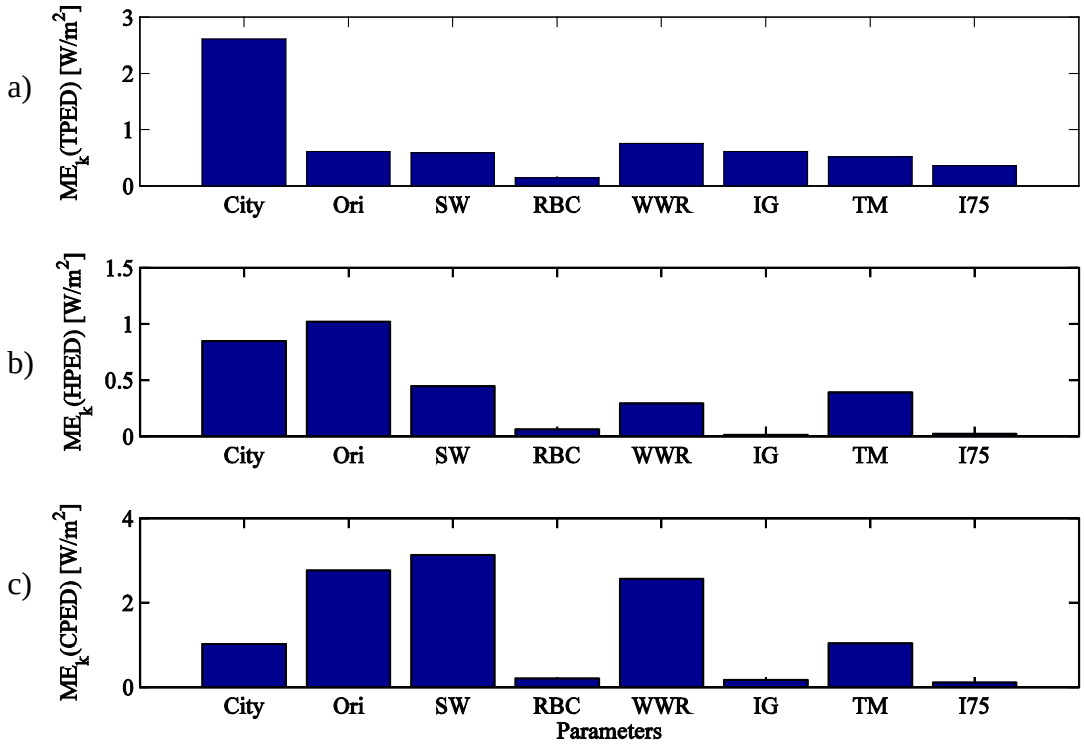

Figure 5.8: Main effect of the parameters (model inputs) on change in peak energy demand due to using SW for a) Total, b) Heating and c) Cooling)

As for the energy outputs, the reader should keep in mind that the peak energy demand outputs refer to the difference of peak demand between buildings using a SW and the same building designs with a passive window (passive state S1). Figure 5.9 presents the total averaged peak energy demand outputs for each city. In Figure 5.9, one could observe that the integration of a SW involves an increased total peak demand for some locations (positive values) and a peak reduction for other locations (negative values). This behavior is mainly explained by the fact that the annual peaks could occur either during the heating or cooling period. Since controlled SWs can increase heating loads, but reduce cooling loads (as mentioned in Section 5.4), locations for which the annual peak occurs during a heating period see their total peak increase and locations having their peak during the cooling period see their total peak decrease. The spread between the results for Miami and Montreal in Figure 5.9 explains the ME_k(TPED) value of the city in Figure 5.8a.

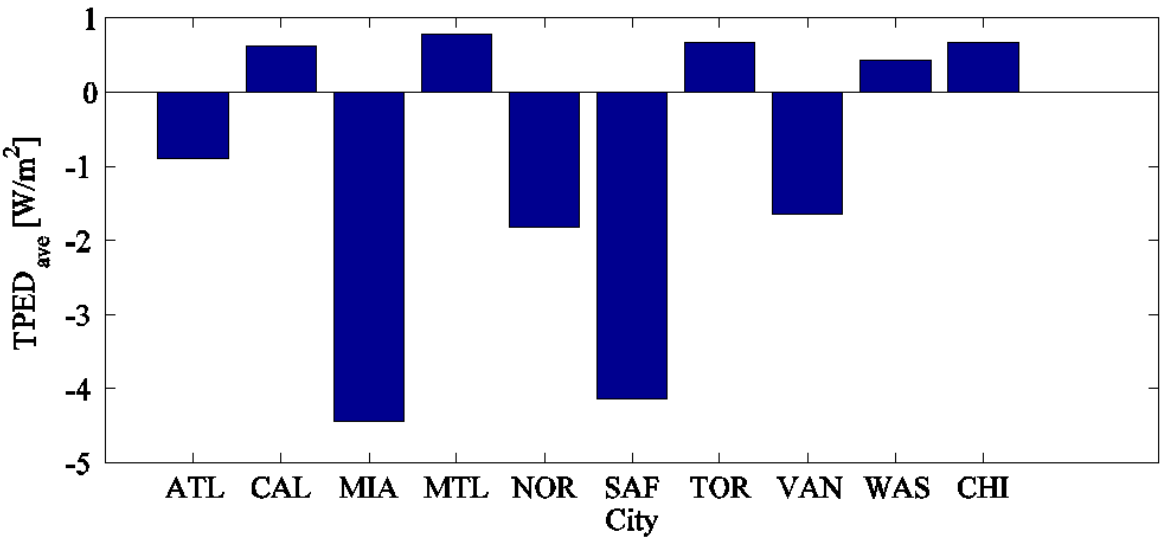

Figure 5.9: Total reduction (or increase) of averaged peak energy demand for each city

The individual assessment of the heating and cooling peaks gives valuable information for sizing these systems. From Figure 5.10a, one could note that the heating peak load is slightly increased for all cities (since SWs tend to limit solar heat gains). The integration of SW could thus likely force the heating system to be slightly larger compared to the base case scenario. However, Figure 5.10b revealed that cooling peak loads are reduced which means that the cooling system could be downsized accordingly compared to the base case scenario. All in all, the integration of SW into building design could thus potentially lead to net initial cost savings considering for the HVAC systems. However, further studies on the topic should be carried on to properly assess the impact of SW on HVAC systems costs.

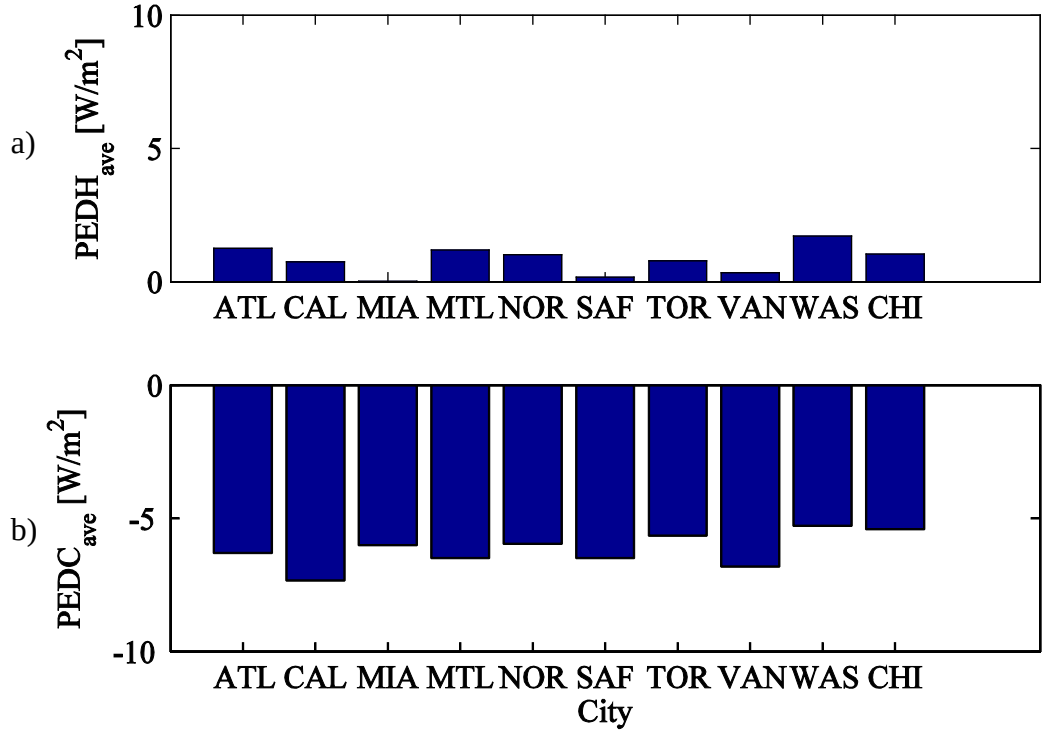

Figure 5.10: Averaged peak energy demand reduction (or increase) for each city (i.e. a) heating peak increase and b) cooling peak reduction)

The influence of the orientation, the SW control type and the WWR on total peak reduction presents a behavior very similar to the one of the total energy presented in the previous section. In terms of the orientation, the peak savings are greater for the east, south and west façades. As for the SW control type, the peak is more affected (higher savings) by the fact that a controlled SW is present (compared to the base case scenario) than by the difference between the different types of RBC (with RBC2 offering the best averaged total peak reduction, i.e. 1.18 W/m^2). Finally, the higher the WWR, the higher the peak reductions are when a controlled SW is considered.

Figure 5.11 presents the reduction of total averaged peak energy demand due to using a SW for the two values of thermal mass. Based on the results of Figure 5.11, one could realize that adding smart windows into building designs with lower thermal mass leads to greater peak reductions compared to designs with higher thermal mass. This behavior is explained by the fact that the thermal mass smooths out the cooling energy demand (time shifting of the

radiative gains) even when no SW is used. This being said, including a SW properly controlled in a building design reduces the importance of having a high thermal mass to achieve a high level of performance regarding energy.

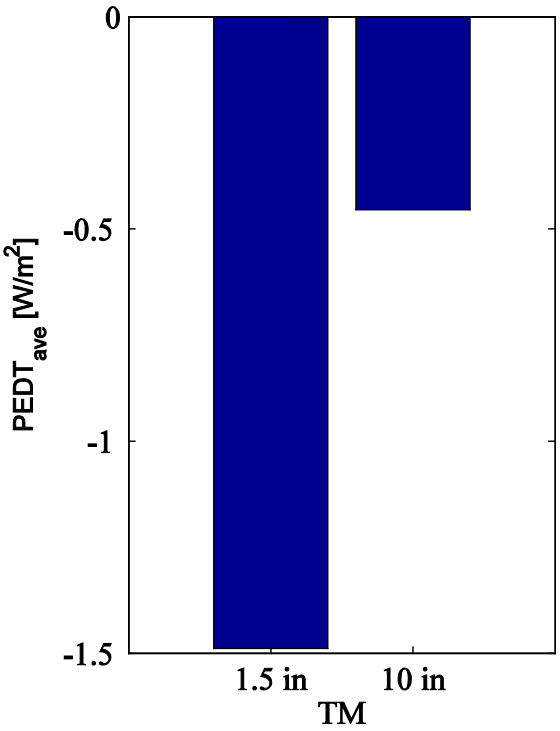

Figure 5.11: Averaged peak energy demand reduction for the two thermal mass designs

5.6 Main effects of building parameters on visual and thermal comfort improvements

Figure 5.12 illustrates the ME of the eight building parameters on the visual and thermal comfort. One could observe that the presence of a SW influences the visual and thermal comfort indicators (UDI and PPD), as illustrated in Figure 5.12a and b respectively. However, while the RBC has a low effect on the PPD (Figure 5.12b), it has the greatest influence on the UDI (Figure 5.12a). Considering absolute ME values, one could realize that the use of smart windows in building designs could largely influence the visual comfort (ME_k(UDI) up to 36.8% in Figure 5.12a). On the other end, even if some parameters (such as the city or the presence of a SW) are influencing thermal comfort, the ME_k(PPD) values only vary by up to 1.5%, thus revealing that SWs have a lot more influence on the visual comfort than on the thermal comfort. While the thermal model in this study was kept simple,

further studies could focus on more detailed thermal comfort models to assess the impact of the use of SW on thermal comfort.

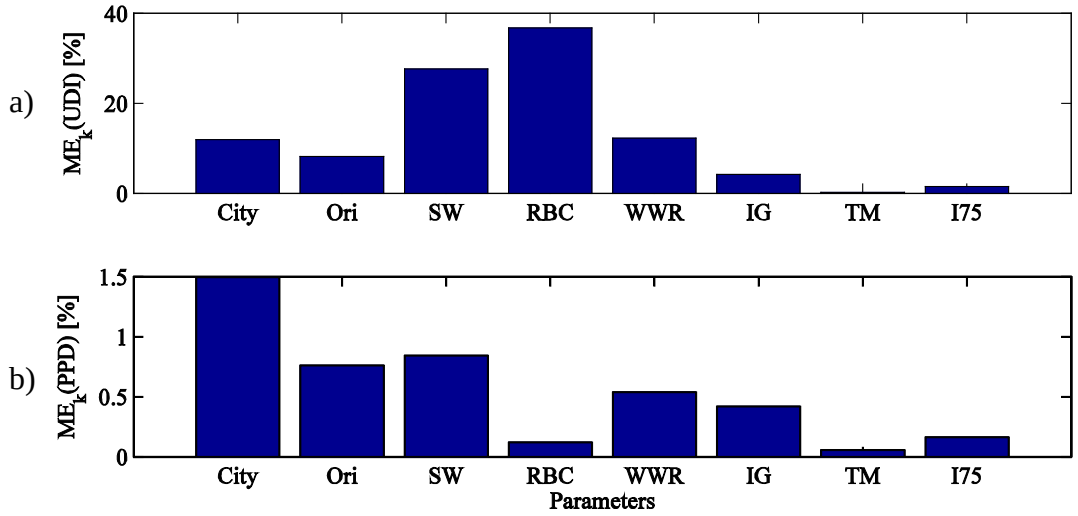

Figure 5.12: Main effect of the parameters on change in visual and thermal comfort due to using a SW (i.e. a) UDI and b) PPD, respectively)

Figure 5.13 presents the averaged UDI changes due to the SW for the eight RBCs. As illustrated, only two types of RBC actually improve the UDI on average, i.e. RBC2 and RBC6 that are both four state controllers with their control either based on daylight on the workplane and incident solar radiation, respectively. The analysis of the simulation results revealed that the RBC2 strategy leads to 89% of the scenarios improving the UDI compared to the base case (all other scenarios leading to the same values of UDI compared to the base case). In all cases for RBC2, scenarios leading limited UDI improvements or no UDI improvements at all were for north oriented façades and/or building façades with a low WWR (i.e. WWR = 33%). In such situations, a conventional passive window offers almost as much useful daylight on the workplane as a controlled SW would (with RBC2 control). However, in situations where the façade is facing east, south or west and for higher values of WWR, the daylight on the workplane exceeds more often the upper range limit of 2000 lx. In these situations, the use of a SW with RBC2 enables to maintain the daylight illuminance level on the workplane within the acceptable limits. The behavior for RBC6 is similar to RBC2, although performances are reduced. RBC6 strategy also leads to UDI deteriorations compared to the base case for north façades and the lowest WWR ratio. As mentioned

previously, in order to keep the computational time and the length of the paper acceptable, results presented in this study are limited to building designs without overhangs. As presented in previous studies [78], overhangs combined with smart windows can further reduce glare. It is thus expected that ME results would have been reduced if the analysis was considering overhangs in the base case.

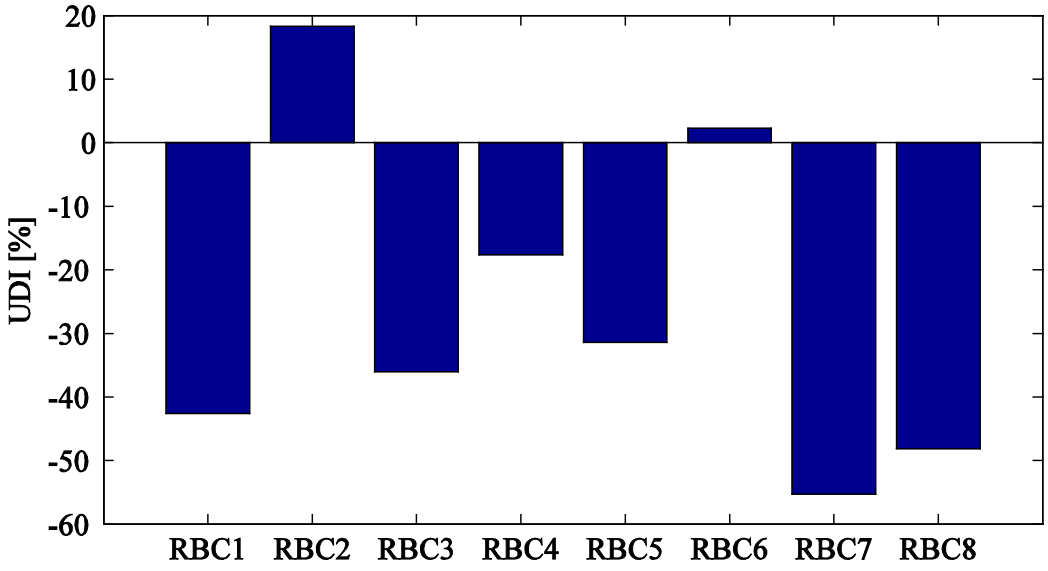

Figure 5.13: Averaged UDI reduction (or increase) for the eight RBC

5.7 Conclusions

This paper presents the sensitivity analysis of different design building parameters on energy and comfort indicators for buildings with electrochromic SWs. A representative office building zone was modeled considering an exterior glazed wall exposed to ambient conditions and all other surfaces (interior walls, ceiling and floor) exposed to adjacent zones with identical zone conditions.

The building parameters considered in the analysis were the location (10 different cities in Canada and in the U.S.), the façade orientation (north, east, south or west), the presence of a smart window and its applied control (8 different types of RBC), the WWR (33%, 50% or 75%), the internal gains density (low and high), the thermal mass (low and high) as well as the building air tightness (thigh and leaky envelopes). Simulations were performed for every combination of the aforementioned parameters, leading to a total of 7680 scenarios. Results

for every scenario were compared to their respective reference case considering a passive window. Improvements or degradation of performance presented in this work are with respect to the reference scenarios.

The sensitivity analysis was performed considering the ME of the building parameters on the energy consumption savings (total, heating, cooling and lighting), the peak energy demand reductions (total, heating, and cooling), the increase of useful daylight index (UDI) and the reduction of predicted percentage of dissatisfied (PDD). The ME was used to target the most influential parameters.

It was shown that the presence of SWs has quite a considerable influence on the energy consumption results (mainly on the total, cooling and lighting energy consumptions). The SW actually has as much influence on the change of total and cooling energy consumptions as the location, the façade orientation or the WWR. While SWs tend to slightly increase heating and lighting energy consumption by limiting solar gains and daylight, they provide considerable cooling savings. These behaviors resulted in total energy savings for approximately 85% of the scenarios under study, with the remaining 15% of the scenarios leading to energy consumption deteriorations (occurring for south facing building zones located in northern climates with low internal gains and/or high infiltration rates). The greatest total energy savings considering SWs are to be expected for warmer climates, for east, south or west façades and for high WWR values. While the different RBCs have very little impact on the heating and cooling, they influence the total energy consumption through the lighting loads. The RBC strategies RBC2 and RBC6 were found to be the most performant in terms of energy savings.

The analysis of the ME results on the peak energy demands revealed that the presence of a smart window mostly influences the cooling peak loads and that the choice of the RBC strategy has very little impact on the peak reduction. Due to the fact that SWs limit solar gains and that the annual peak load could occur either during the heating or cooling season, the integration of SW involves an increased annual total peak demand for colder climates and an annual peak reduction for warmer climates. In all cases, the use of a SW leads to

increased heating and reduced cooling peak loads (compared to the reference scenarios). It was also shown that adding smart windows into building designs with lower thermal mass leads on average to greater peak reductions compared to designs with higher thermal mass. While the choice of the RBC is having a limited impact on the energy savings and an even lower impact on the peak loads, the ME analysis revealed that this parameter has a very large impact on the UDI. Only two RBC strategies, i.e. RBC2 and RBC6, were found to offer visual comfort improvements (on average) compared to the reference scenarios with passive windows (with RBC2 outperforming RBC6). As for thermal comfort, the results showed that the use of smart windows has a limited effect on PPD.

The results presented in this work aim at helping the decision-making related to electrochromic SWs in the building design process. While total energy savings, peak load reductions and visual/thermal comfort indicators were assessed in this paper, further studies using a similar approach should include additional relevant decision making information regarding SW. Among other, future studies should include the relative effect of overhang designs [120], active load management window strategies [121], integrated control strategies [122] and should consider the economic challenges related to the integration of smart windows. The main effect of the building variables on the total cost (initial and operational) could also be studied.

While this work focused on the decision-making related to electrochromic SWs in the building design process, the methodology developed in this work could be applied to alternative technologies such as dynamically controlled shading systems. Further studies could focus a comparison of such technologies.

CHAPTER 6 CONCLUSIONS

The main objective of this thesis was to gain a better understanding of how electrochromic windows could lead to improved performances in terms of energy consumption and thermal comfort. To achieve this goal, this work was elaborated around three main research areas in order to address questions that have so far been left open regarding the design and the performance of window embedded solar sensors, the performance of advanced control systems for smart windows, and the sensitivity analysis of the main building design parameters on energy and comfort. The main contributions that this work brought to the scientific community in the field of smart window control are presented in Sections 6.1 to 6.3. Future perspectives based on the outcomes of this work are presented in Section 6.4.

6.1 Development and assessment of a low cost sensor for solar heat flux measurements in buildings

Smart windows are known for their capacity to manage solar heat gains. Hence, it makes sense in terms of control to measure the actual solar radiation passing through the windows. This information could thus directly serve as an input for SW control. While different types of solar radiation sensors offering good accuracies are readily available on the market (such as photovoltaic detectors or pyranometers), these sensors are either quite sensitive to spectral distribution or to ambient temperature or are very expensive. For the aforementioned reasons, it is unlikely that these types of solar sensor would be broadly used in real building applications such as smart window control. A solution to this issue was presented in Chapter 3 with the proposition of a new type of low cost solar sensor, i.e. a black and white sensor that calculates instantaneous solar heat flux based on a 1D heat transfer model.

With the help of the 1D heat transfer model developed in Matlab, an efficient procedure was proposed to calibrate the sensor. Once calibrated, the results (comparison of the experimental measurements to reference measurements obtained with a pyranometer) have shown that the two proposed designs of this new type of sensor were presenting a good accuracy regardless of the sky conditions for both instantaneous readings and daily integrated values. This work has thus brought new knowledge in the field of dedicated solar sensors through the proposition of a new type of low cost sensor independent of spectral profile that could be embedded in building envelope components such as windows. This sensor technology is now

currently used in a research project funded by the U.S. Department of Energy (DE-FOA-0000823) and led by the Lawrence Berkeley National Laboratory.

While this sensor was originally developed to monitor solar radiation for efficient control of smart windows, this technology could also be used for other applications or spectral profiles.

6.2 Reduced energy consumption and enhanced comfort with smart windows: Comparison between quasi-optimal, predictive and rule-based control strategies

While electrochromic windows could offer different optical properties that are readily known based on their state, a better understanding of the appropriate state to be considered at any time to optimize energy and comfort is still required. The different building considerations (thermal and visual) make the problem of SW control a very complex one. However, with the increased performance of actual computers and the large amount of optimization methods available, the possibility to implement more sophisticated real-time control strategies has now become a reality.

In Chapter 4, four state-of-the-art control strategies are presented and compared to assess the performance of viable control solutions for real-time control of smart windows. The most promising heuristic controllers and a more sophisticated model based predictive controller are proposed as applicable real-time control strategies and are compared to a reference case based on genetic algorithms. This work provided an overview of the potential of different control strategies for smart window control and a methodology to compare these strategies. The GA and MPC controllers were totally new control strategies developed by the authors. It was shown that the energy performances of the MPC are limited by both the internal model simplifications and the form of the objective function. The results reveal that, for the situation studied in this work, having thermal mass in the floor that is only passively interacting with the occurring heat flows does not seem to create the required circumstances for MPC to outperform simpler controllers. It was also shown that the efficiency of the artificial lighting system impacts the relative performance between the different controllers. In the model under study, adopting a more efficient artificial lighting system resulted in a drop of relative performance between controllers. In a context where systems are getting increasingly

complex and difficult to compare, this work brings a better understanding on how SW control strategies behave one against the others.

6.3 Office buildings with electrochromic windows: a sensitivity analysis of design parameters on energy performance, and thermal and visual comfort

In Chapter 5, decision-making information on building design with efficiently controlled electrochromic windows is provided. In order to assess the influence of the major building design parameters on energy performance and comfort, a sensitivity analysis is performed considering simultaneously a large number of design parameters. Given the extensive number of design parameters under study, this work greatly contributed to generalize the outcomes related to potential energy and comfort improvements related to the integration of smart windows into building designs. Furthermore, the proposed methodology to generate decision-making information based on the Main Effect sensitivity analysis method provided results corroborated with many previous related studies. This being said, the methodology proposed in this work is thus of great interest for future studies aiming to generate reliable decision-making information.

Among the most relevant outcomes in terms of decision-making information, it was shown that the presence of SWs has quite a considerable influence (as much as the building location, the façade orientation or the WWR) on the energy consumption results and that the greatest total energy savings considering SWs are to be expected for warmer climates, for east, south or west façades and for high WWR values. It was also shown that adding smart windows into building designs with lower thermal mass leads to greater peak reductions when compared to designs with higher thermal mass. The ME analysis furthermore revealed that the SW control strategy has a very large impact on the UDI, i.e. only two strategies out of eight under study were actually found to offer visual comfort improvements compared to the reference scenarios. As for thermal comfort, the results indicated that the use of smart windows has a limited effect on PPD. All these outcomes are seen as great improvements in terms of additional knowledge when evaluating whether or not it is relevant to invest additional effort to efficiently integrate SW into building designs. Indeed, many factors such as the budget allocated for SW could limit the relative percentage of window being SW for a given project.

Therefore, the outcomes presented in this work are a great step towards the improvement of such design decisions.

6.4 Future perspectives

Many questions were raised in the process of realizing the different steps of this thesis. While many of these questions were answered through the conclusions of this work, some questions remain open and offer great research perspectives to even further increase the knowledge in the field of smart window control. The most promising perspectives are presented in the following paragraphs.

6.4.1 Black and White sensor improvements

As presented in Chapter 3, the work on the solar sensor gave very promising results and its usefulness is confirmed by the fact that some of the best research groups are using it in their research projects. However, some limitations detailed in this work, such as partial shading due to the recess of the solar sensor, could be addressed in order to improve the sensor design. For example, designs considering repetitive patterns of black and white surfaces instead of only one pair of black and white surface could lead to improved measurements in partial shading situations. Moreover, the numerical model developed being 1D, further studies could be conducted in order to assess edge effects for very small sizes of the sensor's black and white surfaces. As for the calibration, long term performance and different locations could be considered to potentially improve and generalize the calibration method. Finally, since photo sensors are largely used for solar irradiance measurements, future research could also compare this kind of sensor to conventional silicon sensors in order to define more precisely the pros and cons of both types (e.g., spectral sensitivity, cost, lifetime, etc.).

6.4.2 Development of efficient SW control strategies

Chapter 4 explores the performance of newly developed optimal control strategies (GA and MPC) based on relatively simple objective function and constraints. This initial work should be seen as a first step in the development process of advanced SW controllers. Since these controllers are capable of dealing with complex thermal interactions for which it is beneficial to increase the intelligence, further studies could broaden the assessment of the MPC and GA controllers' performance by considering more complex objective functions could include, for example, interactions with other zones and/or with the electromechanical systems. The

objective function could also consider the combined contribution of the energy and peak load rather than the total energy only. Moreover, the complexity of the optimal control decisions and human interactions is such that field studies could be performed to corroborate outcomes obtained from the aforementioned numerical study propositions.

6.4.3 Generalization of the effect of design parameters on energy performance and comfort for buildings with SW.

In Chapter 5, annual energy savings, peak load reductions and visual/thermal comfort indicators were assessed while considering the principal design parameters and state-of-the-art heuristic SW control strategies. However, as presented in Chapter 4, there is an increasing interest in the field of SW to include complexity in controls and considerations to improve benefits. For these reasons, further studies using an approach similar to the one presented in Chapter 5 could include additional relevant decision making information regarding SW, such as the relative effect of overhang designs, active load management window strategies, or integrated control strategies. The main effect of the building variables on the total cost (initial and operational) could also be included (or be studied in parallel) to increase knowledge in terms of economic considerations related to SW.

REFERENCES

[1] R. Singh, “Energy in a century of environmental concerns: Responses for creating a bright energy future,” *VGB PowerTech*, vol. 79, no. 9, pp. 26–31, 1999.

[2] M. Abaza, “High performance buildings using whole building integrated design approach,” *Strateg. Plan. Energy Environ.*, vol. 31, no. 4, pp. 19–34, 2012.

[3] J. K. W. Wong, H. Li, and S. W. Wang, “Intelligent building research: a review,” *Autom. Constr.*, vol. 14, no. 1, pp. 143–59, Jan. 2005.

[4] D. Clements-Croome, “Sustainable intelligent buildings for people: A review,” *Intell. Build. Int.*, vol. 3, no. 2, pp. 67–86, 2011.

[5] Yang Han and Lin Xu, “A survey of the Smart Grid Technologies: background, motivation and practical applications,” *Przeglad Elektrotechniczny*, vol. 87, no. 6, pp. 47–57, 2011.

[6] Y. Yan, Y. Qian, H. Sharif, and D. Tipper, “A survey on smart grid communication infrastructures: Motivations, requirements and challenges,” *IEEE Commun. Surv. Tutor.*, vol. 15, no. 1, pp. 5–20, 2013.

[7] M. Sechilariu, B. Wang, and F. Locment, “Building-integrated microgrid: Advanced local energy management for forthcoming smart power grid communication,” *Energy Build.*, vol. 59, pp. 236–243, 2013.

[8] P. J. Werbos, “Computational intelligence for the smart grid-history, challenges, and opportunities,” *IEEE Comput. Intell. Mag.*, vol. 6, no. 3, pp. 14–21, 2011.

[9] Loonen, RCGM Roel, Trcka, M Marija, and Hensen, JLM Jan, “Exploring the potential of climate adaptive building shells.” Technische Universiteit Eindhoven, 2011.

[10] A. Wyckmans, “Intelligent building envelopes,” Norwegian University of Science and Technology, 2005.

[11] G. M. Sottile, “2004 Survey of United States architects on the subject of switchable glazings,” *Mater. Sci. Eng. B Solid-State Mater. Adv. Technol.*, vol. 119, no. 3, pp. 240–5, Jun. 2005.

[12] B. P. Jelle, A. Hynd, A. Gustavsen, D. Arasteh, H. Goudey, and R. Hart, “Fenestration of today and tomorrow: A state-of-the-art review and future research opportunities,” *Sol. Energy Mater. Sol. Cells*, vol. 96, no. 1, pp. 1–28, 2012.

[13] S. C. Sekhar and K. L. C. Toon, “On the study of energy performance and life cycle cost of smart window,” *Energy Build.*, vol. 28, no. 3, pp. 307–16, Nov. 1998.

[14] R. Baetens, B. P. Jelle, and A. Gustavsen, “Properties, requirements and possibilities of smart windows for dynamic daylight and solar energy control in buildings: A state-of-the-art review,” *Sol. Energy Mater. Sol. Cells*, vol. 94, no. 2, pp. 87–105, 2010.

[15] S. K. Deb, S.-H. Lee, C. Edwin Tracy, J. Roland Pitts, B. A. Gregg, and H. M. Branz, “Stand-alone photovoltaic-powered electrochromic smart window,” *Electrochimica Acta*, vol. 46, no. 13–14, pp. 2125–2130, 2001.

[16] S. E. Rudolph, J. Dieckmann, and J. Brodrick, “Technologies for smart windows,” *ASHRAE J.*, vol. 51, no. 7, pp. 104–106, 2009.

[17] A. McWilliams, “Smart Materials: Technologies and Global Markets,” BCC Research, USA, Wellesley, MA, USA, May 2011.

[18] H. J. Han, Y. I. Jeon, S. H. Lim, W. W. Kim, and K. Chen, “New developments in illumination, heating and cooling technologies for energy-efficient buildings,” *Energy*, vol. 35, no. 6, pp. 2647–53, Jun. 2010.
[19] H. M. Yin, D. J. Yang, G. Kelly, and J. Garant, “Design and performance of a novel building integrated PV/thermal system for energy efficiency of buildings,” *Sol. Energy*, vol. 87, no. 1, pp. 184–195, 2013.
[20] R. Loonen, “Climate adaptive building shell.”
[21] W. Chun, S. J. Oh, H. Han, J. T. Kim, and K. Chen, “Overview of several novel thermodiode designs and their application in buildings,” *Int. J. Low Carbon Technol.*, vol. 3, no. 2, pp. 83–100, 2008.
[22] Na Zhu, Zhenjun Ma, and Shengwei Wang, “Dynamic characteristics and energy performance of buildings using phase change materials: a review,” *Energy Convers. Manag.*, vol. 50, no. 12, pp. 3169–81, décembre 2009.
[23] B. P. Jelle, C. Breivik, and H. D. Rokenes, “Building integrated photovoltaic products: A state-of-the-art review and future research opportunities,” *Sol. Energy Mater. Sol. Cells*, vol. 100, pp. 69–96, May 2012.
[24] S. Macka and Y. Yasar, “The effects of window alternatives on energy efficiency and building economy in high - Rise residential buildings in cold climates,” *Gazi Univ. J. Sci.*, vol. 24, no. 4, pp. 927–944, 2011.
[25] R. A. Khire, A. Messac, and S. Van Dessel, “Design of thermoelectric heat pump unit for active building envelope systems,” *Int. J. Heat Mass Transf.*, vol. 48, no. 19–20, pp. 4028–4040, 2005.
[26] J.-M. Dussault, L. Gosselin, and T. Galstian, “Integration of smart windows into building design for reduction of yearly overall energy consumption and peak loads,” *Sol. Energy*, vol. 86, no. 11, pp. 3405–16, Nov. 2012.
[27] R. Sullivan, E. S. Lee, K. Papamichael, M. Rubin, and S. E. Selkowitz, “Effect of switching control strategies on the energy performance of electrochromic windows,” *Proceedings of SPIE - The International Society for Optical Engineering*, pp. 443–455, Sep. 1994.
[28] A. Piccolo and F. Simone, “Effect of switchable glazing on discomfort glare from windows,” *Build. Environ.*, vol. 44, no. 6, pp. 1171–1180, 2009.
[29] G. Wu *et al.*, “All-solid state electrochromic smart window,” *Zhenkong Kexue Yu Jishu XuebaoVacuum Sci. Technol.*, vol. 17, no. 4, pp. 275–282, 1997.
[30] D. Cupelli *et al.*, “Self-adjusting smart windows based on polymer-dispersed liquid crystals,” *Sol. Energy Mater. Sol. Cells*, vol. 93, no. 11, pp. 2008–2012, 2009.
[31] S. Bains, “Windows of opportunity [smart windows for light/heat blocking],” *IEE Rev.*, vol. 51, no. 4, pp. 40–3, Apr. 2005.
[32] V. Wittwer, M. Datz, J. Ell, A. Georg, W. Graf, and G. Walze, “Gasochromic windows,” in *International Solar Energy Society World Congress 2003, June 14, 2003 - June 19, 2003*, 2004, vol. 84, pp. 305–314.
[33] R. Arutjunjan, T. Markova, I. Halopenen, I. Maksimov, A. Tutunnikov, and O. Yanush, “Smart thermochromic glazing for energy saving window applications,” in *Optical Materials and Applications, 6-9 July 2004*, 2005, vol. 5946, pp. 594618–1.
[34] C. M. Lampert and C. G. Granqvist, “Application of Large-Area Chromogenics to Architectural Glazings,” in *Large Area Chromogenics: Materials and Devices for Transmittance Control*, Bellingham, WA: Optical Engineering Press, 1989.

[35] S. E. Selkowitz, M. Rubin, E. S. Lee, and R. Sullivan, “Review of electrochromic window performance factors,” *Opt. Mater. Technol. Energy Effic. Sol. Energy Convers. XIII*, vol. 2255, pp. 226–248, Sep. 1994.

[36] R. Sullivan, M. D. Rubin, and S. E. Selkowitz, “Energy performance analysis of prototype electrochromic windows,” *ASHRAE Trans.*, vol. 103, no. pt 2, pp. 149–156, 1997.

[37] R. Sullivan, M. Rubin, and S. Selkowitz, “Reducing Residential Cooling Requirements Through the Use of Electrochromic Windows,” in *Thermal Performance of the Exterior Envelopes of Buildings VI Conference*, Clearwater, Florida, 1995.

[38] R. Sullivan, E. Lee, M. Rubin, and S. Selkowitz, “The Energy Performance of Electrochromic Windows in Heating-Dominated Geographic Locations,” presented at the SPIE International Symposium on Optical Materials Technology for Energy Efficiency and Solar Energy Conversion XV, Freiburg, Germany, 1996.

[39] M. Moeck, E. S. Lee, M. D. Rubin, R. T. Sullivan, and S. E. Selkowitz, “Visual quality assessment of electrochromic and conventional glazings,” *Sol. Energy Mater. Sol. Cells*, vol. 54, no. 1–4, pp. 157–64, Aug. 1998.

[40] E. S. Lee, D. L. DiBartolomeo, J. H. Klems, M. Yazdanian, and S. E. Selkowitz, “Monitored Energy Performance of Electrochromic Windows Controlled for Daylight and Visual Comfort,” *ASHRAE Trans.*, vol. 112, no. 2, pp. 122–141, Oct. 2006.

[41] E. Lee, “A Design Guide for Early-Market Electrochromic Windows,” Lawrence Berkeley National Laboratory, LBNL-59950, 2006.

[42] J.-J. Kim and J. Jones, “A conceptual framework for dynamic control of daylighting and electric lighting systems,” in , *Conference Record of the 1993 IEEE Industry Applications Society Annual Meeting, 1993*, 1993, pp. 2358–2364 vol.3.

[43] J. Karlsson, B. Karlsson, and A. Roos, “CONTROL STRATEGIES AND ENERGY SAVING POTENTIALS FOR VARIABLE TRANSMITTANCE WINDOWS VERSUS STATIC WINDOWS,” in *Eurosun-2000*, Copenhagen, 2000.

[44] J. Karlsson, “CONTROL SYSTEM AND ENERGY SAVING POTENTIAL FOR SWITCHABLE WINDOWS,” presented at the Seventh International IBPSA Conference, Rio de Janeiro, Brazil, 2001.

[45] A. Azens, C.-G. Granqvist, J. Karlsson, G. Niklasson, and A. Roos, “Climate control system and method for controlling such,” Patent number US6965813 B2, 2005.

[46] A. Davies, “The application and control of chromogenic switchable glazing,” *Light. J. Rugby Engl.*, vol. 67, no. 5, pp. 12–19, 2002.

[47] E. S. Lee and D. L. DiBartolomeo, “Application issues for large-area electrochromic windows in commercial buildings,” *Sol. Energy Mater. Sol. Cells*, vol. 71, no. 4, pp. 465–91, Mar. 2002.

[48] H. Arsenault, M. Hébert, and M.-C. Dubois, “Effects of glazing colour type on perception of daylight quality, arousal, and switch-on patterns of electric light in office rooms,” *Build. Environ.*, vol. 56, pp. 223–231, Oct. 2012.

[49] F. Gugliermetti and F. Bisegna, “Visual and energy management of electrochromic windows in Mediterranean climate,” *Build. Environ.*, vol. 38, no. 3, pp. 479–492, 2003.

[50] M. N. Assimakopoulos, A. Tsangrassoulis, G. Guarracino, and M. Santamouris, “Integrated energetic approach for a controlable electrochromic device,” *Energy Build.*, vol. 36, no. 5, pp. 415–422, May 2004.

[51] M. N. Assimakopoulos, A. Tsangrassoulis, M. Santamouris, and G. Guarracino, “Comparing the energy performance of an electrochromic window under various control strategies,” *Build. Environ.*, vol. 42, no. 8, pp. 2829–2834, 2007.
[52] F. Gugliermetti and F. Bisegna, “A model study of light control systems operating with electrochromic windows,” *Light. Res. Technol.*, vol. 37, no. 1, pp. 3–20, 2005.
[53] R. D. Clear, V. Inkarojrit, and E. S. Lee, “Subject responses to electrochromic windows,” *Energy Build.*, vol. 38, no. 7, pp. 758–79, Jul. 2006.
[54] A. Jonsson and A. Roos, “Evaluation of control strategies for different smart window combinations using computer simulations,” *Sol. Energy*, vol. 84, no. 1, pp. 1–9, Jan. 2010.
[55] J. Soussa, “Energy Simulation Software for Buildings: Review and Comparison,” in *Proceedings of the 1st International Workshop on Information Technology for Energy Applications*, 2012, vol. 923, pp. 57–68.
[56] W. H. Kwon and S. Han, *Receding Horizon Control - Model Predictive Control for State Models*. Springer-Verlag, 2005.
[57] P. Ngendakumana, *Modélisation simplifiée du comportement thermique d’un bâtiment et vérification expérimentale*. LIEGE, 1991.
[58] L. Gosselin, M. Tye-Gingras, and F. Mathieu-Potvin, “Review of utilization of genetic algorithms in heat transfer problems,” vol. 52, no. 9–10, pp. 2169–88, Apr. 2009.
[59] J. Lofberg, “YALMIP : a toolbox for modeling and optimization in MATLAB,” in *2004 IEEE International Conference on Robotics and Automation (IEEE Cat. No.04CH37508)*, 2004, pp. 284–289.
[60] R. C. G. M. Loonen, M. Trčka, D. Cóstola, and J. L. M. Hensen, “Climate adaptive building shells: State-of-the-art and future challenges,” *Renew. Sustain. Energy Rev.*, vol. 25, pp. 483–493, Sep. 2013.
[61] R. Lollini, L. Danza, and I. Meroni, “Energy efficiency of a dynamic glazing system,” *Sol. Energy*, vol. 84, no. 4, pp. 526–537, 2010.
[62] A. de Gracia, L. Navarro, A. Castell, D. Boer, and L. F. Cabeza, “Life cycle assessment of a ventilated facade with PCM in its air chamber,” *Sol. Energy*, vol. 104, pp. 115–23, Jun. 2014.
[63] F. Mancilla-David, F. Riganti-Fulginei, A. Laudani, and A. Salvini, “A Neural Network-Based Low-Cost Solar Irradiance Sensor,” *Ieee Trans. Instrum. Meas.*, vol. 63, no. 3, pp. 583–591, Mar. 2014.
[64] H. A. Krishna, N. K. Misra, and M. S. Suresh, “Solar Cell as a Capacitive Temperature Sensor,” *Ieee Trans. Aerosp. Electron. Syst.*, vol. 47, no. 2, pp. 782–789, Apr. 2011.
[65] B. Plesz, A. Foldvary, and E. Bandy, “Low cost solar irradiation sensor and its thermal behaviour,” *Microelectron. J.*, vol. 42, no. 4, pp. 594–600, Apr. 2011.
[66] J. J. Michalsky, R. Perez, L. Harrison, and B. A. LeBaron, “Spectral and temperature correction of silicon photovoltaic solar radiation detectors,” *Sol. Energy*, vol. 47, no. 4, pp. 299–305, 1991.
[67] W. E. B. D. L. King, “Improved accuracy for low-cost solar irradiance sensors,” 1997.
[68] Z. Chuan, J. Michalsky, and L. Harrison, “Comparison of irradiance measurements made with the multi-filter rotating shadowband radiometer and first-class thermopile radiometers,” *Sol. Energy*, vol. 55, no. 6, pp. 487–491, 1995.
[69] D. R. Myers and A. Lester, “A method for improving global pyranometer measurements by modeling responsivity functions,” *Sol. Energy*, vol. 80, no. 3, pp. 322–31, Mar. 2006.

[70] F. P. Incropera, D. D. Dewitt, T. L. Bergman, and A. S. Lavine, *Fundamentals of Heat and Mass Transfer*, 6th edition. John Wiley & Sons , Inc., 2007.
[71] J. H. Klems and S. E. Selkowitz, "MOBILE WINDOW THERMAL TEST FACILITY (MoWiTT).," *Chang. Energy Use Futur. Int Conf Energy Use Manage 2nd Oct. 22 1979 - Oct. 26 1979*, vol. 4, pp. A72–A79, 1979.
[72] Kipp & Zonen, *CM 11 Pyranometer Instruction manual*, 0805 ed. Delft, Holland, 2000.
[73] The MathWorks, Inc., *Optimization Toolbox User's Guide*, vol. R2014 b. Natick, MA, 2014.
[74] E. Monstvilas, V. Stankeviius, J. Karbauskait, A. Burlingis, and K. Banionis, "Hourly calculation method of building energy demand for space heating and cooling based on steady-state heat balance equations," *J. Civ. Eng. Manag.*, vol. 18, no. 3, pp. 356–368, 2012.
[75] C. E. Ochoa, M. B. C. Aries, E. J. van Loenen, and J. L. M. Hensen, "Considerations on design optimization criteria for windows providing low energy consumption and high visual comfort," *Appl. Energy*, vol. 95, pp. 238–245, 2012.
[76] A. Piccolo, "Thermal performance of an electrochromic smart window tested in an environmental test cell," *Energy Build.*, vol. 42, no. 9, pp. 1409–17, Sep. 2010.
[77] S. E. Selkowitz, E. S. Lee, and O. Aschehoug, "Perspectives on Advanced Facades with Dynamic Glazings and Integrated Lighting Control," presented at the International Conferences on Solar Energy in Buildings, Lausanne, Switzerland, 2003.
[78] E. Lee, "Energy and visual comfort performance of electrochromic windows with overhangs," *Build. Environ.*, vol. 42, no. 6, pp. 2439–2449, 2007.
[79] A. Shehabi *et al.*, "U.S. energy savings potential from dynamic daylighting control glazings," *Energy Build.*, vol. 66, pp. 415–423, 2013.
[80] M.-C. Dubois, F. Cantin, K. Johnsen, and W. K. E. Osterhaus, "The effect of coated glazing on visual perception: A pilot study using scale models," *Light. Res. Technol.*, vol. 39, no. 3, pp. 283–304, 2007.
[81] E. S. Lee *et al.*, "Advancement of Electrochromic Windows," *Lawrence Berkeley Natl. Lab.*, Apr. 2006.
[82] T. Hilliard, M. Kavgic, and L. Swan, "Model predictive control for commercial buildings: trends and opportunities," *Adv. Build. Energy Res.*, vol. 0, no. 0, pp. 1–19, Sep. 2015.
[83] B. Delcroix and M. Kummert, "Conduction transfer functions in TRNSYS multizone building model: current implementation, limitations and possible improvements," in *Fifth National Conference of IBPSA-US*, Madison, WI, 2012.
[84] M.-C. Dubois and A. Blomsterberg, "Energy saving potential and strategies for electric lighting in future north european, low energy office buildings: A literature review," *Energy Build.*, vol. 43, no. 10, pp. 2572–2582, 2011.
[85] K. Fisekis, M. Davies, M. Kolokotroni, and P. Langford, "Prediction of discomfort glare from windows," *Light. Res. Technol.*, vol. 35, no. 4, pp. 360–369, Dec. 2003.
[86] A. Borisuit, J.-L. Scartezzini, and A. Thanachareonkit, "Visual discomfort and glare rating assessment of integrated daylighting and electric lighting systems using HDR imaging techniques," *Archit. Sci. Rev.*, vol. 53, no. 4, pp. 359–373, Nov. 2010.
[87] C. Reinhart and P.-F. Breton, "Experimental validation of 3ds Max® design 2009 and Daysim 3.0," in *11th International IBPSA Conference - Building Simulation 2009, BS 2009, July 27, 2007 - July 30, 2007*, Glasgow, Scotland, 2009, pp. 1514–1521.

[88] G. J. Ward, "The RADIANCE lighting simulation and rendering system," in *Proceedings of 21st International SIGGRAPH Conference, 24-29 July 1994*, 1994, pp. 459–72.
[89] A. Pandharipande and D. Caicedo, "Daylight integrated illumination control of LED systems based on enhanced presence sensing," *Energy Build.*, vol. 43, no. 4, pp. 944–950, Apr. 2011.
[90] EnergyPlus™ Version 8.5 Documentation, "Engineering Reference." U.S. Department of Energy, 31-Mar-2016.
[91] A.-T. Nguyen, S. Reiter, and P. Rigo, "A review on simulation-based optimization methods applied to building performance analysis," *Appl. Energy*, vol. 113, pp. 1043–1058, Jan. 2014.
[92] S. J. Qin and T. A. Badgwell, "A survey of industrial model predictive control technology," *Control Eng. Pract.*, vol. 11, no. 7, pp. 733–764, Jul. 2003.
[93] B. Coffey, "Integrated control of operable fenestration systems and thermally massive HVAC systems: Methods and simulation studies of energy savings potential," California Energy Commission Public Interest Energy Research (PIER) Program, 2012.
[94] M. Sourbron and L. Helsen, "Sensitivity analysis of feedback control for concrete core activation and impact on installed thermal production power," *J. Build. Perform. Simul.*, vol. 7, no. 5, pp. 309–325, Sep. 2014.
[95] F. Oldewurtel *et al.*, "Use of model predictive control and weather forecasts for energy efficient building climate control," *Energy Build.*, vol. 45, pp. 15–27, Feb. 2012.
[96] M. Kummert and P. Andre, "Simulation of a model-based optimal controller for heating systems under realistic hypothesis," in *Proceedings of the 9th IBPSA Conference, Building Simulation 2005*, IBPSA, 2005, pp. 555–562.
[97] P. Geyer and A. Schlüter, "Automated metamodel generation for Design Space Exploration and decision-making – A novel method supporting performance-oriented building design and retrofitting," *Appl. Energy*, vol. 119, pp. 537–556, Apr. 2014.
[98] S. V. Vasilyeva, P. M. Beaujuge, S. Wang, J. E. Babiarz, V. W. Ballarotto, and J. R. Reynolds, "Material Strategies for Black-to-Transmissive Window-Type Polymer Electrochromic Devices," *ACS Appl. Mater. Interfaces*, vol. 3, no. 4, pp. 1022–1032, Apr. 2011.
[99] A. Piccolo and F. Simone, "Performance requirements for electrochromic smart window," *J. Build. Eng.*, vol. 3, pp. 94–103, Sep. 2015.
[100] E. S. Lee, D. L. DiBartolomeo, and S. E. Selkowitz, "Daylighting control performance of a thin-film ceramic electrochromic window: Field study results," *Energy Build.*, vol. 38, no. 1, pp. 30–44, Jan. 2006.
[101] J.-M. Dussault, M. Sourbron, and L. Gosselin, "Reduced energy consumption and enhanced comfort with smart windows: Comparison between quasi-optimal, predictive and rule-based control strategies," *Energy Build.*, vol. 127, pp. 680–691, Sep. 2016.
[102] A. L. Dyer, R. H. Bulloch, Y. Zhou, B. Kippelen, J. R. Reynolds, and F. Zhang, "A Vertically Integrated Solar-Powered Electrochromic Window for Energy Efficient Buildings," *Adv. Mater.*, vol. 26, no. 28, pp. 4895–4900, Jul. 2014.
[103] M. Pittaluga, "The electrochromic wall," *Energy Build.*, vol. 66, pp. 49–56, Nov. 2013.

[104] M. H. Kristensen and S. Petersen, “Choosing the appropriate sensitivity analysis method for building energy model-based investigations,” *Energy Build.*, vol. 130, pp. 166–176, Oct. 2016.
[105] R. Singh, I. J. Lazarus, and V. V. N. Kishore, “Uncertainty and sensitivity analyses of energy and visual performances of office building with external venetian blind shading in hot-dry climate,” *Appl. Energy*, vol. 184, pp. 155–170, Dec. 2016.
[106] F. Bre, A. S. Silva, E. Ghisi, and V. D. Fachinotti, “Residential building design optimisation using sensitivity analysis and genetic algorithm,” *Energy Build.*, vol. 133, pp. 853–866, Dec. 2016.
[107] R. C. G. M. Loonen, F. Favoino, J. L. M. Hensen, and M. Overend, “Review of current status, requirements and opportunities for building performance simulation of adaptive facades,” *J. Build. Perform. Simul.*, vol. 0, no. 0, pp. 1–19, Mar. 2016.
[108] S. J. Emmerich and A. K. Persily, “U.S. Commercial Building Airtightness Requirements and Measurements,” in *AIVC Conference 2011*, Brussels, 2011.
[109] K. Gowri, D. W. Winiarski, and R. E. Jarnagin, “Infiltration modeling guidelines for commercial building energy analysis,” PNNL-18898, 968203, Sep. 2009.
[110] L. Guan, “The influence of internal load density on the energy and thermal performance of air-conditioned office buildings in the face of global warming,” *Archit. Sci. Rev.*, vol. 58, no. 2, pp. 162–173, Apr. 2015.
[111] ISO Standard 7730, “Moderate thermal environments - Determination of the PMV and PPD indices and specification of the conditions for thermal comfort.” ISO, 1994.
[112] M. De Carli, B. W. Olesen, A. Zarrella, and R. Zecchin, “People’s clothing behaviour according to external weather and indoor environment,” *Build. Environ.*, vol. 42, no. 12, pp. 3965–3973, décembre 2007.
[113] Solar Energy Laboratory, University of Wisconsin-Madison, “TRNSYS 17 a TRaNsient SYstem Simulation program - Volume 5 - Multi zone Building modeling with Type56 and TRNBuild.” 2012.
[114] J. Wienold and J. Christoffersen, “Evaluation methods and development of a new glare prediction model for daylight environments with the use of CCD cameras,” *Energy Build.*, vol. 38, no. 7, pp. 743–757, juillet 2006.
[115] A. Nabil and J. Mardaljevic, “Useful daylight illuminance: a new paradigm for assessing daylight in buildings,” *Light. Res. Technol.*, vol. 37, no. 1, pp. 41–57, Mar. 2005.
[116] G. van Moeseke, I. Bruyère, and A. De Herde, “Impact of control rules on the efficiency of shading devices and free cooling for office buildings,” *Build. Environ.*, vol. 42, no. 2, pp. 784–793, Feb. 2007.
[117] S. Firląg *et al.*, “Control algorithms for dynamic windows for residential buildings,” *Energy Build.*, vol. 109, pp. 157–173, Dec. 2015.
[118] J.-M. Dussault, C. Kohler, H. Goudey, R. Hart, L. Gosselin, and S. E. Selkowitz, “Development and assessment of a low cost sensor for solar heat flux measurements in buildings,” *Sol. Energy*, vol. 122, pp. 795–803, Dec. 2015.
[119] A. Saltelli *et al.*, “2.4.4 Fractional Factorial Sampling,” in *Global sensitivity analysis*, John Wiley & Sons Ltd, 2008.
[120] A. Tavil and E. S. Lee, “Effects of Overhangs on the Performance of Electrochromic Windows,” *Archit. Sci. Rev.*, vol. 49, no. 4, pp. 349–356, Dec. 2006.

[121] E. S. Lee, S. Selkowitz, V. Bazjanac, V. George, and C. Kohler, “High-Performance Commercial Building Façades.” LBNL-50502, Lawrence Berkeley National Laboratory, Jun-2002.
[122] E. S. Lee, C. Gehbauer, B. E. Coffey, A. McNeil, M. Stadler, and C. Marnay, “Integrated control of dynamic facades and distributed energy resources for energy cost minimization in commercial buildings,” *Sol. Energy*, vol. 122, pp. 1384–1397, Dec. 2015.
[123] S. Reilly, D. Arasteh, and S. Selkowitz, “Thermal and optical analysis of switchable window glazings,” *Sol. Energy Mater.*, vol. 22, no. 1, pp. 1–14, 1991.
[124] A. Llordes, G. Garcia, J. Gazquez, and D. J. Milliron, “Tunable near-infrared and visible-light transmittance in nanocrystal-in-glass composites,” *Nature*, vol. 500, no. 7462, pp. 323–6, Aug. 2013.
[125] P. Rocha, A. Siddiqui, and M. Stadler, “Improving energy efficiency via smart building energy management systems: A comparison with policy measures,” *Energy Build.*, vol. 88, pp. 203–13, Feb. 2015.
[126] A. S. Bahaj, P. A. B. James, and M. F. Jentsch, “Potential of emerging glazing technologies for highly glazed buildings in hot arid climates,” *Energy Build.*, vol. 40, no. 5, pp. 720–31, 2008.
[127] J.-M. Dussault and L. Gosselin, “Pre-design Tools and procedures for efficient integration of smart Windows,” 2014.
[128] B. P. Jelle, A. Hynd, A. Gustavsen, D. Arasteh, H. Goudey, and R. Hart, “Fenestration of today and tomorrow: A state-of-the-art review and future research opportunities,” *Sol. Energy Mater. Sol. Cells*, vol. 96, no. 1, pp. 1–28, 2012.
[129] A. Arnault, “Simulation et optimisation de l’intégration de matériaux à changement de phase dans une zone thermique,” Université Laval, 2012.
[130] H. Poirazis, Å. Blomsterberg, and M. Wall, “Energy simulations for glazed office buildings in Sweden,” *Energy Build.*, vol. 40, no. 7, pp. 1161–1170, 2008.
[131] C. Tian, T. Chen, H. Yang, and T. Chung, “A generalized window energy rating system for typical office buildings,” *Sol. Energy*, vol. 84, no. 7, pp. 1232–1243, Jul. 2010.
[132] T. Miyazaki, A. Akisawa, and T. Kashiwagi, “Energy savings of office buildings by the use of semi-transparent solar cells for windows,” *Renew. Energy*, vol. 30, no. 3, pp. 281–304, Mar. 2005.

APPENDIX

Appendix A1: Smart Windows Control Strategies for Building Energy Savings in Summer Conditions: A Comparison between Optimal and Model Predictive Controllers

Abstract

Advanced control strategies for smart windows (SW) are discussed in this paper. Since smart windows are used both to reduce energy consumption and to improve thermal and visual comfort, the optimal solar flux passing through the window is the result of a complex trade-off between daylighting and heat flow balance. A typical office building zone is modeled in TRNSYS with an integrated electrochromic smart window. Two types of advanced SW controllers, i.e. (i) a genetic algorithm based controller and (ii) a model predictive control based controller, are studied and compared to a base case scenario. The advanced controllers evaluate the hour-by-hour state of the smart window required to minimize the overall energy consumption (heating, cooling, lighting) while respecting constraints related to thermal and visual comfort. Results have shown that the two controllers, while presenting different control strategies, offer very similar and promising results in terms of energy savings and peak load reductions. Finally, opportunities resulting from the present work are discussed.

A1.1 Introduction

Smart windows (SW) [12] retained the attention of many researchers over the years since the early 90s. Research was initially oriented toward the development of potential technologies and the evaluation of the thermal and optical performance of idealized SW [123]. Then, simple control strategies applied to real SW technologies have been simulated and it was showed that SW could reduce the peak loads and the overall energy consumption compared to conventional “passive” glazings [35]. Later on, the notion of visual comfort was added in the control strategies in order to increase the market acceptance [54].

Nowadays, althought there are still many research projects on the development of materials offering enhanced performances for smart windows [124], the focus on smart windows is moving toward a deeper understanding of the optimal use of the existing SW technologies. With the increasing amount of available data (current weather and/or weather forcasts) and the highly sofisticated building energy management systems available [125], it is now possible to think about the optimal implementation of control systems for active façades such as SW.

The main purpose of this paper is to investigate the performance of two different SW controllers, i.e. a controller based on a genetic algorithm (GA) strategy and a controller based on a model predictive control (MPC) strategy. Since literature reveals that SW present higher energy savings in hot climates [126], this study is focused on the analysis of these control strategies during summer conditions.

A1.2 building model

The building model considered in the present work represents a typical single zone office space developed in TRNSYS [113] with Type 56. All simulations were performed with a time step of one hour. Since the focus of this work is about control strategies in summer conditions, the simulation period covered the months of June and July. While the hours simulated during the month of June were used as a warm up period as suggested by [83], every hours of the month of July were used for the analysis presented in the next sections.
The building was located in the city of Montreal (Quebec), Canada, with EnergyPlus weather data for Montreal (.epw file) being used as the weather file.

The building geometry consists of a 10 m (32.8 ft) × 10 m (32.8 ft) × 3 m (9.8 ft) (width (L) × depth (P) × height (H)) building zone with a south facing exterior wall (see Figure A1.1). The exterior wall considers a 10 m (32.8 ft) wide (L) by 2 m (6.6 ft) high (Hsw) double insulated unit electrochromic SW [12] on the upper part of the wall and an opaque wall (U-Value = 0.45 W/m^{2}K (0.08 Btu/hr-ft^2-°F) at the bottom (the wall construction being, from outside to inside: concrete siding, lightweight frame and gypsum indoor finishing). The thermal mass is accounted for in the envelope and in the floor (0.10 m (4 in) concrete floor slab). All other surfaces were defined as adiabatic interior surfaces. For the sake of illustration, Table A1.1 provides the SW center of glazing properties at normal incidence. However, the model uses the complete and detailed properties varying with the angle of incidence obtained in the IGDB.

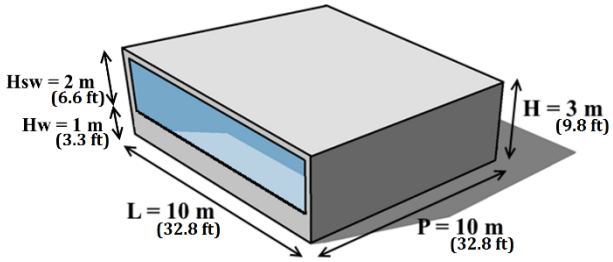

Figure A1.1: Building zone dimensions.

Table A1.1: Smart Window Center-of-Glazing Properties

Smart window states	U-Value [W/m^{2}K]	U-Value [Btu/h-ft^2-°F]	SHGC [-]	Tvis [%]	Tsol [%]
State 1 (S1) (bleached)	1.63	0.287	0.47	62.1	38.1
State 2 (S2)	1.63	0.287	0.17	21.2	8.6
State 3 (S3)	1.63	0.287	0.11	5.9	2.4
State 4 (S4) (fully tinted)	1.63	0.287	0.09	1.5	1.0

Gains and Schedules

Internal gains include artificial lighting, people and equipment. Table A1.2 presents the building zone heat gains with their radiative and convective fractions. Only sensible heat has been considered in the model.

Table A1.2: Building Zone Heat Gains

Gain Types	Max. Heat Gains		Convective Fraction	Radiative Fraction
	[W]	[Btu/hr]	[%]	[%]
Occupants (10)	730	2491	30	70
Equipment	800	2730	30	70
Light	352	1201	41	59

As presented in Table A1.2, the zone could accept up to 10 occupants (73W/occupant (249 Btu/hr/occupant)) and contains a power density of 8 W/m^2 (2.54 Btu/hr-ft^2) (floor area) for office equipment. The building lighting model calculates the illuminance distribution on interior surfaces of the zone considering daylight and artificial light from the lighting system (eight T8 lamps of 55 W (188 Btu/hr) each, i.e.: 440 W (1501 Btu/hr) totals). The artificial lighting system considers a 20 % heat to return. Illuminance levels from daylight were calculated using Daysim simulation software [87]. On the other hand, illuminance levels from the artificial lighting system were directly calculated from Radiance [88] and considered lamps uniformly distributed over the ceiling area. Since this paper was designed to compare SW control strategies, a simplified representation of the lighting system was considered, i.e.: a linear relation between lighting and power (no ballast factor and standby power loss considered). In order to offer proper luminosity on the work plane, a sensor has been set in the middle of the room's width and at two thirds of the room's depth (from the glazed wall). The minimal required luminosity at the sensor is labeled WP_{req} and has been set to 500 lux (46.5 fc) during occupancy hours [84]. The installed artificial lighting system is assumed to provide only the necessary amount of artificial light to meet the illuminance requirements during occupancy hours (dimmable system to prevent over lighting). Occupancy and work plane lighting requirements are presented in Figure A1.2.

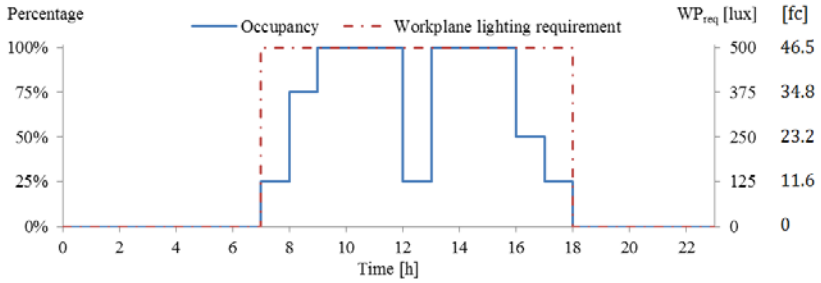

Figure A1.2: Week days schedule for occupancy (left axis) and work plane lighting requirement (right axis).

HVAC&R System

The HVAC&R system is simplified to a convective heating load Q_{heat} and a cooling load Q_{cool} that act directly on the air node of the building model. The indoor minimal and maximal temperature set points are 21°C (69.8 °F) and 25°C (77 °F) which are respectively lowered and raised by 3°C (5.4°F) outside the occupation hours. The system sizing considered the maximum heating and cooling loads for the building with the smart window in its clearer state (33 W/m^2 (10.5 Btu/hr-ft^2) and 83 W/m^2 (26.3 Btu/hr-ft^2) (floor area), respectively). A constant air volume ventilation system was installed. The volume flow rate was roughly estimated at 340 m^3/h (200 cfm). A heat exchanger was used to transfer heat between the air exhaust and make up air with 60 % efficiency.

A1.3 Smart window Control strategies

Base Case Scenario

The SW base case controller considers a SW set at its clearest state (S1) at all time. This passive approach is used to define the reference energy consumption of the building zone. It represents the energy consumption of an office building zone whose envelope is composed of a typical passive low-E window (low-E on surface #2). No shading system is installed in the base case. The control strategies presented in the following subsections are all compared to this base case scenario in order to assess the benefits of advanced control strategies.

Genetic Algorithm

The purpose of the genetic algorithm controller (optimal control) is to establish the possible minimum overvall energy consumption of the zone (heating, cooling and artificial lighting) [127]. Results of other control strategies, such as MPC, could then be compared to the results achieved with the GA in order to assess their performance. To achieve such optimal control

for active SW, a controller based on a genetic algorithm [58] assuming a perfect building model representation and perfect weather forecast (i.e. one perfectly knows the future weather parameters) have been used. The algorithm minimizes an objective function (in this case, the overall energy consumption) by evaluating a certain number (population) of different combinations (phenotypes) of the design variables (SW state at each time step). The initial population evolves generation by generation by keeping the phenotypes of a generation that give the best results and by creating the following generation from those phenotypes and newly created ones (children) by crossovers and mutations.

The design variables involved are thus the SW states at each simulated hour where sunlight is available. To minimize computational time, hourly artificial lighting variables have not been considered as design variables, but rather as values adjusted to meet requirements depending on the SW state, the lighting control strategy and the lighting set point.

The objective function to minimize is the overall energy consumption (Q_{Tot}), in Wh/m^2 (Btu/ft^2) of floor area, defined as:

$$Q_{Tot} = (Q_{Heat} + \frac{Q_{Cool}}{COP} + Q_{Light}) \quad \text{(A1.1)}$$

where Q_{Heat} is the total energy consumed for heating in [Wh/m^2] (Btu/ft^2), Q_{Cool} is the total heat removal required for cooling in [Wh/m^2] (Btu/ft^2), COP is the coefficient performance of the cooling system (COP = 3 in this case) and Q_{Light} is the total lighting energy consumption in [Wh/m^2] (Btu/ft^2). Constraints of minimal light requirements were defined.

Optimization parameters and convergence criteria used for the optimization runs are presented in Table A1.3. It is important to understand that the GA optimization is not intended for real-time control of SW since the required computational time is too long for such applications. It serves here only to establish the optimal achievable level of performance with an “optimal control” against which real-time strategies could be compared.

Table A1.3: Parameters of the Genetic Algorithm

Parameters	Value	Units
Number of phenotypes per generation	40	-
Maximum number of generations	75	-
Number of generations with unchanged Q_{Tot} value before convergence	30	-
Proportion of children per generation	80	%
Children mutation probability	5	%
Number of chromosomal crossovers	2	-

Model Predictive Control (MPC)

In the MPC approach (see Figure A1.3), a linearized internal model (based on a simplified space-state resistance-capacitance thermal model of the building developed in Matlab [26] runs as a closed-loop observer of the building states ($\hat{x}$) in parallel to the "real" process (TRNSYS model). These states are then used to calculate the predictions $\hat{Y}$ of the building outputs T over the prediction horizon Hp. These predictions are then optimized considering the possible design variables (SW states) in order to minimize Q_{tot} (Eq. (A1.1)) over the entire prediction horizon. U_c represents the inputs to supply to the building energy management system (heating/cooling loads, lighting load and SW state). The optimization environement used in this work was YALMIP with the GUROBI Solver. The optimization constraints were the minimum lighting requirements (hard constraints), the HVAC&R system maximal capacities (hard constraints) and the temperature setpoints (soft constraints). The MPC controller includes the observer, the predictor and the optimization procedure. In this work, the prediction horizon considered in the MPC controller was 24 hours.

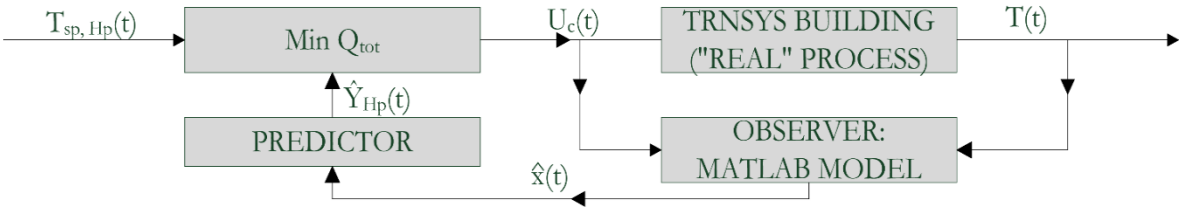

Figure A1.3: Model based predictive control architecture.

Besides the optimization solvers, the MPC controller is different from the GA controller by the fact that it contains an internal model that is different from the "real" process and introduces model errors in the predictions. For this reason, the states of the internal model are updated at each time step with the measured outputs of the TRNSYS model in order to

maintain convergence. As presented in Figure A1.3, the architecture of the MPC controller is developed for real-time control applications. However, as for the GA controller, prefect weather forecast is used in the MPC controller in order to assess its maximal performances.

A1.4 Results

A comparison of the base case scenario, the GA and the MPC controllers is illustrated in the following subsections on a monthly and an hourly basis. From the results, one could clearly see that the two advanced controllers show considerable savings.

Monthly Results

Table A1.4 presents results of energy consumption (cooling, lighting and total) as well as the maximum peak load for the month of July. Fan power was not considered in the results analysis presented in this section. Table A1.4 illustrates the fact that GA and MPC controllers reduce the overall energy consumption by 33% and 32 % respectively, compared to the base case scenario. For both the GA and the MPC controllers, this overall energy reduction is the result of a trade-off between cooling energy consumption (36% and 35% decrease, respectively, compared to the base case) and lighting energy consumption (approximatively 0.22 kWh/m^2 (70 Btu/ft^2) increase in both cases). Total energy savings are mainly explained by the fact that the darker states of the SW reduce dramatically the solar heat gains entering the building while forcing the artificial lighting system to operate a little more to respect illuminance requirements. Table A1.4 also illustrates cooling peak load reductions of 26% and 25% for the GA and MPC, respectively, compared to the base case. This reduction in peak load suggests that buildings equipped with SW and advanced controllers could be designed with smaller cooling equipment, thus reducing equipment initial costs.

Table A1.4: Results - Month of July

SW controllers	Cooling energy consumption		Lighting energy consumption		Total energy consumption		Cooling Peak load	
	[kWh/m^2]	[Btu/ft^2]	[kWh/m^2]	[Btu/ft^2]	[kWh/m^2]	[Btu/ft^2]	[W/m^2]	[Btu/hr-ft^2]
Base case	7.49	2375	0.10	32	7.59	2407	47.16	14.95
GA	4.76	1509	0.32	101	5.08	1611	35.03	11.11
MPC	4.81	1525	0.33	105	5.14	1630	35.27	11.18

Montly results presented in Table A1.4 also illustrates the fact that the two advanced controllers present very similar results in term of energy consumption and cooling peak load. The MPC thus seems a very promising type of controller for real-time SW control applications.

Hourly Results

In order to present representative hourly results for the month of July, results for each hour between July 16th (Monday) and July 22nd (Sunday), inclusively, are presented in Figure A1.4.

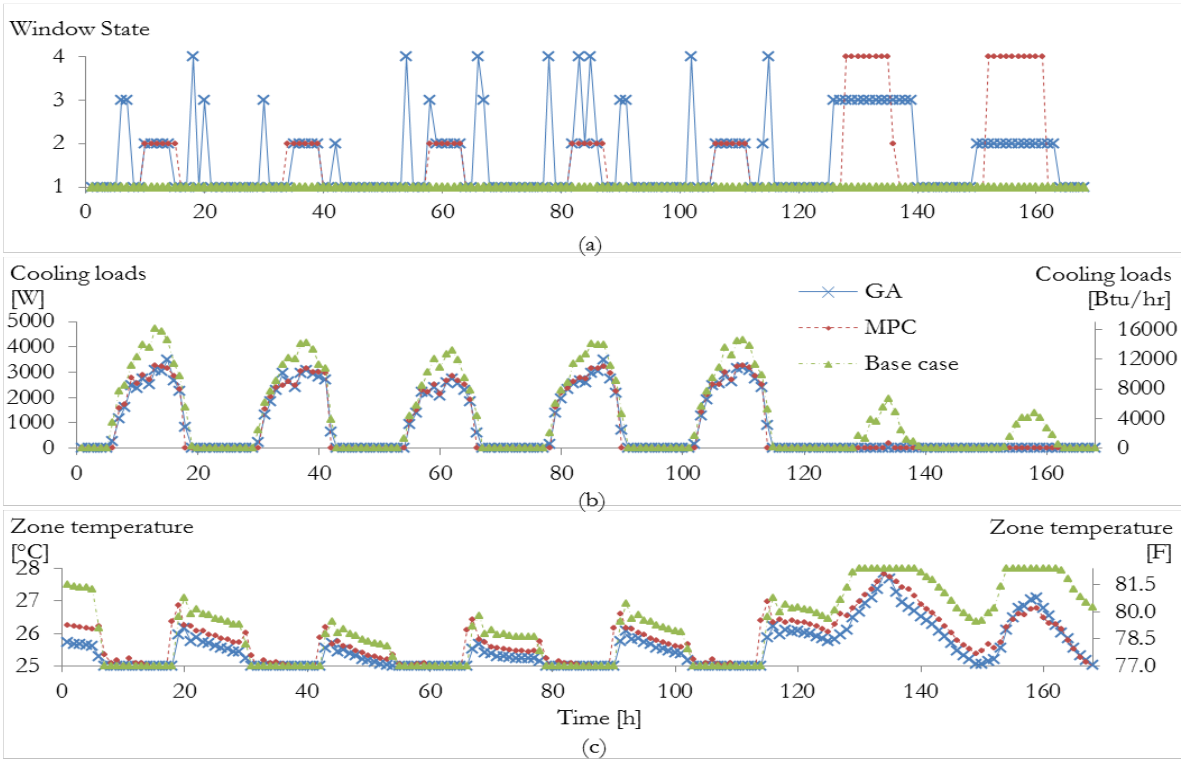

Figure A1.4: Hourly results from July 16th (Monday) to July 22nd (Sunday), inclusively: (a) Window states, (b) Cooling loads and (c) Zone temperature.

The SW states presented in Figure A1.4a show that the GA and MPC controllers have a quite different control approach during weekday off-occupancy hours. During these hours with sunlight (early morning and evening), the GA controller tends increase the opacity of the SW in order to limit as much as possible solar heat gains (even if solar intensities are very low) while the MPC waits for higher solar intensities to select darker states. This difference of control strategies impacts the total energy consumption results for the GA and MPC in Table

A1.4 and is visible in Figure A1.4b. During occupied weekday hours both the GA and MPC select the state S2 (Figure A1.4a) as the best trade-off between cooling and lighting loads. During the weekend (no occupancy and illuminance requirements), both the GA and MPC limit the cooling loads (Figure A1.4b) by setting the SW states to darker states (Figure A1.4a). Again, the control strategies of the GA and MPC are different. The GA sets the SW states to clearer states, but for a longer period of time (including hours of low solar intensities) compared to the MPC. In Figure A1.4c, the profiles of zone temperature reveal that while the base case and GA controllers respect the comfort conditions at all time (25°C (77 °F) maximum during occupancy hours), the soft constraints of the MPC controller tolerate slight deviations from the temperature requirements. This violation of the constraints is mainly due to the fact that the MPC controller contains model errors.

A1.5 Conclusions

This paper presents the performance comparison of two advanced SW controllers aiming to optimize energy savings and peak loads reduction. The developed controllers were based on either a genetic algorithm or a model predictive control strategy. Results of a base case scenario considering a SW at its clearest sate at all time were also considered as the reference values. All results were analyzed considering summer conditions (month of July) for the city of Montreal and were based on a typical office building zone with a south oriented façade modeled in TRNSYS.

The analysis of the different control strategies allowed assessing the fact that advanced control strategies could potentially offer energy savings (cooling + lighting) of the order of 33% and peak load reduction of about 26% while maintaining temperature set points and lux levels to maintain a comfortable built environment. It was shown that the MCP yields to a total energy consumption very similar to the theoretically optimal control of the GA. Therefore, the MPC controller is thus a promising type of controller for real-time SW control applications. Results have also shown that different control strategies could lead to similar overall results.

In future work, it would be important to release some of the assumptions that were made in this work. For example, further studies could consider a conventional shading system

installed to the base case scenario as well as a higher lighting power density for a more realistic comparison with advanced control strategies. Also, MPC controllers should be tested by taking into account uncertainties such as that of the weather forecast or occupancy with simulations covering a complete year and different façade orientations. Furthermore, the performance of MCP controllers should also be compared to rule based control strategies, which are often easier to implement but not as efficient.

Appendix A2: Pre-design tools and procedures for efficient integration of smart windows

Abstract

In this paper, design tools are proposed to architects, engineers and other building professionals involved in the pre-design stage of a project, in order to facilitate the integration of smart windows into the envelope. Smart window technologies can influence the building energy performance and the occupants' visual comfort. Therefore, it is of prime importance for building professionals to possess sufficient tools and knowledge to evaluate properly the pros and cons of smart windows. One of the aspects complicating the analysis is that the overall performance of smart windows is largely influenced by how they are operated, and by a variety of parameters such as the building features (thermal mass, etc.), the occupants, etc. A numerical model was developed to simulate the dynamic modeling of a zone, with a façade occupied by a smart window, and was coupled to an optimization toolbox to determine the optimal control of the opacity. This work thus helps to gain a better understanding of how smart window opacity states and their control affect the overall energy performance of buildings. Finally, modeling strategies as well as preliminary control guidelines to assess energy performance of buildings with smart windows are proposed based on this analysis.

A2.1 Introduction

In early stage of building design, a good estimate of heating, cooling and lighting demands is required in order to assess the performance of the design. Nowadays, for environmental and economic reasons, enhanced building technologies are developed and integrated into designs to reduce energy consumption. Actually, many envelope components have evolved from previously passive [128] to active technologies often qualified of “smart” [9].

Among these technologies, smart windows [12] present opportunities to reduce building energy consumption by controlling solar heat gains. However, the complexity of heat transfer interactions in buildings can make optimal control of such technologies quite complex to reduce efficiently the energy consumption while maintaining at the same time occupants’ comfort.

Research in the field of smart windows was initiated in the late 80s and early 90s by the Environmental Energy Division of the Lawrence Berkeley National Laboratory. At that time, results were presented mainly for idealized electrochromic [35][123] windows and demonstrated a potential regarding energy loads reduction and the possibility to reduce the size of the mechanical systems. Later, the evolution of smart window technologies enabled the assessment of the performance of real electrochromic glazings in different climates and with different simple control strategies [49]. Results confirmed that real smart windows present energy consumption reduction opportunities and showed that better performances are obtained when daylight is maximized to achieve visual requirements. Today, research on smart windows is highly oriented towards more complex and efficient control strategies optimizing the trade-offs between solar gains and daylight requirements [54]. Despite the work conducted up to now, it is usually agreed that more research on smart window dynamics is required to develop more efficient predictive control strategies and to offer more simplified tools to architects and building designers, in order to truly benefit from the potential of these technologies.

This paper presents a model to simulate a perimeter zone with smart windows, and optimization results of the overall building energy consumption considering the control of

the smart window and artificial lighting system. The objectives of this work are: 1- Increase the understanding of the effect on energy performance of relevant parameters related to design, control or climate, 2- Assess the relevance of advanced control on a smart window/artificial lighting combined system, 3- Develop tools (procedures) to evaluate properly smart window potential benefits and design strategies for building perimeter zones.

A2.2 Methodology

Building model description

A building model was developed to calculate the overall energy consumption (i.e., heating, cooling and artificial lighting demands). Thus, the model considers a building located in Montreal, Québec, Canada, and is subdivided into a lighting model created in Matlab [26] and a thermal model developed in TRNSYS. Both lighting and thermal considerations are based on previously validated models [26][129].

To limit computational time, the building model considers a single perimeter zone (5 m width × 5 m depth × 3 m height) maintained at a constant temperature (T_{in}=20°C) with a double glazed south façade and five interior adiabatic surfaces. The floor surface is a massive 0.254 m thick concrete slab and all other surfaces are modeled with non-massive materials. Surface and floor properties are presented in Table A2.1.

Table A2.1: Surface and floor properties

	Values	Units
Surface solar and IR emissivities		
ε_{window}	0.84	-
$\varepsilon_{interior\ surfaces}$	0.90	-
Floor slab properties		
$c_{p,floor}$	837	J/kgK
ρ_{floor}	2243	kg/m^3
k_{floor}	1.73	W/mK

Since todays' architecture values building designs with highly glazed façades [130], the exterior wall is modeled with a window-to-wall ratio (WWR) of 1, even though it is known

that buildings with WWR between 0.3 and 0.5 consume less energy [131][132]. Consequently, results presented with WWR=1 should be considered as an upper limit in terms of energy performance enhancement provided by smart windows since smaller WWR will reduce the influence of smart windows on the overall energy consumption.

The smart window considered in the model is a double pane insulated glass unit (IGU) electrochromic (EC) window with four possible states of opacity. The IGU has 6 mm thick glass panes and a 12.7 mm gap (90% argon/10% air). EC layer is located on surface 2 of the IGU (i.e. interior surface of the exterior glass pane). Table A2.2 presents center-of-glazing values for each state, obtained from the International Glazing DataBase (IGDB) via the Window6 software. Note that the simulation model actually uses detailed angular values of the glazing properties, but incident values are reported in Table A2.2 for the sake of comparison between the different states.

Table A2.2: Center-of-glazing properties of a smart window

Smart window states	**U-Value** W/m^2K	**SHGC** -	**Tvis** %	**Tsol** %
State 1 (S1) (bleached)	1.63	0.47	62.1	38.1
State 2 (S2)	1.63	0.17	21.2	8.6
State 3 (S3)	1.63	0.11	5.9	2.4
State 4 (S4) (fully tinted)	1.63	0.09	1.5	1.0

Internal gains are related to artificial lighting, occupancy and equipment. They are summarized in Table A2.3, with their radiative and convective fractions. Only sensible heat has been considered in the model.

Table A2.3: Internal gains

Gain types	**Heat gains** W/h	**Convective fraction** %	**Radiative fraction** %
Occupants (3)	219	30	70
Equipment	200	30	70
Light	200	41	59

As presented in Table A2.3, gains for occupants consider 3 occupants doing moderate office work (73W/h/occupant). Furthermore, lighting gains consider a heat-to-return percentage of 20% that is thus not accounted for in the energy balance.

The building lighting model calculates the illuminance distribution on interior surfaces of the building considering combined daylight and artificial light. In order to offer proper luminosity on the workplane, a sensor has been set in the middle of the room's width and at two thirds of the room's depth (from the glazed wall). The minimal required luminosity at the sensor is labeled WP_{req} and has been set to 500 lux [84] during occupancy hours. Although more visual comfort considerations could have been included, the aims of the ongoing research are more energy-oriented. Further studies will consider more exhaustive visual comfort models and their impacts on control strategies and building energy consumption.

To represent a typical transient variation of internal gains and lighting requirements in office buildings, schedules have been created. Figure A2.1 presents the schedule of occupancy and workplane light requirement for week days. The use of miscellaneous equipment follows the same pattern as occupancy. For simplicity, internal gains are set to zero at all time during week-ends.

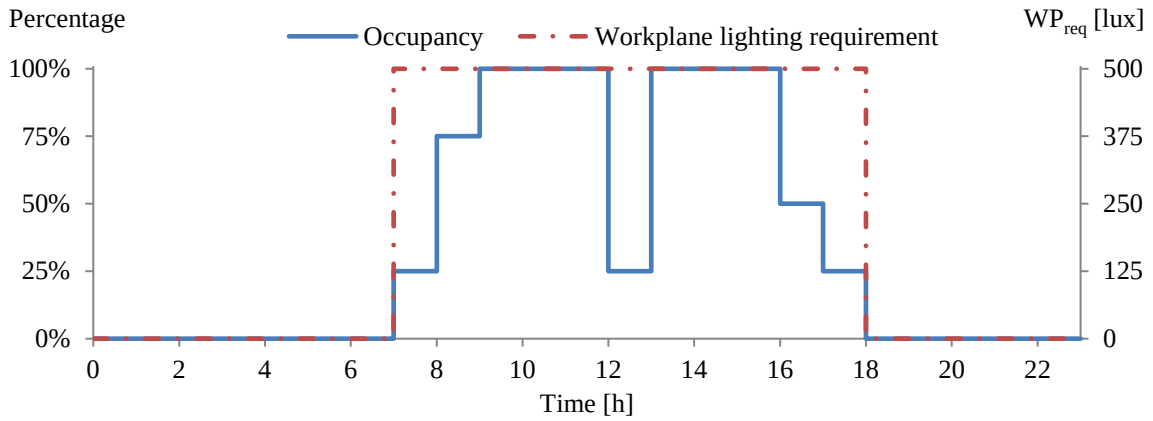

Figure A2.1: Week days schedule for occupancy and workplane lighting requirement.

Control systems

The two building systems designed to control solar heat gains and lighting on the workplane are the smart window and the artificial lighting systems. Figure A2.2 illustrates the influence of the control systems on the overall energy consumption.

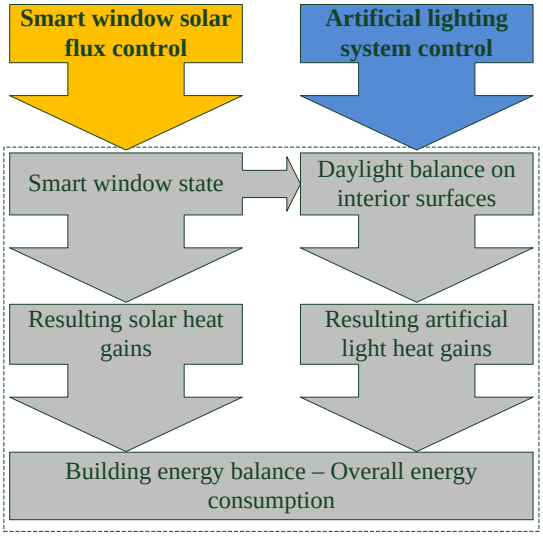

Figure A2.2: Systems control scheme.

Many different control strategies could be used [49] in order to achieve energy savings and visual comfort. To assess the relative effectiveness of different strategies, overall energy consumption results have been obtained considering the design control parameters presented in Table A2.4.

Table A2.4: Active systems control types

	Smart window	**Artificial lighting**
Control types	SW-1S	LCS1
	SW-4S	LCS2
		LCS3

In Table A2.4, there are two types of control for the smart window and three types for the artificial lighting. For the smart window, all control types begin with “SW” (standing for Smart Window) and are followed by a term “#S” defining the number of possible opacity states:

- 1S refers to a passive glazing, i.e. no control. The window remains at the same state (S1, S2, S3 or S4) during the entire simulation;
- 4S refers to four possible states, i.e. Clear, Fully tinted and two other intermediary states as presented in Table A2.2.

For the artificial lighting system, all control types begin with "LCS" (standing for Lighting Control System) and are followed by a number referring to the complexity of the control strategy:

- LCS1 refers to a basic artificial light control system always "On" during occupancy hours;
- LCS2 refers to an active control that can turn On/Off the lighting system depending on available daylight at the workplane sensor;
- LCS3 refers to an advanced artificial light control system that adjusts artificial light power to supply enough visible light at the workplane sensor during occupancy hours without over lighting (dimmer).

Simulation results presented in this paper were obtained by considering the 13 control strategy combinations of Table A2.5.

Table A2.5: List of control strategy combinations for simulations

Strategy combination #	SW	Light
1	SW-1S $_{State\ 1}$ (S1)	LCS1
2	SW-1S $_{State\ 2}$ (S2)	LCS1
3	SW-1S $_{State\ 3}$ (S3)	LCS1
4	SW-1S $_{State\ 4}$ (S4)	LCS1
5	SW-1S $_{State\ 1}$ (S1)	LCS2
6	SW-1S $_{State\ 2}$ (S2)	LCS2
7	SW-1S $_{State\ 3}$ (S3)	LCS2
8	SW-1S $_{State\ 4}$ (S4)	LCS2
9	SW-1S $_{State\ 1}$ (S1)	LCS3
10	SW-1S $_{State\ 2}$ (S2)	LCS3
11	SW-1S $_{State\ 3}$ (S3)	LCS3
12	SW-1S $_{State\ 4}$ (S4)	LCS3
13	SW-4S (optimization)	LCS3

The first strategy combination of Table A2.5 is the base case scenario considering a passive window having the properties of State 1 of the EC window, with lights "On" during all

occupancy hours. This scenario has been set as the base case since it represents a typical perimeter building office with a passive low-e ($\varepsilon_{EC,layer}$=0.147) double insulated glazing unit with only manual control for light. Combinations 2 to 12 allow determining the optimal passive state as a function of the lighting strategy. Finally, combination 13 considers optimization runs (see the following section for details about the optimization procedure) that evaluate optimal hourly smart window states to minimize overall energy consumption with four possible SW states (States 1 to 4). Optimization runs consider a totally bleached SW state (State 1 in Table A2.2) between sunset and sunrise.

Optimization procedure

Before analyzing the behavior of a combined smart window/artificial lighting system, one must first determine which control gives optimal results. To obtain such control for active SW strategies (i.e., strategy 13 of Table A2.5), a genetic algorithm [58] has been used. This algorithm minimizes an objective function (in this case, the overall energy consumption) by evaluating a certain number (population) of different combinations (phenotypes) of the design variables (SW State at each time step). The initial population evolves generation by generation by keeping the phenotypes of a generation that give the best results and by creating the following generation from those phenotypes and newly created ones (children) by crossovers and mutations.

The design variables involved are thus the SW states at each simulated hour where sunlight is available. To minimize computational time, hourly artificial lighting variables have not been considered as design variables, but rather as values adjusted to meet requirements depending on the SW state, LCS and the lighting set point.

The objective function to minimize is the overall energy consumption (C_{OEC}), in Wh/m^2 of floor area, defined as:

$$Q_{Tot} = \left(Q_{Heat} + \frac{Q_{Cool}}{COP} + Q_{Light}\right) \quad \text{(A2.1)}$$

where Q_{Heat} is the total energy consumed for heating in [Wh/m^2], Q_{Cool} is the total energy consumed for cooling in [Wh/m^2], COP is the coefficient performance of the cooling system and Q_{Light} is the total lighting energy consumption in [Wh/m^2].

Optimization parameters and convergence criteria used for the optimization runs are presented in Table A2.6.

Table A2.6: Parameters of the Genetic Algorithm

Number of phenotypes per generation	40	
Maximum number of generations	2000	
Number of generations with unchanged C_{OEC} value before convergence	250	
Proportion of children per generation	80	%
Children mutation probability	4	%
Number of chromosomal crossover	1	

A2.3 Results

Effect of light control strategy with fixed opacity state

To integrate properly smart windows into building designs, one must first understand the behavior of each possible state of smart windows over a complete year. This way, the state leading to the lowest energy consumption could be determined for each season as a function of the lighting strategy.

Figures A2.3 to A2.5 present, for the artificial lighting controls LCS1, LCS2 and LCS3 respectively, the overall energy consumption for a typical day of each season for the four different fixed SW states (passive mode, i.e. no control is applied to the SW). These figures also present the approximate yearly behavior (average) for each state which is the average of the results for each typical day.

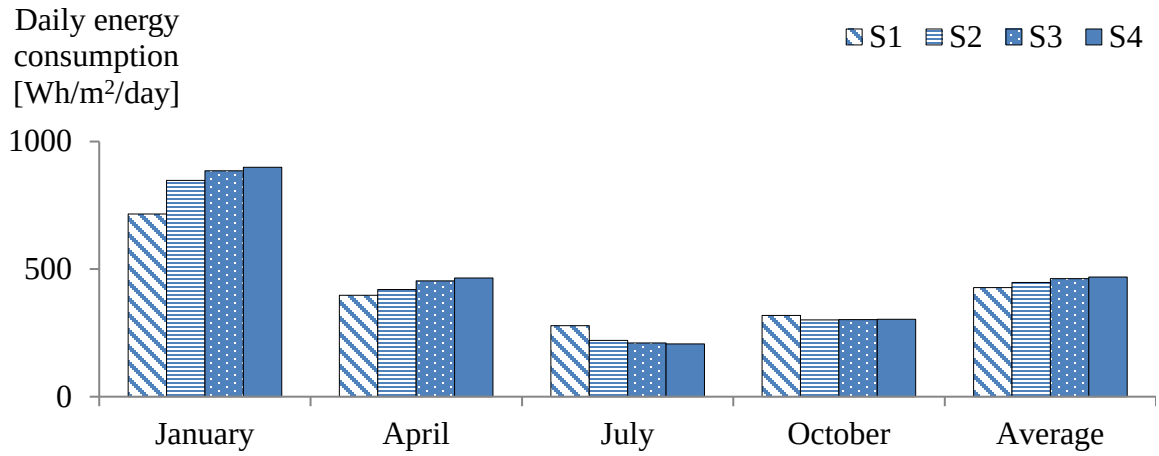

Figure A2.3: Effect of window passive opacity state on building loads with light control LCS1.

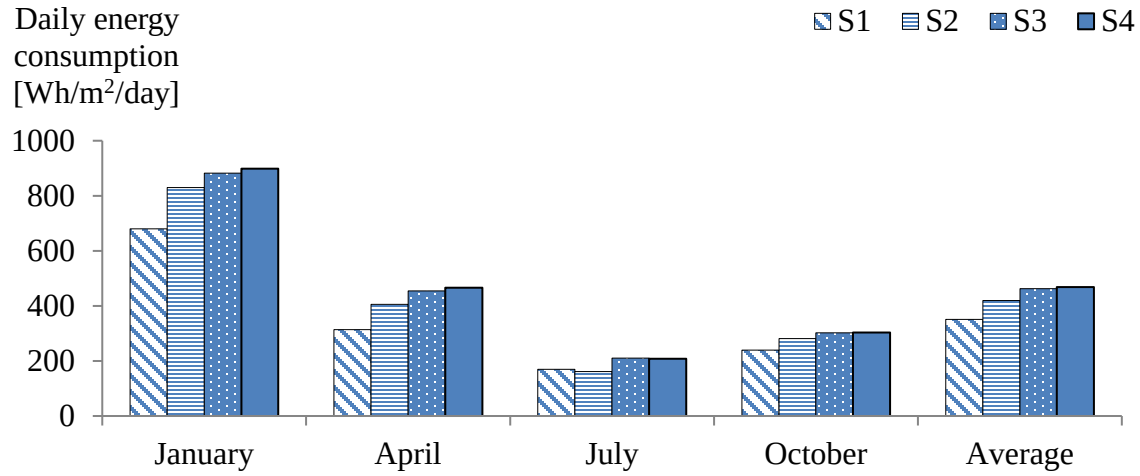

Figure A2.4: Effect of window passive opacity state on building loads with light control LCS2.

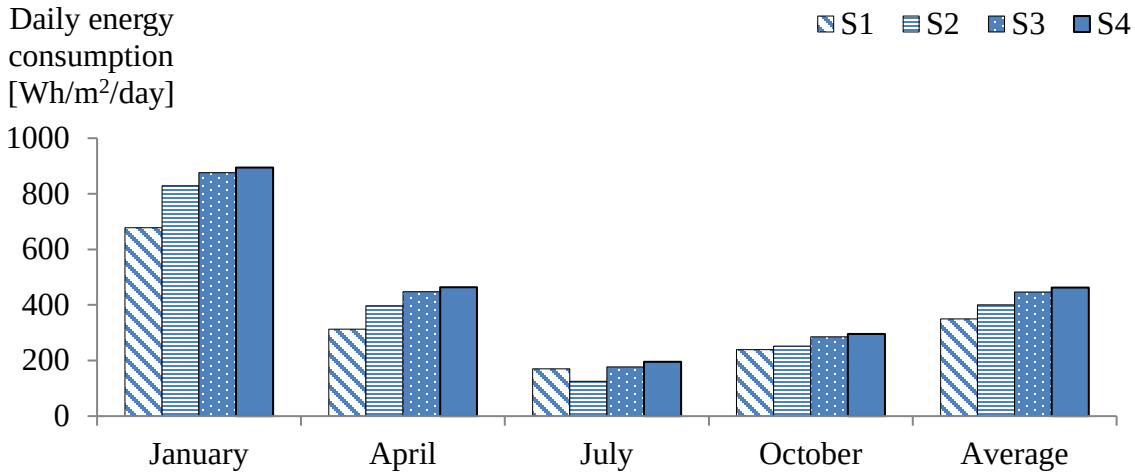

Figure A2.5: Effect of window passive opacity state on building loads with light control LCS3.

From Fig. A2.3, we realize that a passive window with the sate S1 (clear state) combined with artificial lighting always on during office hours (LCS1) offers the lowest energy consumption values for January and April (where outside temperature values are lower, i.e.: mean daily temperatures around -13°C and 0°C, respectively) while passive windows with states S4 and S3 offer the lowest values for July and October (where outside temperature values are higher, i.e.: mean daily temperatures around 19°C and 8°C, respectively).

In Figure A2.4, it is observed that the on/off control strategy (LCS2) for the artificial lighting system has the following effects compared to the situation with lights always turned on (LCS1): 1 – There are now changes for January and April, 2- The best passive state changes from S4 to S2 in July and from S3 to S1 in October. Figure A2.5 (with LCS3) exhibits similar trends compared to Figure A2.4 (LCS2).

Regardless of the lighting control strategy considered, Figs. A2.3, A2.4 and A2.5 show that even if different passive states are more adapted for different seasons, S1 seems to be the most appropriate state for a passive use on an annual basis for the building considered. To benefit from optimally varying window properties at all time, a building designer must integrate a smart window control to reduce energy consumption.

To assess the increase in performance associated to different controls, one could use the behavior obtained from those figures in a building simulation software to evaluate more precisely benefits of smart windows by dividing passive states by season. For example, if a designer is interested in a building with lighting control LCS1, he/she could run a simulation over a year using S1 for days of winter and spring seasons and S4 and S3 for summer and fall respectively. This procedure applied to the present building reduces the yearly energy consumption from 150.64 kWh/m^2 (S1-LCS1) to 143.71 kWh/m^2 ($S1_{winter-spring}$+$S4_{summer}$+$S3_{fall}$-LCS1), which corresponds to a reduction of about 4.6% only by considering a simplified control with four opacity changes per year. The same procedure applied for lighting control LCS3 reduces the yearly energy consumption from 118.16 kWh/m^2 (S1-LCS3) to 111.01 kWh/m^2 ($S1_{winter-spring-fall}$+$S2_{summer}$ –LCS3), which corresponds to savings of about 6.1%.

Effect of smart window control on building loads

The procedure presented in the previous section based on optimal seasonal SW states to approximate SW thermal performance could be followed for a particular project by building designers for a preliminary evaluation of potential savings. For designers interested to assess more precisely potential savings, a procedure taking into account more finely the modularity of smart windows should be elaborated. This section presents avenues that might offer solutions with this respect.

Figure A2.6 reports the results of a full hour-by-hour optimization of the SW opacity, combined with the advanced lighting control (LCS3). As presented in the previous section, S1 represents the most efficient passive state over a complete year for the building considered. For this reason, the three S1 results of the previous section are repeated in Figure 6 for the sake of comparison.

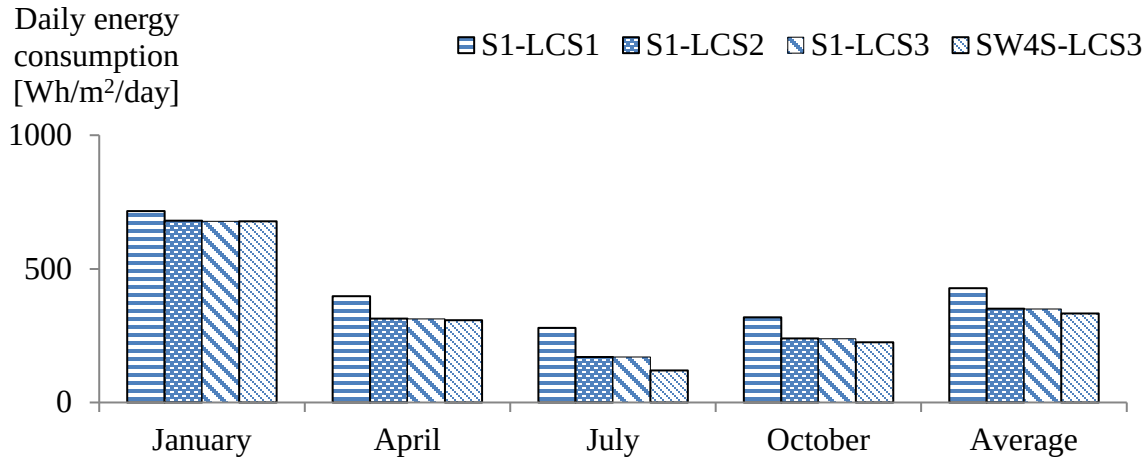

Figure A2.6: Effect of smart window opacity state control with lighting control LCS3 on building energy consumption compared to passive states**.**

From Figure A2.6, we can observe that the hourly control (optimization) of the smart window brings more energy savings, with average reductions of the energy consumption of 22.3%, 5.2% and 4.9 % compared with S1-LCS1, S1-LCS2 and S1-LCS3, respectively.

Moreover, it is clear from Figure A2.6 that the highest energy consumption reduction is happening during the hot season (July) which corroborates results of other studies on the subject [38]. In July, reductions of the energy consumption are 57%, 18% and 18% compared

with S1-LCS1, S1-LCS2 and S1-LCS3, respectively. Savings for S1-LCS2 and S1-LCS3 are the same since daylight illuminance values on the workplane are higher than the required set point for all hours in both cases.

Compared to passive season control (S1winter-spring-fall+S2summer –LCS3), hourly control optimization (SW4S-LC3) of the smart window brings average reductions of the energy consumption of about 1.8%, meaning that the simplified seasonal control approach could provide a fairly good estimation of smart window potential.

Figure A2.7 presents results for July of hourly opacity states optimized to reduce the overall energy consumption and its influences on cooling, heating and lighting loads compared to S1-LCS3 (best passive state over all seasons) and S2-LCS3 (best passive state for summer).

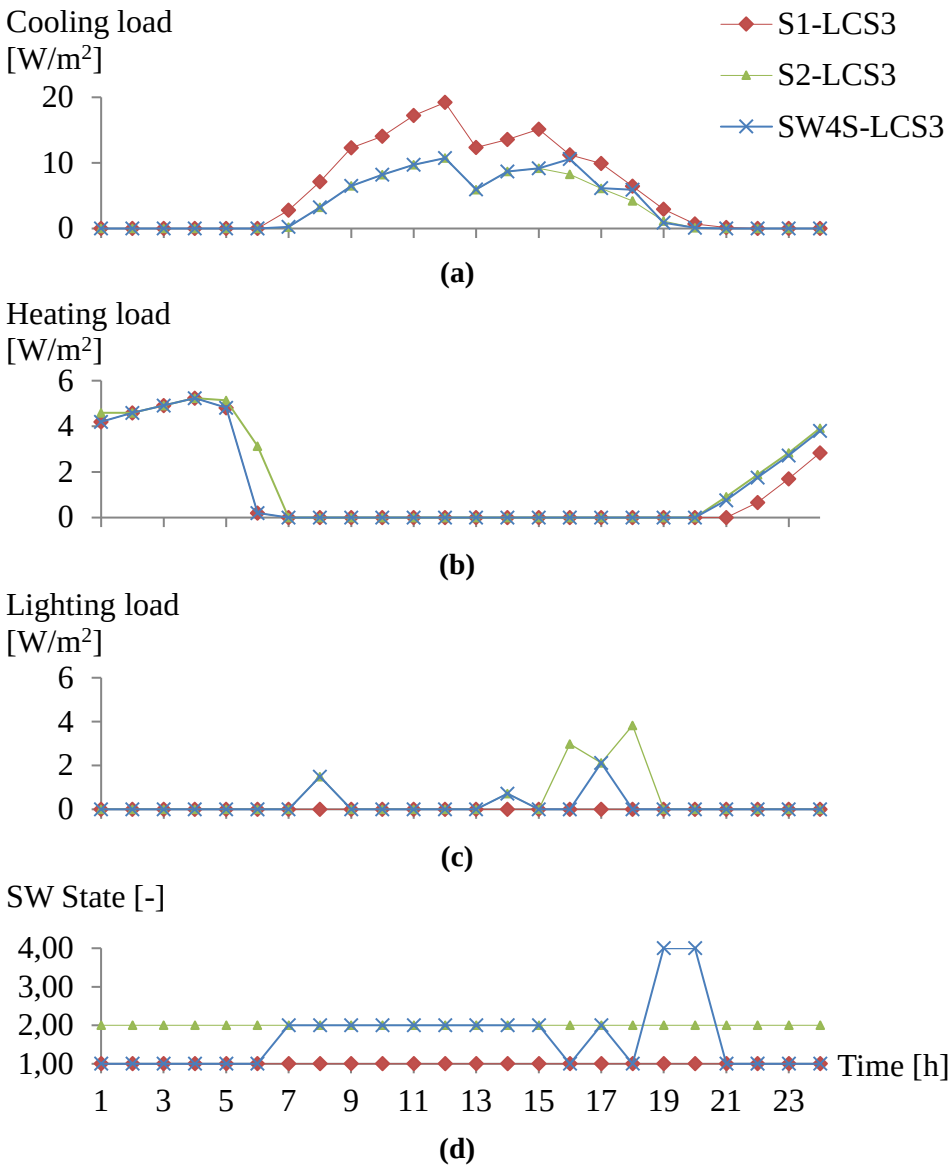

Figure A2.7: Hourly results for a typical day of July – a) Cooling loads, b) Heating loads, c) lighting loads and d) Smart window optimized opacity state.

From Figure A2.7, we can realize that the optimal hourly control of the smart window states (Fig. A2.7d) influences in a complex manner the cooling load (Fig. A2.7a). It is reduced due to lower solar heat gains at high opacity compared to S1-LCS3 and slightly increased due to higher solar heat gains (16h and 18h) compared to S2-LCS3. The heating load is also affected (Fig. A2.7b); it is increased slightly during evening and at night compared to S1-LCS3 due to the fact that the thermal mass of the floor slab has not received as much solar energy during the day. Compared to S2-LCS3, the optimal solution reduces heating due to higher solar heat

gains. Furthermore, heating load results highlight the fact that a 24 hours period does not take into consideration the charging and discharging of the thermal mass for hours previous to the simulation start time. Finally, for the artificial lighting demand (Fig. A2.7c), some hours require additional artificial lighting since less daylight reaches the workplane compared to S1-LCS3. Compared to S2-LCS3, less artificial lighting is required due to higher visible transmittance states at some hours.

From the results presented in this section, it is thus clear that an efficient hourly control of SW states provide higher savings than passive states. This being said, simple procedures shall be offered to building designers in order to roughly evaluate SW performance based on an optimal or nearly optimal control. The following guidelines are preliminary avenues that are proposed to address this need. They are based on the observations of optimized opacity such as that presented in Figure A2.7. The following optimal SW behaviors can be noted:

- At night (solar radiation = 0 W/m^2) → Switch to state S1
- While $Q_{heating,S1} > 0$ → Switch to S1 to allow as much solar radiation as possible in the building
- While $Q_{cooling,S1} > 0$ AND Workplane lighting requirement = 0 lux → Switch to S4

Otherwise, i.e. when there is a cooling load at a given time ($Qcooling,_{S1} > 0$) and also a workplane lighting requirement larger than 0, the optimal state of the SW, S_{opt}, varies. Based on the optimization results, it was found that the best SW state was mostly correlated with the total solar irradiation incident on the window, G_{tot}. The approximate range of G_{tot} for which the optimal state is S1 is reported in the first line of Table A2.7, for each season. Similarly, the next lines of this table correspond to the range of G_{tot} for which the best state is S2, S3 or S4.

Table A2.7: Range of total façade incident solar radiation for which the best SW state is as indicated, during cooling hours with a lighting requirement of 500 lux.

Optimal SW state	G_{tot} [W/m^2]			
	Winter	Spring	Summer	Fall
S1	All values	0 - 225	0 - 100	0 - 110
S2	-	225 and over	100 and over	110 and over
S3	-	-	-	-
S4	-	-	-	-

Table A2.7 also reveals that the range of G_{tot} for which each state is optimal depends on the season considered. In other words, there are other aspects than just total solar incident irradiation to consider. For example, the indoor-to-outdoor temperature difference also affects to some respect which state is best at a given time.

Further studies will focus on the development of a more general correlation for the optimal state selection considering G_{tot}, the exterior-to-interior temperature difference, and internal gains. To ensure that the procedure and guidelines presented in this section are applicable to different building projects, annual simulations for different types of building, orientations and climates should be conducted. Further research will cover these elements.

A2.4 Discussions and conclusions

This paper presents thermal and daylight analysis results based on simulations for south perimeter building zones located in Montreal.

Considering an approach with passive opacity states (i.e., no optimized hour-by-hour changes of opacity), we determined the energy consumption as a function of the opacity state, the climate and the lighting strategy. The bleached state was better during cold exterior temperatures while darker states were preferred for warmer seasons. However, regardless of the selected artificial lighting control strategy, the bleached state is preferred to other darker passive states over an annual basis for climates as in Montreal. Considering these results, a preliminary design assessment procedure was proposed for designers. The procedure consists in calculating the building energy consumption with glazing properties for all passive states

for a typical day of each season to evaluate which passive state is best (season by season). Then, a calculation combining these results could be performed, using the best selected passive state at each season to estimate total energy consumption with the integration of smart windows at a given season. Annual energy savings could thus be estimated compared to a base case building. It was found that this approach can provide a fairly good estimate of the SW performance on an annual basis.

To assess the relevance of advanced active SW control strategies, a genetic algorithm optimized hour-by-hour the opacity of a SW. Results have shown that optimal control is desirable mostly for warmer seasons and could offer savings between 5% and 22% compared to the best yearly passive state, depending on the artificial lighting strategy. Also, since the highest savings have been obtained for the summer, a more detailed results comparison have been made with the best yearly state (S1) and the best passive summer state (S2). It was shown that optimized control outperforms the passive state S1 mostly by reducing cooling loads and the passive state S2 mostly by reducing heating and lighting loads. Preliminary guidelines for control have been proposed based on the results of optimization. These guidelines consider the optimal state selection at each hour depending on heating or cooling conditions, lighting requirements and total solar radiation incident on the glazing.

As mentioned previously, reported results are relevant for South oriented perimeter zones of an office building, in a moderate climate. For different climates and/or façade orientations, one could follow the methodology presented in this article to obtain a relevant assessment of SW in terms of building energy consumption. Further studies will examine the influence of relevant building parameters (façade orientation, thermal mass, COP of systems, acceptable interior T° ranges, and other climates) on optimal results. More generic performance indicators and procedures will be developed for predesign of buildings with integrated SW.